

2003

# Experimental investigation of push-pull precast cladding connections

Kevin Chan  
*San Jose State University*

Follow this and additional works at: [https://scholarworks.sjsu.edu/etd\\_theses](https://scholarworks.sjsu.edu/etd_theses)

---

## Recommended Citation

Chan, Kevin, "Experimental investigation of push-pull precast cladding connections" (2003). *Master's Theses*. 2435.  
DOI: <https://doi.org/10.31979/etd.dzhx-7zfz>  
[https://scholarworks.sjsu.edu/etd\\_theses/2435](https://scholarworks.sjsu.edu/etd_theses/2435)

This Thesis is brought to you for free and open access by the Master's Theses and Graduate Research at SJSU ScholarWorks. It has been accepted for inclusion in Master's Theses by an authorized administrator of SJSU ScholarWorks. For more information, please contact [scholarworks@sjsu.edu](mailto:scholarworks@sjsu.edu).

**EXPERIMENTAL INVESTIGATION OF PUSH-PULL PRECAST CLADDING  
CONNECTIONS**

**A Thesis**

**Presented to**

**The Faculty of the Department of Civil and Environmental Engineering**

**San Jose State University**

**In Partial Fulfillment**

**Of the Requirements for the Degree**

**Master of Science**

**by**

**Kevin Chan**

**August 2003**

UMI Number: 1417471

### INFORMATION TO USERS

The quality of this reproduction is dependent upon the quality of the copy submitted. Broken or indistinct print, colored or poor quality illustrations and photographs, print bleed-through, substandard margins, and improper alignment can adversely affect reproduction.

In the unlikely event that the author did not send a complete manuscript and there are missing pages, these will be noted. Also, if unauthorized copyright material had to be removed, a note will indicate the deletion.

**UMI**<sup>®</sup>

---

UMI Microform 1417471

Copyright 2004 by ProQuest Information and Learning Company.

All rights reserved. This microform edition is protected against unauthorized copying under Title 17, United States Code.

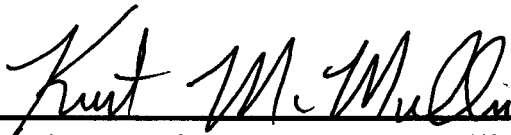
ProQuest Information and Learning Company  
300 North Zeeb Road  
P.O. Box 1346  
Ann Arbor, MI 48106-1346

© 2003

Kevin Chan

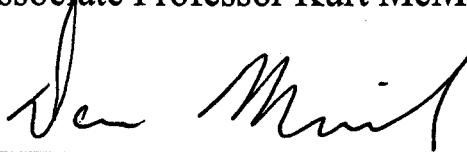
ALL RIGHTS RESERVED

APPROVED FOR THE DEPARTMENT OF  
CIVIL AND ENVIRONMENTAL ENGINEERING



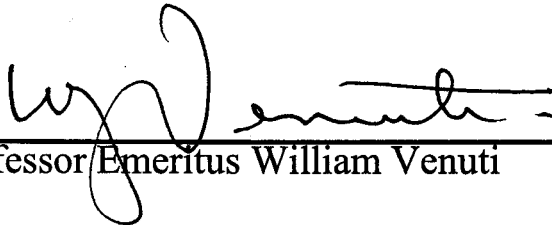
---

Associate Professor Kurt McMullin



---

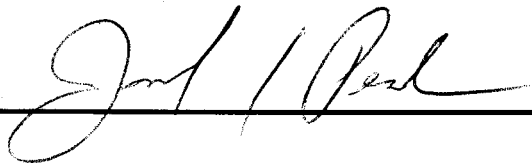
Daniel Merrick



---

Professor Emeritus William Venuti

APPROVED FOR THE UNIVERSITY



## **ABSTRACT**

### **EXPERIMENTAL INVESTIGATION OF PUSH-PULL PRECAST CLADDING CONNECTION**

**by Kevin Chan**

Four monotonic experiments of push-pull precast concrete cladding connections were performed to simulate the cladding connection under two orthogonal loading directions. The goal was to investigate the behavior of these cladding connections under bending and axial forces. Axial tension and compression occurs as a result of out-of-plane panel movement and represents the forces that the rods are intended to resist. Bending of the rods occurs as a result of in-plane panel movement, which these rods are not traditionally expected to resist.

Two of the experiments tested the bending strength of the connections using a cantilever test. The threaded rods of the two cantilever tests had a length of 460 mm and 150 mm. The other two tests evaluated the axial strength of the connection with 460 mm threaded rods. Analytical models were developed using basic mechanics to predict the behavior of the connection and estimate a possible failure sequence.

## **ACKNOWLEDGMENTS**

I would like to express my gratitude to San Jose State University and the Department of Civil and Environmental Engineering for providing me this research opportunity. This research provided me valuable hands-on experience in all aspects of research. I would also like to express my gratitude and appreciation to Daniel Merrick and Professor Emeritus William Venuti for their assistance in reviewing this report.

I wish to express my utmost gratitude to the University's technicians who helped with fabrication of the specimens, most notably Dave Hemer and Pat Joice; without their help I would not have been able to finish my project in time. I am especially grateful for Pat Joice's expertise in welding and assistance in setting up the experiments. I will forever remember my experience working in the lab.

I wish to thank Mark Hildebrand from Willis Construction Co., Inc. for providing the drawing of the push-pull precast cladding connection. Without these drawings, accurate representations of the dimensions would not have been duplicated for this study.

In addition, I would like to thank Associate Professor Kurt McMullin for his guidance and wonderful knowledge during this research. I am very grateful for Kurt's assistance in reviewing this report and providing a great experience working on this research.

I wish to thank my fellow student, Carter Choi, for his assistance with this research. This past year has been very memorable, working side by side in the lab and checking each other's work.

Finally, I wish to thank my parents for the support they have given me to continue my education.

## TABLE OF CONTENTS

List of Tables	viii
List of Figures	ix
Chapter 1. Introduction	1
1.1 Problem Statement	1
1.2 Project Goals and Objectives	2
1.3 Scope of Work	3
Chapter 2. Literature Review	4
2.1 Introduction	4
2.2 Experimental Test Programs	4
2.2.1 Studies at Cal Poly University at San Luis Obispo	4
2.2.2 Studies at Georgia Institute of Technology	5
2.2.3 Studies at University of Oklahoma	6
2.3 Analytical Research Programs	7
2.4 Design Issues	9
Chapter 3. Experimental Design	12
3.1 Experimental Variables	12
3.2 Experimental Specimen	13
3.2.1 Specimen Properties	13
3.2.2 Failure Modes	15
3.3 Testing Arrangement	16
3.4 Instrumentation	18
3.5 Testing Procedure	19
3.6 Predicted Results	20
3.6.1 Cantilever Tests	21
3.6.2 Axial Tests	22
Chapter 4. Experimental Results	24
4.1 Behavior of Test Specimens	24



4.2 Observed Failure Modes	26
4.3 Results for Individual Tests	27
4.3.1 Results of PP1	27
4.3.2 Results of PP2	28
4.3.3 Results of PP3	29
4.3.4 Results of PP4	30
4.4 Variation from Expected Test Specimen and Procedure	30
Chapter 5. Comparison of Analytical and Experimental Results	32
5.1 Secant and Tangent Stiffness	32
5.2 Displacement Damage Thresholds	34
5.3 Comparison of Experimental and Predicted Results	35
5.4 Similar Results of All Tests	37
5.5 Effect of Change of Test Variables	37
Chapter 6. Conclusions and Recommendations	39
6.1 Results of Original Research Objectives	39
6.2 Conclusions	40
6.3 Recommendations for Engineering Practice	41
6.4 Recommendations for Continuation of Research	41
References	43
Appendix A. Notation	46
Appendix B. Glossary	48
Appendix C. Tables	51
Appendix D. Figures	63
Appendix E. Summary of Material Tests	96
Appendix F. Calibration Charts of Instrumentation	108
Appendix G. Supporting Calculations	113

## LIST OF TABLES

Table 1 – Properties and Results of Threaded Rod Connection from Rihal	52
Table 2 – Goodno's Results of Response Model: Clip Angle vs. Ductile Rod Cladding Panel Connections	52
Table 3 – Seismic Rehabilitation Guidelines for Nonstructural Performance Levels and Damage	52
Table 4 – Summary of Similar Past Investigations of Push-Pull Precast Cladding Connection	54
Table 5 – Test Matrix	54
Table 6 – Properties of Test Specimens	55
Table 7 – Table of Instrumentation for Cantilever Tests (PP1 and PP2)	55
Table 8 – Table of Instrumentation for Tension and compression Tests (PP3 and PP4)	56
Table 9 – Predicted Failure Mode Sequence of Cantilever Test	57
Table10– Predicted Failure Mode Sequence of Compression Test	58
Table11– Predicted Failure Mode Sequence of Tension Test	59
Table12– Predicted Value of Bending Forces and Corresponding Deflection for the Cantilever Test	60
Table13– Experimental Results	60
Table14– Stiffness Properties of Each Individual Rod of the Tests	60
Table15– Displacement of Damage Thresholds for Performance Limits	61
Table16– Summary of Cantilever Test Results from Various Researchers	61
Table 17– Summary of Cantilever Test Results from Various Researchers	62

## LIST OF FIGURES

Figure 1 – Typical Push-Pull Precast Cladding Connection	64
Figure 2 – Typical Panel Embed Hardware	65
Figure 3 – Rihal’s Threaded Rod Connection Test	66
Figure 4 – Craig’s Typical Push-Pull Connection	66
Figure 5 – Craig’s Push-Pull Connection Test Fixture	67
Figure 6 – Craig’s Push-Pull Cyclic Performance to Failure	67
Figure 7 – Craig’s Push-Pull Comparison with Design Chart	68
Figure 8 – Sack’s Flexible Panel Frame Connection	68
Figure 9 – Sack’s Bearing Panel Frame Connection	69
Figure10– Sack’s Fixed and Pinned End Elastic Stiffness Coefficients vs. Ratio of Rod Length and Diameter for Flexible Panel Frame Connection	69
Figure11– Fillet Weld Size on the Nuts of the Cantilever Tests	70
Figure12– Fillet Weld Size of the Axial Tests	71
Figure13– Tension and compression Tests Arrangement	72
Figure14– Fillet Weld Size on the Nuts of the Axial Tests	73
Figure15– Cantilever Test Arrangement	74
Figure16– Cantilever Tests Instrumentation Lay Out	75
Figure17– Tension and compression Tests Instrumentation Lay Out	76
Figure18– Testing Arrangement of Tension Test (PP3)	77
Figure19– Testing Arrangement of Compression Test (PP4)	78
Figure20– Prediction Model of the Cantilever Test	79
Figure21– Predicted Results of the Cantilever Tests	79
Figure22– Prediction Model of the Axial Tests	80
Figure23– Predicted Results of the Axial Tests	81
Figure24– The Fractured Rod of PP3	82
Figure25– Bending of the Plate and Threaded Rods of PP3	82
Figure26– Gap at Backside of the Flange of the Column Testing Jig of PP4	83

Figure27– Bending of the Plate of PP3	83
Figure28– Yield Lines Caused by Bending on the Plate of PP3	84
Figure29– Initial Deformation of PP4	84
Figure30– Bending of the Rods of PP4	85
Figure31– Force vs. Overall Displacement Curve of PP1	86
Figure32– Force vs. Displacement of Two Ends of WT Beam of PP1	86
Figure33– Force vs. Displacement of Rod A of PP1	87
Figure34– Force vs. Displacement of Rod B of PP1	87
Figure35– Force vs. Displacement of Rod C of PP1	88
Figure36– Force vs. Displacement of Rod D of PP1	88
Figure37– Force vs. Overall Displacement of PP2	89
Figure38– Force vs. Displacement of Two Ends of WT Beam of PP2	89
Figure39– Force vs. Displacement of Rod A of PP2	90
Figure40– Force vs. Displacement of Rod B of PP2	90
Figure41– Force vs. Overall Displacement of PP3	91
Figure42– Force vs. Column Plate and Rods Displacement of PP3	91
Figure43– Force vs. Overall Displacement of PP4	92
Figure44– Force vs. Column Plate and Rods Displacement of PP4	92
Figure45– Comparison of Recorded Overall Displacement and Equation 9	93
Figure46– Definition of Secant and Tangent Stiffness	93
Figure47– Method of Finding Yield Displacement	94
Figure48– Comparison of Actual and Predicted Results for Cantilever Loading	94
Figure49– Comparison of Actual and Predicted Results for Axial Loading	95

# CHAPTER 1

## Introduction

### 1.1 Problem Statement

Precast concrete cladding systems are a common type of enclosure system for many steel and concrete buildings. Past research has shown that the cladding system has significant influence on the response of the structure during strong ground motion (Craig et al. 1988). The cladding can stiffen the building and change the response of the structure. Due to this effect, the researchers believed it important to investigate the behavior of the cladding connections. The authors investigated one type of connection used to connect the precast cladding to the building framing. This style of connection is often called a push-pull precast cladding connection and an example is shown by Figure 1 in Appendix D. The study presented in this report is an initial part of an extended research initiative regarding seismic and blast loading behavior of precast cladding systems.

Push-pull precast cladding connections are also called threaded rod lateral connections. As shown in Figure 1, a typical connection consists of a steel plate welded to the structural column. One end of the two threaded rods is bolted to the corner of this column plate. At the other end, the threaded rods are welded to panel hardware which has been embedded into the precast concrete panel. Figure 2 shows an enlarged view of one typical piece of panel hardware, the concrete embeds.

The purpose of precast cladding connections is to transfer the loads of individual concrete panels to the building's primary structural members. The intended design of the push-pull connection is to resist out-of-plane movement, the direction of movement that is perpendicular to the face of the claddings. Under

out-of-plane movement, the threaded rods in the connection will experience compression or tension loading. Push-pull connections are not designed to resist in-plane panel movement. The in-plane movement will cause the threaded rods to experience bending force.

The purpose of this study is to determine the bending and axial stiffness of 25 mm diameter rods used as a component of the push-pull precast cladding connection. Varying lengths of threaded rods were tested and analytical models of the connection were conducted to predict possible failure modes and sequence. Evaluation of the predicted analytical results to the experimental results was completed. The stiffness value obtained in this study will be incorporated into related analytical work (Kwong 2002). Kwong performed pushover analysis of the cladding panel based on relatively simple assumptions about deflections and forces of the connection. The results from this study will provide Kwong's model with more accurate information of deflection and forces of the connection.

## **1.2 Project Goal and Objectives**

Experimental work on precast cladding connection was conducted because of the limited amount of published testing available. The goal of this project is to observe the characteristics of threaded rods and the connecting element of current push-pull precast cladding connections to improve understanding of the connection. It is hoped that results gathered in this study will be used in the future by engineers to have a better understanding of the behavior of the connection.

The objectives of this project are the following:

1. Measure force-deflection relationship of the push-pull connection under in-plane and out-of-plane movement.
2. Develop predictive models for the connection.
3. Determine the accuracy of the predictive model by comparing the predicted results to experimental results.

The project objectives were accomplished by four experimental tests that simulate various geometric configurations of push-pull connections, and with three different loading directions. Rod length was varied for different configurations. Specimens tested were assemblies of threaded rods, column plates, welds between the structural column and column plate, and panel hardware to simulate the primary components of a typical push-pull precast cladding connection. Quantitative data measured during the four tests include the strength and ductility of each specimen. The analytical models were used to predict force-deflection curves, failure modes, and sequence of limit states for all tests.

### **1.3 Scope of Work**

A literature review was conducted that found a limited number of studies related to push-pull precast cladding connection. There were four experimental tests performed in this study. The two cantilever tests were combined with existing published work to form a larger test matrix. No existing results similar to the tension and compression tests were found. All design and fabrication was conducted in the Engineering building at San Jose State University. The design phase included design of a new testing arrangement and test specimens. The length of time to complete design, fabrication, testing, and completion of the report was approximately one and a half years.

A prediction model was developed for each of the loading types to estimate the ductility, stiffness, and strength of the push-pull precast cladding connection. The data collected from the four tests was compared to these predictions.

## **CHAPTER 2**

### **Literature Review**

#### **2.1 Introduction**

The author found a limited number of published test results of various components of the precast concrete cladding systems. A review of the testing performed by past investigators provided information about push-pull precast cladding connections to initiate this study. The testing performed by past researchers included experimental tests of connections and concrete embedment, and analytical studies of building systems.

#### **2.2 Experimental Test Programs**

##### **2.2.1 Studies at Cal Poly University at San Luis Obispo**

Rihal tested ten push-pull connections (1989). The objective was to investigate the static load-deflection behavior of 19 mm (5/8 inch) diameter threaded rods of different lengths. A drawing of Rihal's test is shown on Figure 3. Table 1 lists the properties and results of Rihal's test. The threaded rod was bolted to a WT 4x12 with two nuts. The size of the hole on the WT beam was not reported. The panel end of the rod was connected to a plate with a ferrule insert and embedded in the precast concrete cladding. A vertical load was applied at the top of the WT beam. Rihal also performed an axial tension test on a 19-mm diameter threaded rod to investigate the behavior of such a rod in axial tension and establish the rod's deformation properties. Rihal concluded from the result of the tensile test that strain hardening must be considered for the rods.



Through his experiments, Rihal concluded that the load capacity decreased with increased rod length and experimental data showed good correlation with his predicted analytical data. Rihal developed a predictive model for the load-deflection relationship of cantilevered threaded-rod specimens. Additional information about Rihal's experimental and analytical data, and prediction model are apparently discussed in another report (Rihal, 1988). However, a copy of this report could not be located through our university library exchange program.

### **2.2.2 Studies at Georgia Institute of Technology**

Craig et al. performed tests on bolt-insert and ductile rod push-pull connections (1988). The purpose of their research was to characterize the kinematic and constitutive properties of the precast cladding connections. Figure 4 shows the typical push-pull connection that Craig was simulating. They tested the connection with various length of 19-mm threaded A-36 steel rod. The rod was connected to the ferrule insert embedded in concrete cladding panel. Figure 5 showed their test set-up.

Tests of the connection were conducted with cyclic in-plane (shear) loading. The lengths of threaded rods varied from 205 to 305 mm. The panel end of the threaded rods was attached to the concrete by a ferrule insert. At the other end, the rod was connected to an angle by nuts and washers. The nuts were spot welded to the threaded rods and the opening on the angle that the threaded rod passes through was significantly larger than the rod. The researchers concluded that the common design of push-pull connections led to details susceptible to low-cycle fatigue failure. Ten consecutive cycles of equal amplitude in-plane displacements were applied to the connection. After this sequence, the amplitude of the displacement increased. This series of displacement was repeated until failure occurred. Figure 6 summarizes the results of the tests. All threaded rods fractured at between 47 to 90 cycles of loading and all failures occurred at

displacements of less than 50 mm (2 inches). The 50 mm displacement was less than the UBC requirement for interstory drift of a 3.35 m (11 ft) height story. Three of the eight tests performed exhibited slip of the rods in the enlarged holes. Slip actually increased the number of cycles to failure by decreasing the connection stiffness. However, the researchers stated that slip can be eliminated if the washers were tack welded to the angle.

Based on their testing results, Craig et al. suggested that the actual connection in the building could reach low cycle fatigue cracking after experiencing several strong earthquakes over a period of time. Figure 7 summarized the test by comparing the test results with a typical set of design curves used in practice. These design curves were created on the basis of simple elasto-plastic beam models with either pinned or fixed end supports. Based on the comparison, they concluded that the measured deflection limits from the tests were approximately two times the design values while the load limits fell almost right on the design curve. The complete results and data of the tests performed were included in another report by Leistikow (Leistikow, 1988). However, this report could not be located through library exchange program as well.

Pinelli et al. tested precast concrete embedment cladding connections (Pinelli et al. 1990). Their tests were designed to evaluate several different types of insert arrangement. All tests were loaded cyclically. Pinelli et al. concluded that inserts located on the edge of cladding performed better than inserts located on the corners, because the existence of concrete on three sides of the inserts provided higher strength values and higher stiffness.

### **2.2.3 Studies at University of Oklahoma**

Sack et al. tested two different types of precast concrete cladding connection (1989). They designated them the flexible panel frame connection and bearing panel frame connection. The two types of insert were modeled using different

assumptions about the structural model of the load path. One was considered as pinned at the panel face and the other fixed. The details of the two connections are shown in Figures 8 and 9. The flexible panel connection was similar to the push-pull connection in this study. Instead of using threaded rods and welding the steel column plate to the structural column like the push-pull connection, their flexible connection used steel rods with threads at the two ends and a steel angle bolted to the structural column. Rod lengths varying from 75 to 230 mm were tested (3, 5, 7, and 9 inches). Each rod length was tested twice with different types of insert connecting the rods to the panel. Figure 10 shows the elastic stiffness coefficients of both pinned and fixed vs. the ratio of rod length and diameter. According to the figure, the rods that had fixed-end inserts had higher stiffness coefficient than the pinned-end insert. Considering all the tests performed, they concluded that the stiffness of the connection depended on three factors: the length of the rods, the thickness of the structural angle, and the stiffness of the panel where the connection is attached which would depend on the type of inserts used.

### **2.3 Analytical Research Programs**

Goodno et al. developed an analytical response model (Goodno et al. 1988). The model consisted of two panels that were assumed to be flat and rigid with elastic spring elements. The two panels were placed next to each other. The eight elastic spring elements were connected to the two panels at their four corners to represent the connections and inserts. The model was run in nonlinear dynamic time history. Two different kinds of connection configurations were used in the model. The first model used eight clip angle connections to attach to the panel. The second model used four clip angle connections at the top of the panel and four push-pull connections at the bottom. The spring stiffness values used in the response model were obtained from the results of the push-pull connection tests

that Craig et al. performed (1988). The complete experimental results were included in another report by Leistikow (Leistikow, 1988). This second report could not be located through library exchange program. The average in-plane linear stiffness of the 300-mm (12 inch) rods was 0.08 kN/cm (0.46 k/in). The stiffness value was used as the elastic spring elements for the response model. Table 2 showed the results of the model with the two different types of connection configurations. In Table 2, the top connection stiffness refers to the stiffness of the connections that attached to the top of the panels while the connector force refers to the peak force experienced by the connections.

This study concluded that the push-pull connection was effective in isolating the cladding from interstory drift compared to clip angle connection, based on the results of the model response shown in Table 2. The results showed that the interstory shear stiffness per bay was reduced by a factor of five and forces in the connection were also reduced.

Craig et al. performed simulations using a hysteretic model to predict cladding influence on building during strong ground motion (1986). Their model used strength and stiffness data they obtained from testing three 19 mm (3/4-inch) diameter wedge-type inserts subjected to moment and shear pull out. The analytical results showed that this type of insert experienced linear displacement behavior up to 44.3 kN (10,000 lbs) and to failure at 48.8 to 53.2 kN (11,000 to 12,000 lbs). The linear region had narrow hysteretic loops indicating little energy dissipation. In the nonlinear region above 44.3 kN, the hysteretic loops increased significantly, indicating more energy dissipation due to deformation of the reinforcing steel.

Another goal of past investigations of precast cladding connection has been to determine if there is a significant influence on a building's response to strong ground motion (Goodno et al. 1991). Nonlinear analytical models were developed using DRAIN-2D of a structure; one with cladding, the other without cladding. Frame members were modeled as beam-column elements with flexural and axial

stiffness with bilinear hysteretic behavior. The model without cladding had its masses lumped at nodes and served as a reference. The results of the analysis showed that the frame with cladding had 70% less drift than the frame without. This was due to the ductile inelastic action in the concrete cladding connections provided significant levels of damping capability.

Other researchers have also concluded that the use of ductile cladding panel systems can significantly reduce the response and increase the lateral stiffness of the structure (El-Gazairly et al. 1990; Craig et al. 1991; and Weston et al. 2002). A review of these reports provided little additional information beneficial to the current study. These publications discussed the subject of insert performance and influence of cladding on the overall structure. The results of these studies may be beneficial for the future analysis of connection/cladding influence on the overall structure.

## **2.4 Design Issues**

Some researchers have discussed possible changes in the process of designing cladding system. Cohen stated that in spite of life-safety problems of concrete panels during the 1994 Northridge earthquake, the influence of cladding system on buildings continues to be ignored by designers and most of the research studies have not been extensive enough to have an effect on the profession (1995). Cohen discussed the shortcomings in codes and practice, and changes that should be made for the future. Likewise Pietroforte discussed possible changes to be made in the coordination between subcontractors and manufacturers regarding the design of cladding system (Pietroforte, 1995). The existing contractual agreement assumes that the design process is concluded ahead of construction. Pietroforte stated that a number of gaps need to be filled in the design and build process to ensure the consistent development of the design process due to the complexity of modern buildings.

Federal Emergency Management Agency 273 Seismic Rehabilitation Guidelines define the nonstructural performance levels expected of a structure after an earthquake. Table 3 lists the four different levels FEMA 273 discusses for the condition of cladding. These levels are Hazards Reduced (N-D), Life Safety (N-C), Immediate Occupancy (N-B), and Operational (N-A). Each level defines a certain condition of the cladding after an earthquake.

The Uniform Building Code 1997 provides design criteria for the total seismic force to be resisted by nonstructural components supported by structures. The design of lateral seismic force,  $F_p$  is shown in Equations 1 and 2. However,  $F_p$  shall not be less than  $0.7C_aI_pW_p$ .

$$F_{p-max} = 4.0C_aI_pW_p \quad \text{Equation 1}$$

$C_a$  = seismic coefficient listed in Table 16-Q in UBC

$I_p$  = component importance factor, varies from 1.00 to 1.50

$W_p$  = component operating weight

$$F_p = (a_pC_aI_p/R_p) (1+3h_x/h_r) W_p \quad \text{Equation 2}$$

$a_p$  = component amplification factor, varies from 1.00 to 1.50

$h_x$  = elemental or component attachment elevation with respect to grade

$h_r$  = structure roof elevation with respect to grade

Drake et al. recommended a value of 1.00 for  $I_p$  for exterior-wall panels, 1.00 for  $a_p$  the component amplification factor, and 3.00 for  $R_p$  the component-response modification factor (1996). Drake et al. compared the new requirement of NEHRP provisions 1994 with 1991 NEHRP provisions and the 1994 UBC requirements. The 1994 provisions included the revised seismic-force design equations and new relative displacement design which were not included in the 1991 NEHRP and 1994 UBC. Factors in the 1994 NEHRP incorporated the effect of site ground motion, dynamic characteristics of the primary structure, flexibility of the component, the importance of the component's function, and relative displacement.

The Uniform Building Code 1997 also discusses design requirements for exterior elements in Section 1633.2.4.2. The building code states that cladding shall accommodate movements of the structure based on  $\Delta_M$  (maximum inelastic response deformation) and temperature changes. Maximum inelastic response deformation is the total story drift expected during a future ground motion, including both elastic and inelastic deformation. Section 1633.2.4.2 lists the following provisions (UBC 1997):

1. Connections and panel joints shall allow for a relative movement between stories of not less than two times story drift caused by wind, the calculated story drift based on  $\Delta_M$  or 1/2 inch (12.7 mm), whichever is greater.
2. Connections to permit movement in the plane of the panel for story drift shall be sliding connections using slotted or oversize holes, connections that permit movement by bending of steel, or other connections providing equivalent sliding, and ductility capacity.
3. Bodies of connections shall have sufficient ductility and rotation capacity to preclude fracture of the concrete or brittle failures at or near welds.
4. The body of the connection shall be designed for the force determined by Equation 2, where  $R_p = 3.0$  and  $a_p = 1.0$ .
5. All fasteners in the connection system, such as bolts, inserts, welds, and dowels, shall be designed for the forces determined by Equation 2, where  $R_p = 1.0$  and  $a_p = 1.0$ .
6. Fasteners embedded in concrete shall be attached to, or hooked around, reinforcing steel or otherwise terminated to effectively transfer forces to the reinforcing steel.

## CHAPTER 3

### Experimental Design

Based on the past published experimental studies, the tests performed by Rihal 1989, Craig et al. 1988, and Sack et al. 1989 were most similar to the tests in this study. The cantilever tests performed in this study will expand the test matrix created by past researchers. Table 4 lists the past experiments performed by Rihal 1989, Craig et al. 1988, and Sack et al. 1989. This study not only dealt with lateral stiffness of the push-pull connection but also the axial stiffness of the push-pull connection under tension and compression.

#### 3.1 Experimental Variables

Four tests were performed in this study. These four tests can be divided into two sets of tests. The first set was the two cantilever tests that simulated the in-plane movement of a concrete panel. This movement would be orthogonal to the loading the connection is designed to resist. These two tests measured the push-pull connection's bending behavior. The design of the two cantilever tests was identical, the only variation being the length of the threaded rods. Rod lengths of 150 and 460 mm (6 and 18 inches) were tested. The purpose of varying the rod length was to observe if failure would occur differently relative to the rod length.

The second set of tests was the axial loading tests. These two tests were testing the axial stiffness of the push-pull connection when the panel moves out-of-plane. This motion represents the original design intent of the connection. These two test specimens were designed identically. The only variation was the loading direction of the tests. The purpose of varying loading direction was to observe the



differences of failure mode, strength, and stiffness depending on the sense of the applied axial load. Table 5 lists the test matrix of the four tests performed.

## **3.2 Experimental Specimens**

Table 6 lists the dimensional properties of a full test matrix of twelve testing specimens that were originally considered. However, due to limitations on the scope of work for this project only Test 1, 3, 7, and 11 were actually performed. The tests with 25 mm (1 inch) diameter rods were chosen, because this rod diameter appears to be the dominant size used in industry.

### **3.2.1 Specimen Properties**

Several potential connection geometries as listed in Table 6 were originally evaluated but at the final stage before testing this list was reduced to four test specimens due to time and budget constraints. All of the test specimens were assembled with 25 mm diameter coil rods. The coil rods were made from low carbon steel with minimum yield stress of 248 MPa (36 ksi) and maximum ultimate stress of 413 MPa (60 ksi). The threads are rolled into the material causing severe cold-working. This cold-working significantly alters the mechanical properties of the steel. With limited information on the extent of cold-working, it was assumed that the properties of the finished rod would be comparable with high strength low alloy steel based on the results of the tension testing of the material. Tension testing of the material used for the threaded rods was completed and is included in Appendix E. High strength low alloy steel has a ratio of minimum yield strength to ultimate strength of about 80% according to AISC Manual Volume I (1994). Using a similar ratio for the coil rod and considering the ultimate stress measured, and listed in Appendix E, an approximate yield stress for the rods was determined to be 486 MPa (70.6 ksi).

The cantilever tests (PP1 and PP2) were designed similar to Rihal's tests (Rihal 1989). The two cantilever tests were intended to expand the test matrix that previous researchers had originally established. One difference was that Rihal's test connected the threaded rods to a fixture built with a concrete panel, while the current tests used an all steel reaction fixture. Rihal wanted to observe if the embedded panel hardware would actually pull out before the connection failed. With modern panel hardware design, it is less likely that panel hardware will pull out of the concrete panel. Due to the expense of trying to include this unlikely failure mode in the test, it was removed from the scope of the project. The threaded rods were connected to the panel hardware by welding the coil nuts on the panel plate with a 6-mm fillet weld (1/4 inch) as shown in Figure 11. This welding was performed by a certified welder from a local shop with E-70XX electrode. Before testing, the actual weld size was measured and is shown in Figure 11 for the two cantilever tests. Also, unlike Rihal's tests of having only the nut connecting the other end of the threaded rod to the WT beam, the cantilever tests in this study used 200-mm square plate washers with nuts on each face. In addition, the holes on the WT beam were cored to a diameter of 75 mm (3 inches).

For the two axial loading tests (PP3 and PP4), a testing jig was fabricated to represent a W12x120 structural column. This column testing jig was welded to a 900 mm x 400 mm x 130 mm (36"x16"x1/2") rectangular plate. This welding was also performed by a certified welder from a local shop with E-70XX electrode. The fillet weld size is 125-mm (5-inch) long and 6-mm (1/4-inch) thick. Similar to Figure 11, Figure 12 shows the exact size of the fillet weld of the two axial tests. The four threaded rods were connected at one end to the corners of the column plate at one end as shown in Figure 13. The other ends of the rods were connected to a W16x40 that represented the concrete embed plate of an actual connection with coil nuts welded to the web with a fillet weld of 6 mm (1/4 inch). Figure 14 shows the actual size of the fillet welds on the nuts for the axial tests. During tension testing, the weld that connects the nuts to the web of the W16x40 is not

expected to resist any force, however during compression test this weld will be required to resist all the force coming from the rod. In the event that these welds fracture, the test will be terminated. In an actual application, the concrete panel will assist in resisting the load transferring from the rods. This assistance will be provided by end bearing of the rod against the concrete. It is expected that the concrete panel will not be able to support a significant load once the weld fractures. Therefore, a conservative assumption was made that the concrete should not be expected to resist any load from the rod.

### **3.2.2 Failure Modes**

The following failure modes were considered for the specimens of PP1 and PP2.

1. Slipping between the plate washers and the supporting element
2. Yielding of the rod due to bending
3. Plastic hinging of the rod due to bending
4. Shear yielding of the rod
5. Bearing of the rod on supporting element

These five failure modes were considered for the cantilever test specimens shown in Figure 15. However, only the first three failure modes are expected to affect the behavior. The load was applied on top of the WT beam. Slip between plate washers and the web of WT beam was expected to occur before any load can be resisted. Once the WT beam came into contact with the rods, the WT beam pushes downward on the rods and causes them to bend. The shear yielding of the rod and bearing of the rod on supporting element were unlikely to occur, because of their expected high load.

The following failure modes were considered for the specimens of PP3 (tension) and PP4 (compression).

1. Yielding of the plate due to bending

2. Plastic hinging of the plate due to bending
3. Yielding of the rod
4. Fracturing of the weld connecting the column testing jig and the column plate (tension test only)
5. Fracturing of the weld connecting the coil nuts to the steel panel plate (compression test only)
6. Buckling of the rod (compression test only)

These six failure modes were considered for tension and compression tests. Load was applied to the top of the column testing jig which pushed downward on the column plate in compression and pulled upward in tension. The load would cause the column plate to bend concave down in tension and concave up in compression. The plate was considered to be the weak spot of the connection and it was assumed that other failure modes were not likely to occur before the plate failed.

Other failure modes might exist for an actual push-pull connection in the field. This is because some potential failure modes were eliminated from the test program due to the need to maintain a symmetric testing arrangement. These failure modes are listed as follow.

1. Fracture of column weld due to tension required to counteract cantilever moment from non-symmetric column plate loading
2. Loss of embedment anchorage into the concrete
3. Interact of axial and bending loading on the rod

### **3.3 Testing Arrangement**

All four tests were designed to simulate the actual bending, tension, and compression forces that the connection will experience in an actual cladding assembly. The testing protocol for test PP1 and PP2 was designated as the cantilever test. The cantilever test protocol consists of a WT beam to represent the

building-side support for the connection as shown in Figure 15. The WT beam was bolted to the top head of the testing machine, and four push-pull coil rods were bolted horizontally through the web of the WT beam. Spacing between the threaded rods was 127 mm on center. The rods were bolted with 100 mm x 100 mm x 13 mm (4"x4"x1/2") plate washers and coil nuts on each side of the web. At the cladding-end, the rods were connected to a vertical steel plate that represents the panel hardware embedded in the concrete panel. The vertical plates were chosen to be thick enough to resist elastically the bending moment that could be transferred from the threaded rods. The rods were threaded into the nuts that were welded to the back of the vertical plate. The welding was performed by a certified welder from a local shop with E-70XX electrodes with nominal strength of 482 MPa (70 ksi). The size of the fillet weld on the nuts was 6 mm (1/4-inch) according to the detail provided by Willis Construction shown in Figure 2. Each of the vertical plates was clamped to two angles. The angles rested on the top of two reaction beams that were positioned in a V shape. High strength C-clamps were used to attach the angles to the beams. The beams provided a reaction to the moment developed between the WT and the vertical plate. During testing, the top head of the testing machine pushed the WT downward and the WT was intended to transfer the force equally to the four threaded rods.

During the literature survey, no compression or tension test literature on push-pull connections was found. Therefore, it was deemed important to investigate the behavior of the connection under both tension and compression forces. An axial testing arrangement was developed for both the tension and compression tests, except the load was applied in opposing directions. The details of the axial test arrangement are shown in Figure 13. The web of the W16x40 represents the panel hardware that would be embedded in the concrete panel. The nuts and washers used to connect the rods on both ends were identical to the configuration of the cantilever tests. For these tests only 460-mm (18-inch)

threaded rods were used for the two axial loading tests. One reason for this choice was due to the inability of installing a shorter push-pull rod in the testing machine.

### **3.4 Instrumentation**

The primary objective for all four tests was measurement of the force and displacement of the rods. For the cantilever test protocol, instrumentation used included six wire potentiometers that measured displacement and the test machine's internal load cell to record the value of force as shown in Figure 16 and Table 7. The coil nuts on the face of the WT were attached to wire potentiometers to measure coil rod deflection away from the concrete panel as shown in Figure 16. Another wire pot was placed at each end of the WT beam. These two wire pots measured the deflection of the two ends of the WT beam. It is assumed that the WT will deflect as a straight line between these two ends. All electronic instrument data channels in the unit of voltage were logged and recorded by a PC-based Omega data acquisition system. Each wire potentiometer was calibrated before the first test. Voltage data readings were converted into inch units based on the measured calibration factor. Appendix F contains graphs of the calibration testing of each instrument.

For the axial loading protocol, six instruments were used as listed in Table 8. Figure 17 illustrates the instrumentation set-up of the axial loading protocol. Five wire pots were used to measure axial displacement of the threaded rods and one 200-kip load cell measured the total force applied by the testing machine. Four wire pots were placed above and below two of the four threaded rods. A limited number of wire pots were available for testing. It was assumed that the deflection of the two sides of the tests would be identical. Therefore only two threaded rods on the same side were connected to four wire pots. The difference between the two wire pots used for a rod was to determine the change in length that the rod experienced during test. The remaining wire pot was used to measure the overall

displacement of the head of the testing machine. Figures 18 and 19 show the testing arrangement of PP3 and PP4 with all instruments mounted before the test. All data channel readings in the unit of voltage were logged at a frequency of one Hz by the Fluke data acquisition system and recorded by a PC. The readings of voltage were converted into engineering units based on the calibration factor.

Photographs were taken of all tests to document testing arrangement and visible damage thresholds.

### **3.5 Testing Procedure**

The procedure for the cantilever test protocol performed in this study was:

1. Test specimens were designed and material ordered, fabricated, assembled, and prepared for testing.
2. Coil rods were installed in the plate and WT, and nuts were tightened manually with a wrench. Plate washers were not tack welded to the WT.
3. Instruments were calibrated to verify the linear relationship of voltage versus measurement.
4. Instruments were placed on the test specimens and connected to the data acquisition system.
5. Loads were applied monotonically for both tests until failure occurred. Failure was defined as complete loss of load resistance or instability of the test specimen.
6. Data were plotted into graphs.

The following is the procedure for the axial test protocol in this study:

1. Test specimens were designed and materials ordered, fabricated, assembled, and prepared for testing.

2. Instruments were calibrated based on a linear relationship of voltage versus measurement.
3. Instruments were placed on the test specimens and connected to the data acquisition system.
4. Specimens were whitewashed with lime to visibly document yielding and slip.
5. Loads were applied monotonically for all two tests until failure occurred. Failure was defined as complete loss of load resistance or instability of the test specimen.
6. Data were plotted into graphs.

### **3.6 Predicted Results**

Several potential failure modes were considered before the tests. These failure modes and their expected sequence were calculated from analysis and tabulated in Table 9, 10, and 11. However, not all failure modes considered actually occurred during test.

The predicted results were calculated using basic steel mechanic equations and appropriate design equations from the AISC-LRFD Manual (AISC 1994). Calculations of the predicted results are included in Appendix G. The yield strength of the steel was assumed to be 248 MPa (36 ksi) for all calculations. The actual yield stress for the threaded coil rods was 486 MPa (70.6 ksi) and the plate used in the axial tests had a yield stress of 366 MPa (53.1 ksi) according to the coupon tests. The design of the test fixture was based on a conservative estimate of the predicted results.



### 3.6.1 Cantilever Tests

It was assumed that the threaded rods acted like cantilevers supported by the panel hardware for the cantilever tests as shown in Figure 20. Force was applied at the tip of the free end of the cantilever rods from the WT beam. Slipping between the web of the WT and the rods was assumed to occur at the beginning of the test with minimal load for the prediction model. However, in reality for bolt slip to occur, the load has must exceed the friction force between the web of the WT and the plate washers. The friction force can be calculated by multiplying the friction coefficient to the clamping force created by tightening the nuts of the threaded rods. However, the friction force was not calculated, because the slip between the WT and plate washer was assumed to occur before load was applied for the prediction model. In addition, the small pretensioning force applied by the lightly tightened nuts would be small.

It was predicted that the four rods would start yielding before any other noticeable failure modes occur. The moment to cause the rods to yield was calculated from Equation 3.

$$M_y = F_y S_x \quad \text{Equation 3}$$

$M_y$  = yield bending moment

$F_y$  = yield stress of the material

$S_x$  = sectional modulus of the specimen

The load coming from the WT beam to cause the rods to yield was  $P_y$ , calculated by Equation 4.

$$P_y = M_y / L \quad \text{Equation 4}$$

$P_y$  = load to create  $M_y$

$L$  = length of the rods

From analysis of the model, the results showed that the four 150-mm rods would reach their plastic bending strength at 12.6 kN, and the four 460-mm rods would resist 4.19 kN. Plastic bending moment was calculated using Equation 5.

$$M_p = F_y Z_x \quad \text{Equation 5}$$

$M_p$  = plastic bending moment

$Z_x$  = plastic modulus of the specimen

The force to cause plastic bending moment in the rods was calculated using Equation 6.

$$P_p = M_p / L \quad \text{Equation 6}$$

$P_p$  = load to create  $M_p$

Potential catenary action of the rod was not considered in the prediction model. Catenary action was excluded because out-of-plane flexibility of the panel will likely prevent axial restraint of the push-pull rod.

Table 9 lists the predicted sequence of the failure modes for the cantilever tests based upon their strength. The predicted force and displacement values of the cantilever tests are tabulated in Table 12 and shown in Figure 21. The elastic bending displacement of the cantilever rods was calculated as:

$$\Delta = PL^3 / 3EI. \quad \text{Equation 7}$$

The moment of inertia,  $I$ , was calculated based on the root diameter of the threaded section ( $d_{rms}$ ) of the rods. As seen in Figure 21, the model with the shorter threaded rods (PP2) showed higher strength and stiffness but less flexible than the longer rods (PP1). Appendix G provides the complete set of equations and calculation of the failure modes.

### 3.6.2 Axial Tests

For the axial test, the column plate was modeled as a beam pinned at the location of the connected rods as shown in Figure 22. The force from the column testing jig was considered as two point loads on the plate. The threaded rods were modeled as pinned at the top and fixed at the bottom and resisting only tension, and compression forces.

This model predicted that the column plate connecting the threaded rods and column testing jig would yield before any other failure modes occur. For both the tension and compression tests, the plate would yield at a total force of 26.6 kN (6 kips) and reach its plastic bending strength at 39.9 kN (9 kips). Equations 3 and 5 were used to calculate the yield and plastic bending moment of the column plate. Based on the model developed, the total force to cause  $M_y$  and  $M_p$  in the plate was determined by dividing by the length of 101.6 mm. The length of 101.6 mm (4 inches) is half of the distance from the column weld to the center of the rod according to the shear and moment diagrams of the model.

The buckling strength of the four threaded rods was calculated based on the assumption that the rods were pinned at the top and fixed at bottom. Tables 10 and 11 list the predicted possible failure modes and sequence for the tension and compression tests. Appendix G provides the complete equations and calculation of the failure modes. Figure 23 shows the predicted values of force and displacement for the axial tests and the load that would cause the rods to yield, the column plate to form plastic hinges, and fracture of the column weld. The prediction curve of force vs. displacement was only drawn until the column plate reaches its yield strength, because the model does not provide a means to predict the displacement after initial yielding of the connection. This prediction curve excluded the failure mode of buckling of the connection, due to the fact that the load to cause the rods to buckle was much higher than other failure modes and exceeds the range of the figure. The stiffness of the assembly is the combination of stiffness of the plate and rods. The models for tension and compression tests were identical, based on the assumption that the threaded rods and column plate had the same behavior in both tension and compression tests. Post buckling displacement of the threaded rods under compression was ignored, but the force to cause rod buckling was included in the development of the failure mode sequence.

## CHAPTER 4

### Experimental Results

Table 13 summarizes the main results of the four tests. This Chapter discusses the result of individual tests. Comparison of different tests and more in-depth evaluation of the results are presented in Chapter 5.

#### 4.1 Behavior of Test Specimens

The first test performed (PP1) was the cantilever test with four 460-mm (18-inch) long 25-mm (1-inch) diameter threaded rods. The four threaded rods were connected to the WT beam at one end and to the steel embedded plate at the other. Details of this connection are described in Section 3.2. Loss of load carrying capacity never occurred during this test. Second-order nonlinear effects appear to have allowed for the development of high catenary axial forces in the rods. According to the predicted results listed in Table 9, the rods should have reached their plastic bending strength at 4.17 kN (0.94 kip). However, a peak load of 39.4 kN (8.88 kips) was achieved during the test, and only small cracks were observed where the rods were bent. The four threaded rods were visibly seen to bend in a double curvature behavior and deflections up to 191 mm (7.5 inches) were recorded. The double curvature bending indicates that the threaded rods should be considered to be fixed at both ends rather than the assumed cantilever model shown in Figure 20. No significant slipping between the threaded rods and the WT beam was recorded even though the plate washers were not tack welded to the WT. The test was eventually stopped because the WT beam was lowered to a point where it was nearly touching the table of the testing machine.

The second test performed (PP2) was the cantilever test with four 150-mm (6-inch) long 25 mm (1-inch) diameter threaded rods. Similar to PP1, loss of load

carrying capacity never occurred for this test. According to the predicted results listed in Table 9, the rods should have reached their plastic bending strength at 12.5 kN (2.83 kips). However, during the test a peak load of 113 kN (25.5 kips) was achieved. Similar to PP1, the four threaded rods were once again bent in double curvature and again no significant slip between the threaded rods and WT beam was observed during the test. The test was eventually stopped at a peak displacement of 39.4 mm because of limitations of the testing jig; the jig was not designed to sustain the amount of force developed in the rods.

The third test (PP3) was the tension test with 460 mm (18 inch) long 25 mm (1 inch) diameter threaded rods. Details of this connection are described in Section 3.2. The test ended when one of the threaded rods fractured due to combined tension and bending at a load of 246 kN (55.4 kips). Figure 24 shows the fractured rod of PP3. At this point the other three threaded rods showed severe inelastic behavior and significant cracking. Bending moment developed in the four threaded rods because as the column plate bent concave downward, the rigidity of the plate washer and coil nut assembly caused the end of the threaded rods to bend with the plate as shown in Figure 25. The extent of this phenomenon was not predicted before the test. At large displacement, the column plate bent significantly and plate yielding was observed near the weld. No cracks were observed on the column plate, even though yield lines were clearly visible on the plate.

Maximum displacement of the entire specimen was 144.8 mm (5.7 inches). The main weld between the column plate and the column testing jig showed no sign of cracking, although the tack weld fractured at a load near 111 kN (25 kips). A poor design of instrumentation resulted in the displacement of the column plate and the rods combined being measured as larger than the maximum displacement of the entire specimen. This error occurred because the string of the wire potentiometer did not remain vertical during testing, resulting in excess displacement to be

recorded. The strings were pulled horizontally due to the bending of the column plate, as shown in Figure 25.

The fourth test (PP4) was the compression test with 460-mm (18-inch) long 25-mm (1-inch) diameter threaded rods. This test ended because of weld fracture of the test fixture. At the end of the test, there were visible cracks on all four threaded rods, even though there was no loss of load carrying capacity of any rod when the test concluded. It did seem apparent that the threaded rods were near a point of fracture. Similar to the tension test, the column plate was bent out of plane causing the top end of the threaded rods to bend with the plate. At around 71.0 kN (16 kips) yield lines were visible on the plate parallel to the weld. The column testing jig that simulated the structural column was welded to the plate at the outside face of the flanges, and no weld was used inside. Because of this weldment design, the plate bent concave upward causing a gap opening on the backside of the flanges. This phenomenon is shown in the photo of Figure 26. At the end of the test, the gaps were approximately 10 mm (0.4 inch) high. During the test, there were several evident occurrences of slipping between the plate washers of the threaded rods and the plate.

## **4.2 Observed Failure Modes**

For both PP1 and PP2, the only failure modes observed during the tests were yielding and plastification of the threaded rods. The threaded rods bent in double curvature and moderate cracks appeared at the location of severe bending of the threaded rods. The predicted slipping between the plate washers and the WT beam did not occur during the tests.

For both PP3 and PP4, the failure modes observed were yielding of the column plate and bending of the threaded rods. The first failure mode observed was that the column plate started to show visible yield lines. Figure 27 shows the bending of the column plate during PP3. The loss of mill scale shown in Figure

28 shows the visible yield lines on the column plate of PP3 after the test. As the column plate bent and reached its plastic hinge strength, the plate rotated the head of the threaded rods and caused the threaded rods to yield due to bending. The final failure mode of PP3 was fracture of the threaded rods caused by bending of the column plate. PP4 ended with test fixture failure, but it is believed that if the test fixture had not failed, PP4 would have ended with fracture of the threaded rods as well. Figure 29 shows the initial deformation of PP4. Figure 30 shows the bending of the rods and that the plate washer has slipped out of the original alignment and the opening on the column plate is no longer fully covered by the plate washer.

### 4.3 Results for Individual Tests

Force vs. displacement graphs of various parameters were plotted for each test and are discussed in this section. Summary results of maximum load, displacement at maximum load, and total energy dissipated are listed in Table 13.

#### 4.3.1 Results of PP1

Test PP1 was the cantilever test with 460 mm (18 inch) length rods. There were a total of six force vs. displacement graphs plotted for this test. Figure 31 shows the overall displacement of the WT beam, while Figure 32 shows displacement at each end of the WT beam. The overall displacement of the WT beam plotted in Figure 31 is calculated by taking the average of the displacements of each end of the WT beam as shown by Equation 8.

$$\Delta_{\text{overall displacement}} = (\Delta_{\text{left}} + \Delta_{\text{right}}) / 2 \quad \text{Equation 8}$$

Figures 33 to 36 are four graphs that show displacement of each of the individual rod. Due to instrumentation difficulties, displacements of rod B, C, D were not properly recorded throughout the test. The data for rods B and C were

collected only for portions of the test, because the wire pots were extended out of their working range. There were not enough wire pots to measure displacement of all the threaded rods. Therefore, a dial gage was used for rod D, but the dial gage was unable to stay mounted on the specimen after 24 mm of displacement.

Figure 32 shows fairly consistent displacement of both ends of the WT beam, hence there was no noticeable tilting of the WT. Figure 33 of rod A shows no sign of slipping of the bolt connection. The other graphs are believed to show similar lack of slip if the data had been accurately recorded. Total energy dissipated during the monotonic test was 1739 kN-mm.

#### **4.3.2 Results of PP2**

Test PP2 was the cantilever test with a 150 mm long threaded rod. Test PP2 had an identical instrumentation setup as PP1. However, due to similar instrumentation difficulties of wire pots being out of range, displacements of rod C and D were not collected. Therefore, for PP2, there were only four graphs plotted. Figure 37 shows the overall displacement of the test, and Figure 38 shows the displacement at each end of the WT beam. Figures 39 and 40 showed displacement recordings of rods A and B. Note that both figures show larger displacements for the rods than the specimen due to instrumentation error. Figure 16, the instrumentation lay out of the cantilever tests, shows that the wire potentiometer was connected on the tip of the rod rather than where the rod passed through the WT beam. Therefore, because of bending of the rods, the rods actually had more displacement at the tip than where they pass through the WT beam.

Figure 38 shows the left end of the WT beam received more displacement than the right indicating slight tilting of the WT beam. The force vs. overall displacement curve for the test shows that there was a small drop of load value at a displacement of 25 mm. The drop of load value could be an error of reading the



load value or possible slipping. However, no occurrence of slipping was visually noticed during the test. Total energy dissipated was 2684 kN-mm.

### 4.3.3 Results of PP3

Test PP3 was the tension test with 460-mm (18-inch) long threaded rod. Figure 41 shows the force vs. overall displacement curve. Overall displacement was measured by Channel 3. Figure 42 shows the force vs. column plate and rods displacement.

$$\Delta_{\text{overall}} = \Delta_{\text{column plate}} + \Delta_{\text{rod}} \quad \text{Equation 9}$$

The value of deflection of the column plate was calculated as the average displacement recorded by the two wire pots connected to the top of the threaded rods as shown in Figure 17 (Channels 2 and 6). The deflection of the column plate was calculated by Equation 9.

$$\Delta_{\text{column plate}} = (\Delta_{\text{top of rod c}} + \Delta_{\text{top of rod d}}) / 2 \quad \text{Equation 10}$$

The value of elongation of the rods was the difference between the reading of the wire pots that connected to the top and bottom of the rod as shown in Figure 17 (for example Channels 5 and 6). The elongation of the rods was calculated by Equation 10.

$$\Delta_{\text{rod}} = \Delta_{\text{top of rod}} - \Delta_{\text{bottom of rod}} \quad \text{Equation 11}$$

As testing progressed the displacement recorded at the top of the rods began to vary from the desired displacement. This occurred because as the plate bent, the tips of the threaded rods were tilted; therefore the strings of wire pots were not vertical as shown in Figure 25. The recorded deflections of the top of the rods were actually more than the true vertical deflection and this error is expected to be about 6%. The maximum load for this test was at 246 kN. The total energy dissipated was 20180 kN-mm.

#### **4.3.4 Results of PP4**

Test PP4 is the compression test with 460-mm (18-inch) length rods. Figure 43 is the force vs. overall displacement and Figure 44 is the force vs. column plate and rods displacement. The maximum load for the test was 94.1 kN. Due to the similarity of instrumentation setup of PP3 and PP4, the data collected in PP4 had developed similar errors as PP3, but the errors were reduced. The attempt to reduce the error was to connect the strings of the wire potentiometers to the plate washers instead of the top of the rods. However, the bending of the column plate caused the strings of wire pots measuring the movement of the plate washer to again be tilted away from vertical. The force vs. overall displacement graph of Figure 43 shows slip of the rod bolted to the plate at four different times near displacements of 150 mm during the test. Each time, the load dropped and a loud noise was audible as potential energy was released. The total hysteretic energy dissipated was 19280 kN-mm.

#### **4.4 Variation from Expected Test Specimen and Procedure**

For both PP1 and PP2, the original plan was to record displacements of all the threaded rods. However, the wire pots did not perform as expected. Several wire pots were out of range, causing some data to not be collected. This error makes direct comparison of displacement between all the threaded rods difficult. However, the data of displacement at the ends of the WT beam were accurately collected throughout the test. Thus, the overall behavior of the push-pull connection was correctly recorded.

All tests were designed for monotonic load. During the testing of PP1, loading was first applied, released, and then reloaded contrary to the intent of applying continuously increasing load to failure. The reason for the unloading was because the specimens had a much higher load capacity than originally expected.

To obtain accurate readings at low loads, the testing machine was originally set at a low scale. When the loads far exceeded expectation, the testing machine was found to be approaching the maximum of the scale. Therefore, unloading the test specimen and choosing a higher scale was necessary if the test was to continue. It is expected that the unloading and reloading had little affect on the results of the test as seen in Figure 31 where the unloading and reloading graphs are nearly identical.

The instrumentation setup for PP3 and PP4 had two wire pots measuring the deflection of the top of two of the threaded rods. During the tests, the column plate connected to the top of the threaded rods bent. The deformation of the column plate caused the string of the wire pot to be tilted out of plumb. Therefore, the data collected from the two wire pots does not equal the desired displacement. Figure 45 shows the actual measurements of overall displacement and that obtained by Equation 9. Theoretically, the overall displacement obtained by Equation 9 should be equaled to the recorded overall displacement. However, due to the instrumentation error, the displacement obtained by Equation 9 does not equal to the recorded overall displacement. As shown in Figure 45, PP3's errors increased as the test proceed. Adjustment of instrumentation was made before PP4. Hence, the error in PP4 was less than PP3 as shown in Figure 45. The line of PP4 is much closer to the theoretical line.

PP4 ended with weld fracture of the column testing jig. Before fracture, it is assumed, the weld had little effect on the results of the test. It is believed that if the weld had not failed, the threaded rods were near the point of fracturing. In addition, the severe distortion of the connection indicates that the useful life of the assembly had been achieved. It is believed that sufficient amounts of data were collected to investigate the behavior of the specimen, even though the failure of the test jig occurred before the specimens reached an unstable state.

## CHAPTER 5

### Comparison of Test Results

Whereas Chapter 4 discussed the results of each experiment, this chapter compares and contrasts the behavior of individual push-pull rod connections. Each of the experiments tested were built with four rod connections and were tested with the intent of each rod carrying one quarter of the test load. To allow for understanding of individual rod performance, the forces discussed in this chapter are the test specimen loads divided by four.

#### 5.1 Secant and Tangent Stiffness

One of the key structural behaviors desired from the test was the stiffness the connection provides. This value determines the force developed under seismic loading, particularly at low levels of loading. Force-displacement relationships are complex and determining actual stiffness from experiments is difficult. For this study, two methods were used for calculating the stiffness: secant stiffness and tangent stiffness. Secant stiffness is calculated using Equation 12 and tangent stiffness is calculated using Equation 13. These two values were calculated for every data point  $i$  using the force denoted as  $F_i$ , and displacement  $\Delta_i$ . Secant and tangent stiffness are also graphically illustrated in Figure 46.

$$k_{si} = F / \Delta. \quad \text{Equation 12}$$

$$k_{ti} = F_i - F_{i-1} / \Delta_i - \Delta_{i-1} \quad \text{Equation 13}$$

One use of the secant and tangent stiffness was to identify the yield point for each test. As can be seen in Figures 31, 37, 41, and 43, no specific point can be clearly identified as the beginning of inelastic behavior of the connections. In an

attempt to provide a consistent method for identifying the yield point, four methods were tried.

1. Method 1 identified the yield point at the displacement where the secant stiffness has a 5 percent drop of the maximum secant stiffness.
2. Method 2 identified the yield point at the displacement where the secant stiffness has a 10 percent drop of the maximum.
3. Method 3 identified the yield point at the displacement where the tangent stiffness has a 5 percent drop of the maximum.
4. Method 4 identified the yield point at the displacement where the tangent stiffness has a 10 percent drop of the maximum.

The stiffness calculated for each point does not follow a smooth function throughout the test. Therefore, the last displacement with stiffness above the 95 percent and 90 percent thresholds was chosen as the yield displacement. This method of finding the yield displacement is illustrated in Figure 47. The results of the methods are shown in Table 14. Based on the results of Table 14, PP1 yielded at a higher displacement according to all four methods compared to PP2's yield displacements of the four methods. PP4 showed higher yield displacement than PP3 for three of the four methods. Method 2 appears to identify the yield point most accurately.

Table 15 lists the stiffness results of all tests. Based on the data collected, the secant stiffness per threaded rod of PP1 and PP2 at maximum load was 0.0539 kN/mm and 0.721 kN/mm. By comparing secant stiffness, it is clear that PP2 was much stiffer than PP1, predominantly because of the shorter length of threaded rods. Based on the testing, the axially loaded specimens had 26% higher maximum secant stiffness in tension than in compression. The maximum load of PP3 was 161% higher than PP4; however this maximum load occurred long after the connection began to yield. PP4 was much more ductile than PP3 and resisted load at much higher displacement.

## 5.2 Displacement Damage Thresholds

Table 16 lists the yield displacement and displacement damage thresholds. Strength degradation and therefore, strength degradation of 75% also, were not recorded for PP1 and PP2, because loss of load carrying capacity never occurred for the tests. Both tests ended, because of limitations of the testing arrangement. Therefore, the displacement value of strength degradation of PP1 and PP2 were taken as the maximum displacement achieved, rather than loss of load carrying capacity. This value thus represents the maximum verified displacement that the connection supports without passing the damage threshold. Likewise, the displacement where strength degradation initiated for PP1 and PP2 were 182.7 mm and 39.2 mm. Initial cracking of metal was not recorded during the tests. The small cracks on the rods were not observed until the end of the tests.

FEMA 273 defines the state of operational (N-A) or immediate occupancy (N-B) when cladding connections yield. Based on the observed failure modes of PP1 and PP2, both tests can be categorized in the level of operational (N-A) and immediate occupancy (N-B) when reaching yield strength. When PP1 and PP2 reached the peak load, the performance limits can be categorized in the level of life safety (N-C).

The displacement of strength degradation of PP3 was recorded at 145.6 mm, when one of the four rods fractured and strength degradation of 75% was recorded at the same displacement. The displacement of strength degradation of PP4 was recorded at 138.3 mm, when the weld on the test fixture cracked. Like the cantilever tests, this value represents the maximum the specimen resisted without exceeding the performance limit.

Initial cracking of metal or weld was not recorded during the tests. In PP3, only one of the four rods completely fractured. Hence, the assembly retained its load carrying capacity. The test ended due to the non-symmetric resistance to

load of the specimen. It is believed that continued loading would quickly fracture the other rods. None of the rods fractured in PP4.

At the beginning of both PP3 and PP4, before the plate starts to bend as shown in Figure 29, the connection can be considered as operational (N-A) or immediate occupancy (N-B) based on FEMA 273. As the plate pulls further away from the flanges of the column testing jig and causes the threaded rods to bend as shown in Figure 30, the cladding connection should be considered as approaching a life safety (N-C) performance level. At the end of PP3 when the threaded rods fractured, the cladding connection should be considered hazard reduced level (N-D), because the gravity stability of the panel is likely lost.

### **5.3 Comparison of Experimental and Predicted Results**

By comparing the data from PP1 and PP2 with their predicted results, it can be seen that the specimen had much higher yield strength and stiffness than originally expected. Figure 48 shows a comparison of actual and predicted results for the cantilever test specimens. According to the figure, it shows that both experiments had higher initial stiffness than predicted by the model. The prediction model expects slip to occur before load can be resisted. The predicted slip between the plate washer and the WT beam seems to have never occurred during the tests. Besides this discrepancy in slip, the large difference in stiffness between the two tests and their predicted results was mainly due to the fact that the threaded rods behaved in double curvature instead of the assumed cantilever. Catenary action is also believed to have increased the post-yield stiffness of the connection. The catenary action developed because the vertical plates representing the panel were clamped to an angle resisting horizontal movement from occurring.

The yield stress of the steel used in the prediction model was 248 MPa (36 ksi). The yield stress of the rods tested was 96% higher than the value used in the model according to the coupon tests. However, due to the large difference between the experimental and analytical results, increasing the yield stress of the rods would not significantly improve the accuracy of the prediction model.

Figure 49 is a comparison of the axial specimens. The predicted results did not account for lower axial strengths due to combined axial and bending load in the rods. Bending of the rods was seen to be directly related to the bending of the plate. Predicted possible failure modes such as fracture of column weld, yielding, and buckling of rods did not occur during the tests.

The stiffness of the model was based on the stiffness of the column plate and the rods combined as shown in Equation 14.

$$k_{\text{model}} = (k_{\text{plate}} k_{\text{rods}}) / (k_{\text{plate}} + k_{\text{rods}}) \quad \text{Equation 14}$$

Figure 49 only shows the prediction curve of the axial specimens until the column plate reaches its yielding stress, thus ending the elastic behavior of the connection. The prediction did not extend beyond the yield point of the column plate because the author was unable to accurately predict the inelastic behavior of the specimens. According to the predicted results, the yield strength of the column plate should occur at 6.65 kN per rod. The predicted displacement at this force is about the same displacement where both specimens began to show yielding. Thus, the model was good in predicting the displacement where yielding occurred, but not the yield strength. The model also predicted the load that will cause the column plate to reach its plastic bending stress, the load to cause fracture of the column weld, and the load to cause the rods to yield.

The nominal yield stress of 248 MPa (36 ksi) was used for the column plates in both of the axial test models, but the actual yield stress obtained from the coupon tests was higher at 366 MPa (53.1 ksi). If this increase in yield stress is considered, the force required to yield the connection would be 9.83 kN per rod, significantly closer to the result of the actual tests.



#### **5.4 Similar Results of All Tests**

Considering the results of all four tests, the coil rods showed very ductile behavior. The rods sustain large displacement with little loss of strength. The rods in PP1 deflected 183 mm laterally and the rods in PP2 had 39.2 mm of displacement, both of which are over 26% of their length. Hence both displacements are fairly large considering the length of the rods. The plates in PP3 and PP4 also showed good ductility, as the plates deflected 179 mm and 107 mm respectively, both of which are over 53% of their plate cantilever length. Based on the force vs. displacement curves of all four tests, it is apparent that all the specimens can resist force far above yield; in fact most of the displacement of each specimen occurred after yield.

Even though PP1 and PP2 had different stiffness, both tests showed no sign of slipping between plate washer and the WT beam. It was originally expected that slipping would occur before any force was resisted. There were also no slips during PP3 and none in PP4 until late in the test. Apparently the small clamping force of the nuts and the eventual binding of components were great enough to prevent relative slip.

For both PP3 and PP4, it was originally suspected that the weld connecting the column testing jig to the column plate would crack leading to complete loss of load-carrying capacity. While the tack welds used for initial alignment on both tests did fracture, the main weld for both tests showed no evidence of cracking.

#### **5.5 Effect of Change of Test Variables**

For the cantilever tests, the only variation was the length of the threaded coil rods. According to the data collected, the shorter rod had higher stiffness and load capacity. This result matches Rihal's conclusion (1989), that the stiffness and

load capacity of the push-pull precast cladding connection are directly related to the threaded rods' length. Table 17 lists the result of the tests performed and comparable results from the literature review. Based on the results of all the similar tests, load capacity decreases as the rod length increases. The same behavior applies to rods under cyclic loading.

For the axial tests, the only variation was the loading direction. PP3 placed the rods in tension, and PP4 compression. Based on Figure 49, the push-pull precast cladding connection had significantly higher strength under tension than compression, but lower ductility. Slip of the bolted assembly, after large displacement, was observed during the compression test. Whether this is truly related to the direction of loading is difficult to establish based on this sole test.

## CHAPTER 6

### Conclusions and Recommendations

#### 6.1 Results of Original Research Objectives

One objective of this investigation of precast cladding connections was to measure force-displacement relationship of the connection under in-plane and out-of-plane movement. There were four tests performed and all four tests had their force-displacement relationship recorded (Figures 31, 37, 41, and 43). These relationships were far from linear, particularly after deflections of approximately 25 mm. Due to difficulty with some instrumentation, displacements of individual components were not fully recorded. However, the overall displacement of the connection was recorded for all the tests. It is expected that Kwong's analysis (2002) will be updated with the results from this study to improve the accuracy of her model. This improvement should result from incorporating the values of strength and stiffness of the push-pull precast cladding connection into the pushover analysis of Kwong's model.

Another objective was to develop a model to predict the behavior of the connection under bending, tension, and compression forces. There were two models developed, one for the cantilever test and another for the axial tests. The assumed model for axial loading considered that the connection behaves in a similar manner under both tension and compression forces.

Evaluating the accuracy of the prediction model was a third objective. The cantilever model was judged inappropriate for estimation. The test specimens had much higher strength than predicted and the expected slip between the plate washers and the WT beam never occurred. However, if the assumed slip was eliminated from the prediction model, the predicted initial stiffness was fairly close

to the actual initial stiffness. The axial model for the tension and compression tests was also less than acceptable. This model was only accurate in predicting the yield displacement, but not the yield strength.

## 6.2 Conclusions

1. The force-deflection relationship obtained defines the elastic and inelastic behavior of the connection. When loaded in flexure, it was found that slip between plate washers and the WT beam never occurred contrary to the original assumption that slip would occur at the beginning of the tests.
2. Rods in push-pull connections resisted significant load during in-plane movement of the panel. PP1 and PP2 resisted maximum load of 9.85 kN and 28.3 kN per rod respectively.
3. The models for PP1 and PP2 were developed as a cantilever system. By comparing the model to the experimental results, the accuracy of the predictive model was poor. The predicted maximum load of PP1 and PP2 were only 10.6% and 11.1% of the actual maximum load recorded during the tests. The accuracy of the model may be improved by changing the cantilever system to a fixed-fixed connection and including second order effects for catenary action.
4. Inelastic bending of the column plate dominated the behavior of the connection under either tension or compression. The column plate of the connection showed high inelastic ductility after yield. There were no fractures of the plate or the weld connecting the column testing jig to the column plate.
5. The fixity of the coil nuts and plate washers transferred significant bending moment to the rods. The bending in the rods was not considered when the predictive models were developed. The tension test ended with one of the rods fractured due to a combination of bending and axial

loading. The fracture of the rods appears to be the final failure for the axial test.

6. The model for axial loading was fairly accurate in predicting the yield displacement of 26.6 mm but was not accurate in predicting yield strength.
7. Of the four methods proposed for yielding of the connection, a 10% drop in secant stiffness consistently identified the highest displacement.

However, it would seem that a larger drop may have been more accurate in defining this point.

### **6.3 Recommendations for Engineering Practice**

1. Tack welding of plate washers during assembly does not appear necessary to eliminate slip as slip appears unlikely to occur during loading.
2. Although push-pull rods are not intended to resist lateral forces on panels via shear, their bending stiffness is significant, particularly if they are short. Concern about fracture of rods due to bending would not seem justified until deflections exceed 25% of their length.

### **6.4 Recommendations for Continuation of Research**

After observing and analyzing the behavior of the push-pull precast cladding connection during the testing, the following recommendations for future research were suggested:

1. The testing arrangement of PP1 and PP2 had the four threaded rods connected to vertical plates that represented the panel. The plates were rigidly attached to the test frame, which did not allow simulation of out-of-plane panel movement. The restraint of movement resulted in catenary action in the threaded rods. Actual cladding connections are not expected to develop catenary action, because the panels would usually

have limited resistance to out-of-plane movement. Thus, future cantilever tests should replicate the ability of the panel embed to move.

2. Based on the data collected for PP1 and PP2, the threaded rods actually have more deflection than the WT beam. It is not physically possible for the threaded rods to have more deflection than the WT beam. This error was caused by error in measuring the deflection at the tip of the threaded rods. Because of bending of the rods, the rods have more displacement at the tip than where they pass through the WT beam. Therefore, a recommendation for future testing is to measure the deflection of the threaded rods closer to the WT beam.
3. The design of PP3 and PP4 was symmetric, and all four threaded rods were connected to a W16x40 that represented the panel. However, in an actual cladding system the four threaded rods would be connected to four different panels. The possibility of relative movement of those panels was not included in these tests. As a result, post-yield stability of the compression loaded rods may have been inaccurately provided. To have a closer resemblance of the actual connection, testing of PP3 and PP4 should continue, but with allowance for the panel ends to move relative to each other.
4. A more definite method of identifying the yield displacement from prototype testing needs to be defined. Assemblies of multiple steel elements do not show clearly defined yield points, and yet such values are particularly necessary in quantifying ductility or conducting analytical bilinear modeling. A drop in secant stiffness was seen to accurately identify the yield displacement in these tests but more extensive research appears warranted.

## References

American Institute of Steel Construction (1994). *Manual of Steel Design-LRFD*, Vol. I, Chicago.

American Institute of Steel Construction (1994). *Manual of Steel Design-LRFD*, Vol. II, Chicago.

Choi, C., McMullin, K.M. (2003). "Experimental Testing of a Lateral Seismic Connection for Precast Concrete Cladding Panel." *Report No. 2003-04*, Department of Civil and Environmental Engineering, San Jose State University, San Jose, California.

Cohen, J.M. (1995). "Seismic Performance of Cladding Responsibility Revisited," *Journal of Performance of Constructed Facilities*, ASCE, 9(4), 254-270.

Craig, J.I., Goodno, B.J., and Fennell, C.J. (1986). "Hysteretic Behavior of Precast Cladding Connections," *Dynamic Response of Structures*, ASCE, New York, 1986, 817-826.

Craig, J.I., Goodno, B.J., Wolz, M.W., and Pinelli, J.P. (1991). "Analytical and Experimental Evaluation of Advanced Cladding Systems for Building," *Proceedings of the Second Conference on Tall Buildings in Seismic Regions*, Los Angeles, California, 99-108.

Craig, J.I., Leistikow, R., and Fennell, C.J. (1988). "Experimental Studies of the Performance of Precast Cladding Connections," *Proceeding of Ninth World Conference on Earthquake Engineering*, Tokyo-Kyoto, Japan, (Vol. VI), 201-206.

Drake, R.M., Bachman, R.E. (1996). "NEHRP Provisions for 1994 for Nonstructural Components." *Journal of Architectural Engineering*, ASCE, 2(1), 26-31.

El-Gazairly, L.F., Goodno, B.J., and Craig, J.I. (1990). "Analytical Investigation of Advanced Connections for Precast Cladding on Buildings," *Proceedings of Fourth U.S. National Conference on Earthquake Engineering*, Palm Springs, California, (Volume 2), 441-450.

Federal Emergency Management Agency (1997). *NEHRP Guidelines for the Seismic Rehabilitation of Buildings*, (FEMA Publication 273), Washington DC.

Goodno, B.J., Craig, J.I., and Hsu, C.C. (1991). "Experimental Studies and Analytical Evaluation of Ductile Cladding Connections," *Pacific Conference on Earthquake Engineering*, New Zealand, 43-54.

Goodno, B.J., Meyyappa, M., and Nagarajaiah, S. (1988). "A Refined Model for Precast Cladding and Connections," *Proceedings of Ninth World Conference on Earthquake Engineering*, Tokyo-Kyoto, Japan, (Vol. VI), 195-200.

International Conference of Building Officials (1997). *Uniform Building Code*. Whittier, California.

Kwong, A. and McMullin, K.M. (2003). "Pushover Analysis and Vibration Characteristics of Precast Cladding Panels." *Report No. 2003-07*, Department of Civil and Environmental Engineering, San Jose State University, San Jose, California.

McMullin, K.M., Chan, K., Choi, C., Kwong, A. (2003). "Performance Engineering of Precast Cladding System." *2003 Structures Conventions*, ASCE, Seattle Washington, May 29-June 1.

PCI (1999). *PCI Design Handbook Precast and Prestressed Concrete*, 5<sup>th</sup> Edition. PCI, Chicago, Illinois, 1-17-18, 6-37-40.

Pietroforte, R. (1995). "Cladding Systems: Technological Change and Design Arrangements," *Journal of Architectural Engineering*, ASCE, 1(3), 100-107.

Pinelli, J.P., Craig, J.I., and Goodno, B.J. (1990). "Development and Experimental Calibration of Selected Dynamic Models for Precast Cladding Connections," *Proceedings of Fourth U.S. National Conference on Earthquake Engineering*, Palm Springs, California, (Volume 2), 147-156.

Rihal, S.S. (1989). "Earthquake Resistance and Behavior of Architectural Precast Cladding and Connections," *Precast Concrete Institute Handbook*, PCI, 1989, 110-140.

Sack, R.L., Beers, R.J., and Thomas, D.L. (1989). "Seismic Behavior of Architectural Precast Concrete Cladding," *Precast Concrete Institute Handbook*, PCI, 1989, 141-158.

Salmon, G.C. and Johnson, J.E. (1996). *Steel Structures: Design and Behavior*, 4<sup>th</sup> Edition. Harper Collins, New York.



Weston, N.R., Craig, J.I., and Goodno, B.J. (2002). "Passive Control of Seismic Response Using Ductile Cladding Panels," Georgia Institute of Technology, Atlanta, Georgia.

**Appendix A**  
**Notation**

## Notation

AISC	American Institute of Steel Construction
$a_p$	Component amplification factor, varies from 1.00 to 1.50
$C_a$	Seismic coefficient listed in Table 16-Q in UBC
CL	Center line
$d_{rms}$	Diameter of the threaded section of the rod.
F	Force
FEMA	Federal Emergency Management Agency
$F_p$	Lateral seismic design force
$F_y$	Yield stress of the material
$h_r$	Structure roof elevation with respect to grade
$h_x$	Elemental or component attachment elevation with respect to grade
$I_p$	Component importance factor, varies from 1.00 to 1.50
k	Stiffness
$k_{si}$	Secant stiffness
$k_{ti}$	Tangent stiffness
L	Length
$M_y$	Yield bending moment
$M_p$	Plastic bending moment
NEHRP	National Earthquake Hazards Reduction Program
PCI	Precast Concrete Institute
PP	Push-pull precast cladding connection
$P_p$	Load to create plastic hinge in specimen
$P_y$	Load to cause yield in specimen
$S_x$	Sectional modulus of the specimen
UBC	Uniform Building Code
$W_p$	Component operating weight
$Z_x$	Plastic modulus of the specimen
$\Delta$	Displacement
$\Delta M$	Maximum inelastic response deformation

**Appendix B**  
**Glossary**

## **Glossary**

Axial arrangement	Describing the non-essential parts to the experiment such as the column testing jig, the W16x40, plate washers and coil nuts. Purpose of these parts was to support the testing specimens.
Cantilever arrangement	Describing the non-essential parts to the experiment such as the vertical plate, reaction beam, the WT beam, angles, clamps, plate washers, and coil nuts. Purpose of these parts was to support the testing specimens.
Column plate	A 900 mm x 400 mm x 130 mm (36"x16"x1/2") rectangular plate that connected the rods and is welded to the structural column of the building.
Column testing jig	A U shape test fixture that represented the structural column of W12x120 of a building. This jig is welded to the column plate.
Column weld	Weld connecting the column plate to the column testing jig representing a W12x120 structural column.
In-plane movement	Movement of the panel that is parallel to the outer surface of the panel. This movement caused bending in the rods.
Intended loading	Axial loading (tension and compression) of the push-pull precast cladding connection. The push-pull connection was designed to resist axial load.

Testing Specimen	Describing the components of the push-pull precast cladding connection that was tested in this study. The components included the 25 mm diameter coil rods and 900 mm x 400 mm x 130 mm rectangular plate.
Out-of-plane movement	Movement of the panel that is perpendicular to the surface of the panel. This movement creates axial load in the rods.
Unintended loading	Bending and shear loading of the push-pull precast cladding connection. The push-pull connection was not originally designed to resist bending and shear loads.
Vertical plate	The steel plate that represented the panel hardware of the connection in PP1 and PP2. See Figure 15.

**Appendix C**  
**Tables**

**Table 1** – Properties and Results of Threaded Rod Connection from Rihal (From m Rihal, 1989)

Specimen No.	Threaded Rod	Max. Test Load (kN)	Max. Rod Deflection (mm)	Max. bending Stress in Rod @
	Length (mm)			Max. Load Based on Analytical Model (MPa)
CST-L4	102	2.1	16.3	531
CST-L4A	102	1.8	19.8	531
CST-L6	152	1.3	22.1	503
CST-L6A	152	1.3	20.1	503
CST-L8	203	0.8	34.0	503
CST-L8A	203	0.8	25.4	503
CST-L10	254	0.6	21.8	448
CST-L10A	254	0.6	24.1	448
CST-L12	305	0.5	28.2	448
CST-L12A	305	0.5	26.9	448

Note: All tests use 16-mm diameter threaded rods.

**Table 2** – Goodno's Results of Response Model: Clip Angle vs. Ductile Rod Cladding Panel Connections (From Goodno et al. 1988)

Response Quantity	Connection Type	Connection Type
	Clip Angle	Push-Pull
INPUT VALUES		
Connection Stiffness (kN/mm)		
Top Connection	65.56	65.56
Bottom Connection	65.56	0.081
Interstory Shear Stiffness V (kN/mm)	2.26	2.26
OUTPUT VALUES		
Connector Forces (kN)		
Top, horizontal	42.43	1.44
Top, vertical	164.71	9.10
Bottom, horizontal	42.24	1.41
Bottom, vertical	130.55	0.01



**Table 3 – Seismic Rehabilitation Guidelines for Nonstructural Performance Levels and Damage (from FEMA 273)**

Performance Level	Damage Threshold
Hazards Reduced Level (N-D)	Severe damage to connections and cladding. Many panels loosened.
Life Safety (N-C)	Severe distortion in connections. Distributed cracking, bending, crushing, and spalling of cladding elements. Some fracturing of cladding, but panels do not fall.
Immediate Occupancy (N-B)	Connections yield; minor cracks (<1/16" width) or bending in cladding.
Operational (N-A)	Connections yield; minor cracks (<1/16" width) or bending in cladding.

**Table 4** – Summary of Similar Past Investigations of Push-Pull Precast Cladding Connection

Research Study	Specimen #	Rod Length (mm)	Rod Diameter (mm)	Loading Protocol
Rihal, 1989	CST-L4	102	16	Monotonic
Rihal, 1989	CST-L4A	102	16	Monotonic
Rihal, 1989	CST-L6	152	16	Monotonic
Rihal, 1989	CST-L6A	152	16	Monotonic
Rihal, 1989	CST-L8	203	16	Monotonic
Rihal, 1989	CST-L8A	203	16	Monotonic
Rihal, 1989	CST-L10	254	16	Monotonic
Rihal, 1989	CST-L10A	254	16	Monotonic
Rihal, 1989	CST-L12	305	16	Monotonic
Rihal, 1989	CST-L12A	305	16	Monotonic
Craig et al. 1988	n/r	305	19	Cyclic
Craig et al. 1988	n/r	279	19	Cyclic
Craig et al. 1988	n/r	229	19	Cyclic
Craig et al. 1988	n/r	203	19	Cyclic
Sack et al. 1989	n/r	229	n/r	Monotonic
Sack et al. 1989	n/r	178	n/r	Monotonic
Sack et al. 1989	n/r	127	n/r	Monotonic
Sack et al. 1989	n/r	76	n/r	Monotonic

**Table 5** - Test Matrix

Test Specimen	Rod Diameter (mm)	Rod Length (mm)	Test Configuration	Plate Washer Attachment	Loading Direction	Panel Movement
PP1	25	460	Symmetric	Not welded	Bending	In-plane
PP2	25	150	Symmetric	Not welded	Bending	In-plane
PP3	25	460	Symmetric	Not welded	Tension	Out-of-plane
PP4	25	460	Symmetric	Not welded	Compression	Out-of-plane

**Table 6** – Properties of Test Specimens

	Test Specimens	Rod Length (mm)	Rod Diameter (mm)
Cantilever Test	Test One (PP2)	150	25
	Test Two	150	19
	Test Three (PP1)	460	25
	Test Four	460	19
Compression Strength Test	Test Five	150	25
	Test Six	150	19
	Test Seven (PP4)	460	25
	Test Eight	460	19
Tension Strength Test	Test Nine	150	25
	Test Ten	150	19
	Test Eleven (PP3)	460	25
	Test Twelve	460	19

**Table 7** – Table of Instrumentation for Cantilever Tests (PP1 and PP2)

Channel	Location	Measuring	Instruments	Serial Number	Calibration Factor
-	-	Load	Riehle Testing Machine	R-84937	-
1	Left side of WT	Displacement	Wire Potentiometer	B1051980	3.2372
6	Rod C	Displacement	Wire Potentiometer	C1054470	0.7746
7	Right side of WT	Displacement	Wire Potentiometer	B1051980	3.2336
8	Rod B	Displacement	Wire Potentiometer	C1054469	3.5487
9	Rod A	Displacement	Wire Potentiometer	A24885	8.1695
-	Rod D	Displacement	Dial Gage	-	-

**Table 8** – Table of Instrumentation for Tension and compression Tests (PP3 and PP4)

Channel	Location	Measuring	Instruments	Serial Number	Calibration Factor
1	-	Load	200-Kip Load Cell	46296	-0.00001201
2	Top of Rod D Head of Testing	Displacement Overall	Wire Potentiometer	B1052679	1.3406
3	Machine	displacement	Wire Potentiometer	C1054469	1.3332
4	Bottom of Rod D	Displacement	Wire Potentiometer	B1051980	1.3414
5	Bottom of Rod C	Displacement	Wire Potentiometer	C1054518	2.6752
6	Top of Rod C	Displacement	Wire Potentiometer	C1054470	1.3259

**Table 9** – Predicted Failure Mode Sequence of Cantilever Test

	Failure Modes	Failure Loads (kN)	Lower Bound (kN)	Upper Bound (kN)
Test 1 (PP2)	Bolt Slip	0.0	0.0	0.0
	Rod Yielding	7.5	6.7	8.2
	Rod Plastification	12.5	11.3	13.8
	Rod Shear	239.5	215.5	263.4
	Web Bearing	533.4	400.0	666.7
Test 2	Bolt Slip	0.0	0.0	0.0
	Rod Yielding	2.7	2.5	3.0
	Rod Plastification	4.7	4.2	5.1
	Rod Shear	123.8	111.4	136.2
	Web Bearing	383.7	287.8	479.6
Test 3 (PP1)	Bolt Slip	0.0	0.0	0.0
	Rod Yielding	2.5	2.2	2.7
	Rod Plastification	4.2	3.8	4.6
	Rod Shear	239.5	215.5	263.4
	Web Bearing	533.4	400.0	666.7
Test 4	Bolt Slip	0.0	0.0	0.0
	Rod Yielding	0.9	0.8	1.0
	Rod Plastification	1.6	1.4	1.7
	Rod Shear	123.8	111.4	136.2
	Web Bearing	383.7	287.8	479.6

Note: Only Test 1 and 3 were performed. The value of load is calculated for the entire specimen containing four threaded rods.

**Table 10 – Predicted Failure Mode Sequence of Compression Test**

	Failure Modes	Failure Loads (kN)	Lower Bound (kN)	Upper Bound (kN)
Test 5	Plate Yielding	26.6	23.9	29.3
	Plate Plastification	39.9	35.9	43.9
	Rod Yielding	398.2	338.5	458.0
	Fracture of Weld on Nut	439.9	395.9	483.9
	Rod Buckling	8901.1	7565.9	10236.3
Test 6	Plate Yielding	26.6	23.9	29.3
	Plate Plastification	39.9	35.9	43.9
	Rod Yielding	206.1	175.2	237.0
	Fracture of Weld on Nut	439.9	395.9	483.9
	Rod Buckling	2384.0	2026.4	2741.6
Test 7 (PP4)	Plate Yielding	26.6	23.9	29.3
	Plate Plastification	39.9	35.9	43.9
	Rod Yielding	398.2	338.5	458.0
	Fracture of Weld on Nut	439.9	395.9	483.9
	Rod Buckling	989.8	841.3	1138.3
Test 8	Plate Yielding	26.6	23.9	29.3
	Plate Plastification	39.9	35.9	43.9
	Rod Yielding	206.1	175.2	237.0
	Rod Buckling	264.8	225.1	304.6
	Fracture of Weld on Nut	439.9	395.9	483.9

Note: Only Test 7 was performed. The value of load is which the load applied by the testing machine. Each test has four threaded rods.

**Table 11** – Predicted Failure Mode Sequence of Tension Test

	Failure Modes	Failure Loads (kN)	Lower Bound (kN)	Upper Bound (kN)
Test 9	Plate Yielding	26.6	23.9	29.3
	Plate Plastification	39.9	35.9	43.9
	Fracture of Weld on Column Plate	353.0	317.7	388.3
	Rod Yielding	398.2	358.4	438.0
Test 10	Plate Yielding	26.6	23.9	29.3
	Plate Plastification	39.9	35.9	43.9
	Rod Yielding	206.1	185.5	226.7
	Fracture of Weld on Column Plate	353.0	317.7	388.3
Test 11 (PP3)	Plate Yielding	26.6	23.9	29.3
	Plate Plastification	39.9	35.9	43.9
	Fracture of Weld on Column Plate	353.0	317.7	388.3
	Rod Yielding	398.2	358.4	438.0
Test 12	Plate Yielding	26.6	23.9	29.3
	Plate Plastification	39.9	35.9	43.9
	Rod Yielding	206.1	185.5	226.7
	Fracture of Weld on Column Plate	353.0	317.7	388.3

Note: Only Test 11 was performed. The value of load is which the load applied by the testing machine. Each test has four threaded rods.

**Table 12** – Predicted Value of Bending Forces and Corresponding Deflection for the Cantilever Test

Stages of Test		Force (kN)	Total deflection (mm)
PP1	Beginning of Test	0.00	0.00
	Slip of Plate Washers Against WT	0.00	25.40
	Yielding of Rod due to Bending	2.46	33.05
	Plastic Hinge of Rod due to Bending	4.19	38.41
PP2	Beginning of Test	0.00	0.00
	Slip of Plate Washers Against WT	0.00	25.40
	Yielding of Rod due to Bending	7.39	26.25
	Plastic Hinge of Rod due to Bending	12.56	26.85

**Table 13** - Experimental Results

Test No.	Date	Maximum Load (kN)	Displacement at Max Load (mm)	Total Energy Dissipated (kN-mm)
PP1	10/31/2002	39.4	182.7	1738.8
PP2	10/31/2002	113.1	39.2	2684.3
PP3	12/4/2002	245.8	145.6	20179.5
PP4	12/12/2002	94.1	138.3	19279.9

**Table 14** - Yield Displacement Results from the Proposed Four Methods

	Specimen PP1 (mm)	Specimen PP2 (mm)	Specimen PP3 (mm)	Specimen PP4 (mm)
Yield Displacement	26.0	16.7	16.3	16.6
Method 1	20.8	13.9	14.1	13.5
Method 2	26.0	16.7	16.3	16.6
Method 3	12.0	7.1	3.2	4.4
Method 4	13.8	9.8	4.4	6.3



**Table 15** - Stiffness Properties of Each Individual Rod of the Tests

Test No.	Secant Stiffness at Maximum Load (kN/mm)	Maximum Secant Stiffness (kN/mm)	Average Tangent Stiffness after Yield (kN/mm)
PP1	0.054	0.141	0.046
PP2	0.721	1.421	0.230
PP3	0.422	0.960	0.403
PP4	0.170	0.762	0.022

**Table 16** - Displacement of Damage Thresholds for Performance Limits

Performance Limit	FEMA - 273 Performance State	Specimen PP1 (mm)	Specimen PP2 (mm)	Specimen PP3 (mm)	Specimen PP4 (mm)
1	2	3	4	5	6
Permanent Deformation	Immediate Occupancy	26.0	16.7	16.3	16.6
<i>Method 1</i>		20.8	13.9	14.1	13.5
<i>Method 2</i>		26.0	16.7	16.3	16.6
<i>Method 3</i>		12.0	7.1	3.2	4.4
<i>Method 4</i>		13.8	9.8	4.4	6.3
Strength Degradation	Life Safety	182.7	39.2	145.6	138.3
Strength Degradation of 75%	Hazards Reduced	n/a	n/a	145.6	n/a
Initial Cracking of Metal or Weld	Life Safety	n/r	n/r	n/r	n/r
Complete Fracture of Component	Not Defined	n/a	n/a	n/a	n/a

n/r = threshold was reached but displacement not recorded.

n/a = threshold was not reached.

**Table 17 - Summary of Cantilever Test Results from Various Researchers**

Researchers	Rod Diameter (mm)	Rod Length (mm)	Test Configuration	Loading Protocol	Maximum Load (kN)	Maximum Deflection (mm)
Chan and McMullin	25	460	Symmetric	Monotonic	9.8	183.8
Chan and McMullin	25	150	Symmetric	Monotonic	28.3	39.4
Rihal	16	102	Non-symmetric	Monotonic	2.1	16.3
Rihal	16	102	Non-symmetric	Monotonic	1.8	19.8
Rihal	16	152	Non-symmetric	Monotonic	1.3	22.1
Rihal	16	152	Non-symmetric	Monotonic	1.3	20.1
Rihal	16	203	Non-symmetric	Monotonic	0.8	34.0
Rihal	16	203	Non-symmetric	Monotonic	0.8	25.4
Rihal	16	254	Non-symmetric	Monotonic	0.6	21.8
Rihal	16	254	Non-symmetric	Monotonic	0.6	24.1
Rihal	16	305	Non-symmetric	Monotonic	0.5	28.2
Rihal	16	305	Non-symmetric	Monotonic	0.5	26.9
Craig et al.	19	305	Non-symmetric	Cyclic	0.8	13.0
Craig et al.	19	279	Non-symmetric	Cyclic	0.9	10.2
Craig et al.	19	229	Non-symmetric	Cyclic	0.9	5.1
Craig et al.	19	203	Non-symmetric	Cyclic	1.0	5.1
Sack et al.	n/r	229	Non-symmetric	Monotonic	n/a	n/a
Sack et al.	n/r	178	Non-symmetric	Monotonic	n/a	n/a
Sack et al.	n/r	127	Non-symmetric	Monotonic	n/a	n/a
Sack et al.	n/r	76	Non-symmetric	Monotonic	n/a	n/a

- Note:
1. All values are based on one rod.
  2. The data from Craig's tests were obtained from the chart given in his report, by approximating the data point on the chart as shown in Figure 7. The actual values were not reported in his paper.
  3. Sack's data were not reported in his paper.

**Appendix D**  
**Figures**

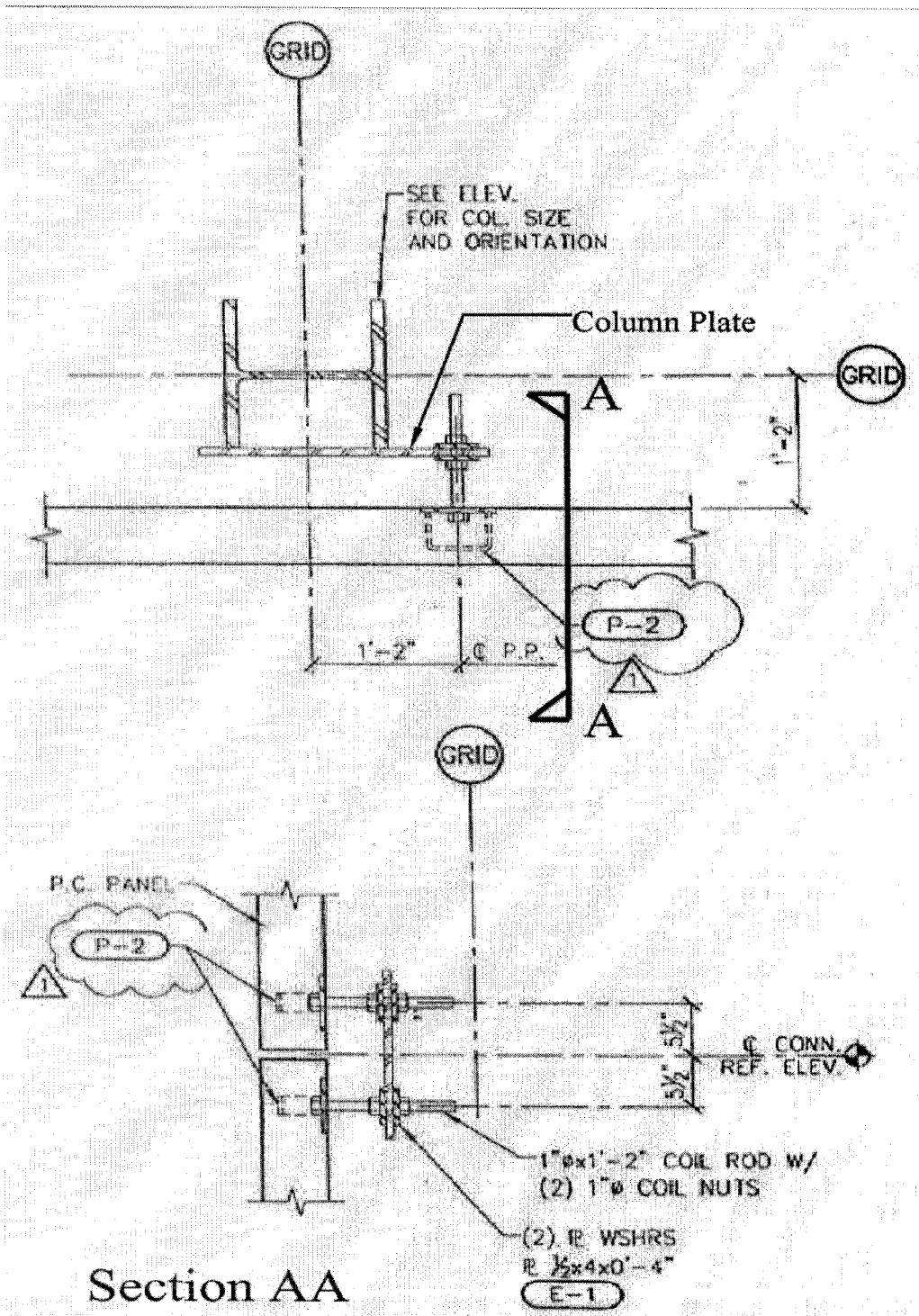


**Figure 1 – Typical Push-Pull Precast Cladding Connection (from Willis Construction)**

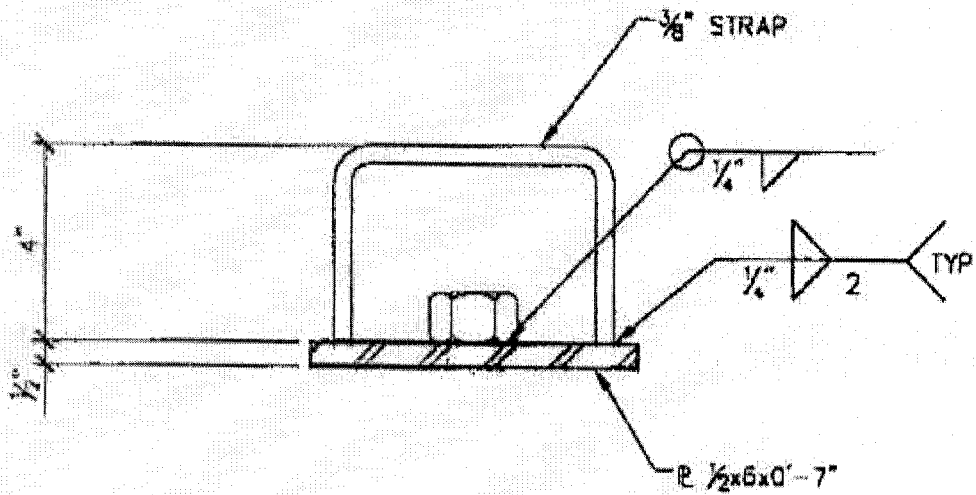
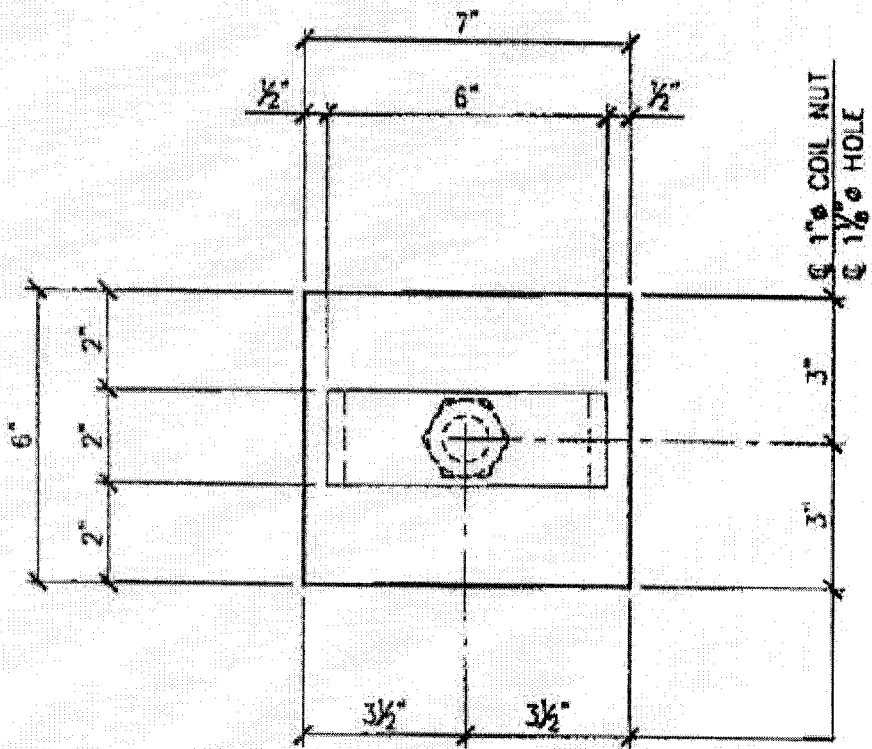


**Figure 2** – Typical Panel Embed Hardware (from Willis Construction)

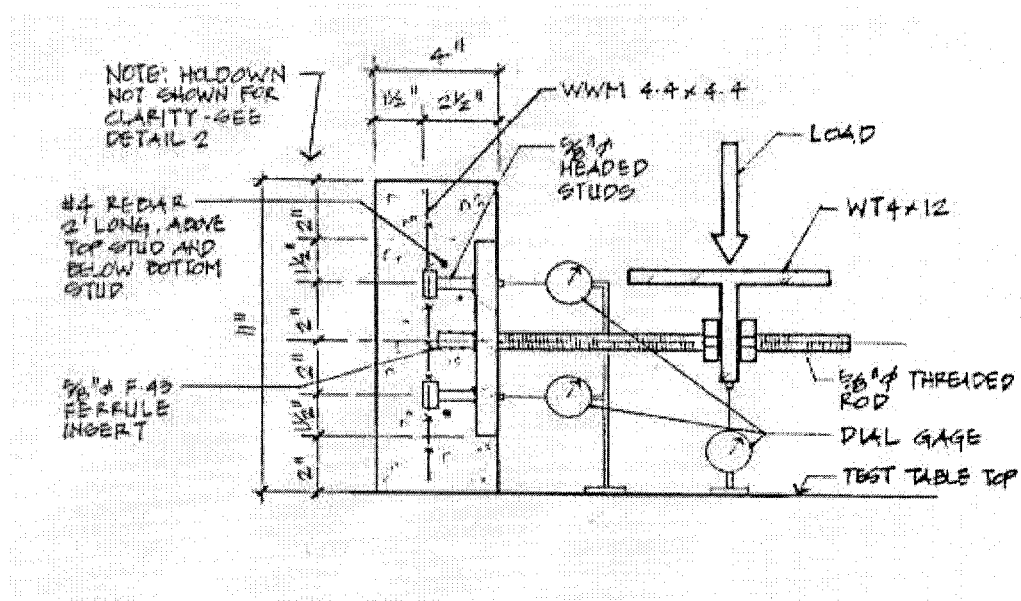


Figure 3 – Rihal’s Threaded Rod Connection Test (from Rihal, 1989)

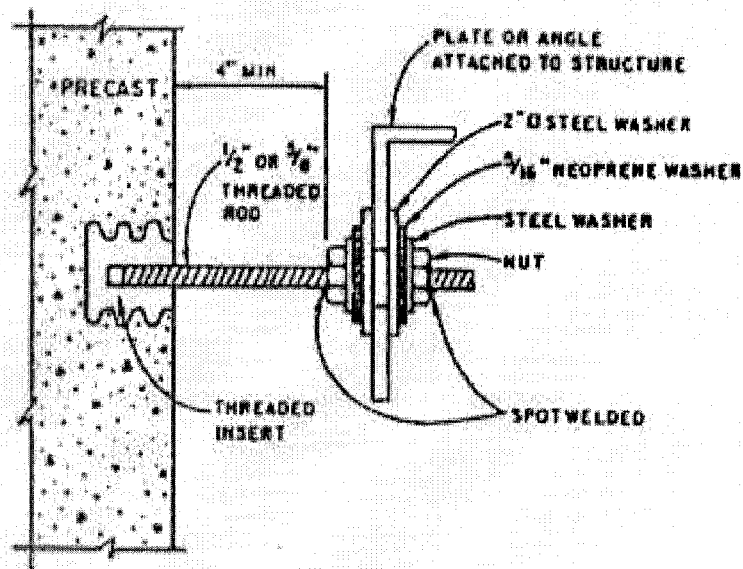
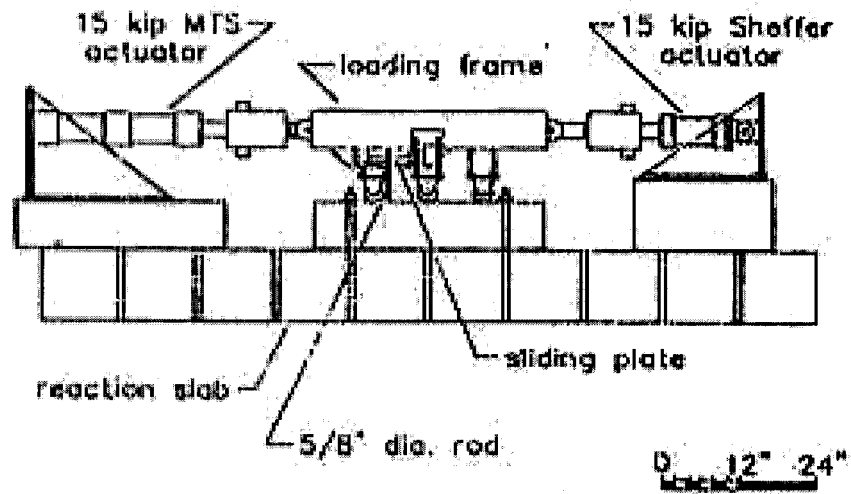
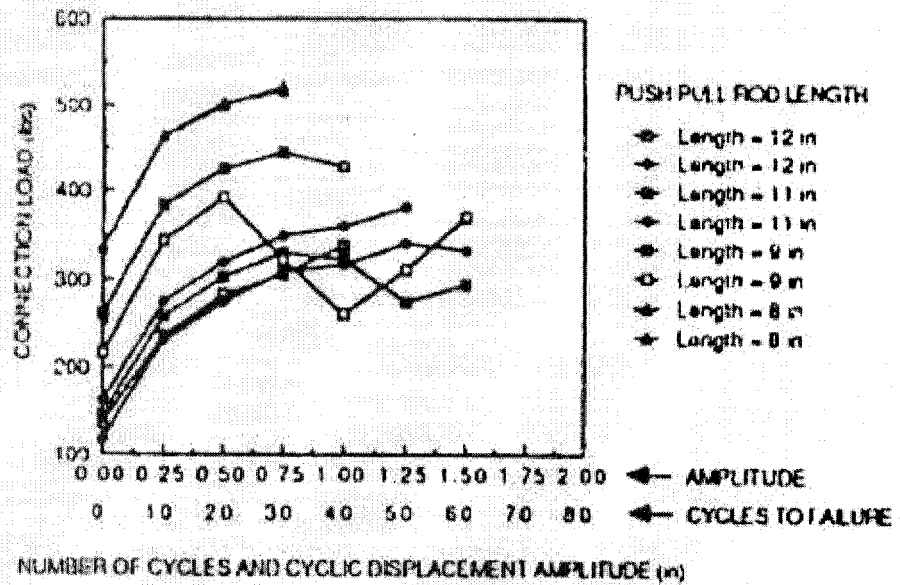


Figure 4 – Craig’s Typical Push-Pull Connection (from Craig et al. 1988)



**Figure 5** – Craig’s Push-Pull Connection Test Fixture (from Craig et al. 1988)



**Figure 6** – Craig’s Push-Pull Cyclic Performance to Failure (from Craig et al. 1988)

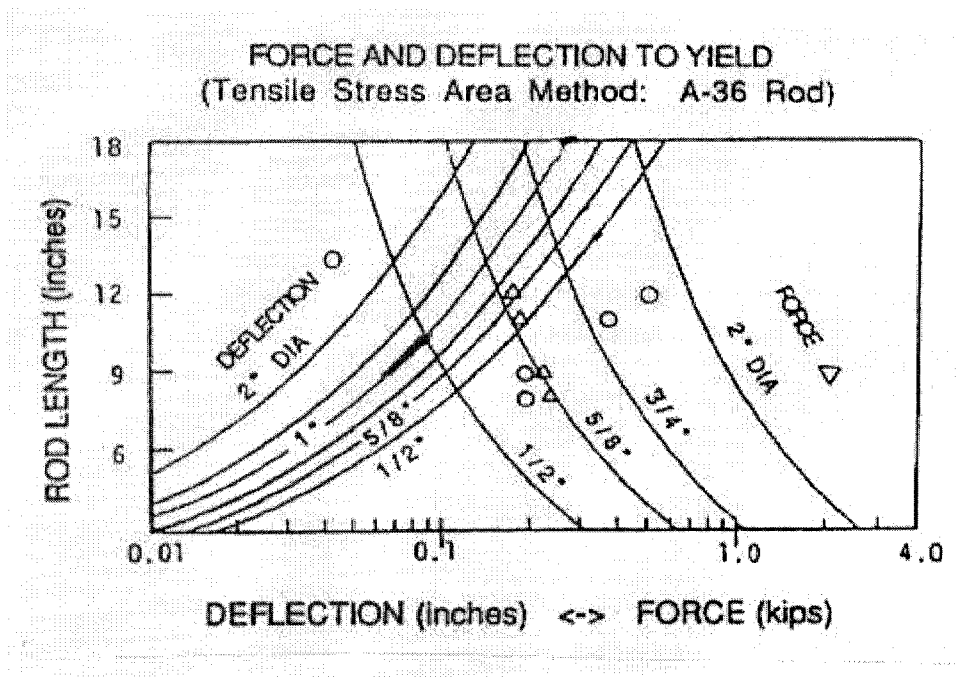


**Figure 7** – Craig’s Push-Pull Comparison with Design Chart (from Craig et al. 1988)

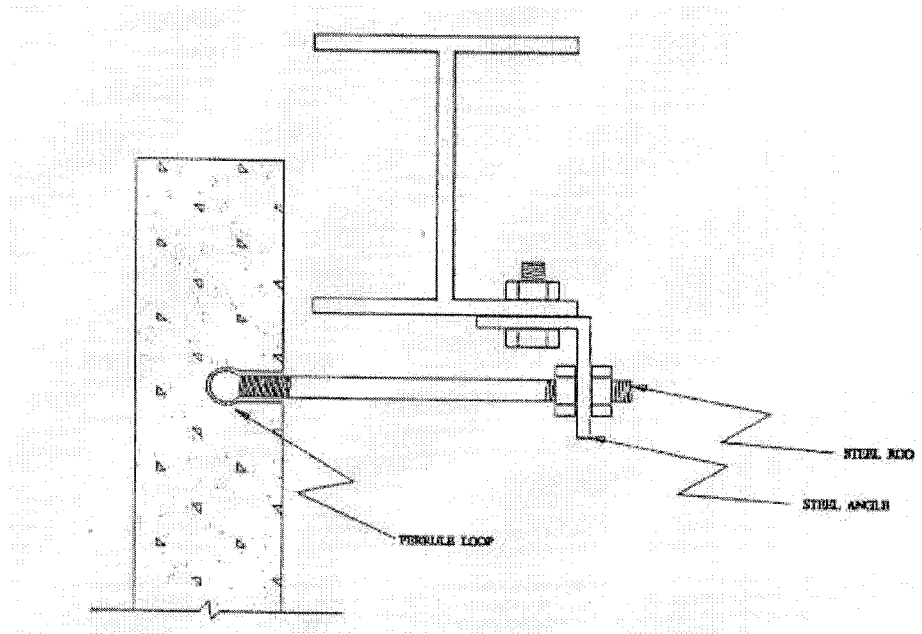


**Figure 8** – Sack’s Flexible Panel Frame Connection (from Sack et al. 1989)



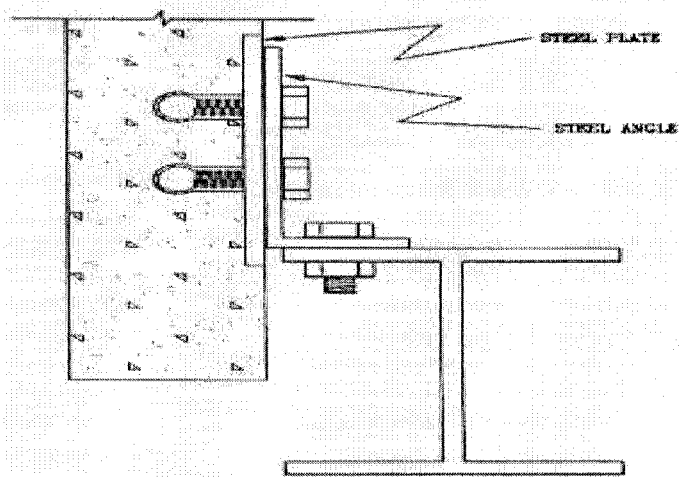


**Figure 9** – Sack’s Bearing Panel Frame Connection (from Sack et al. 1989)

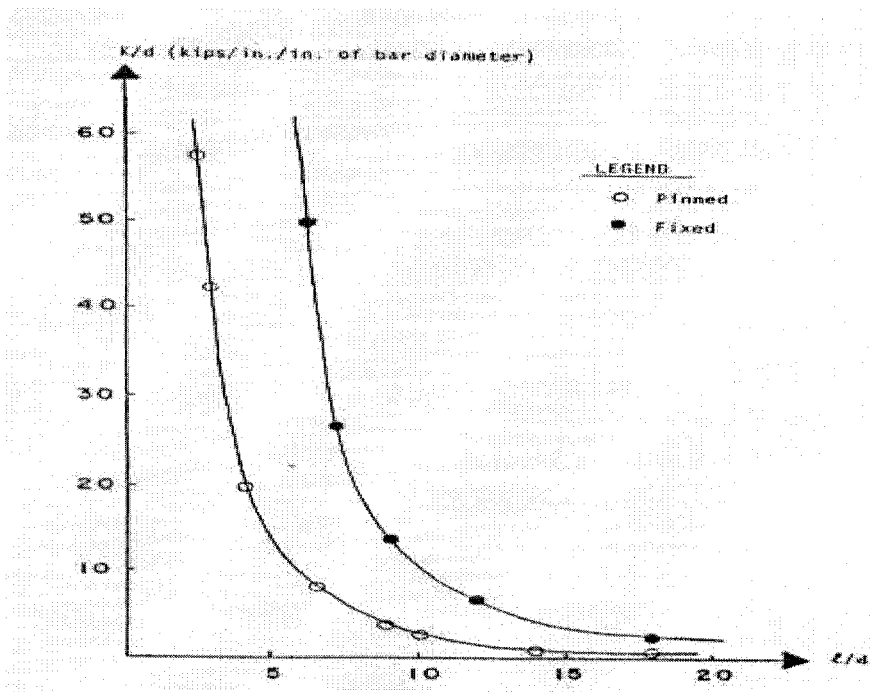
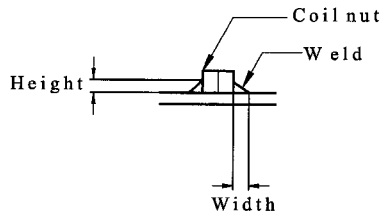
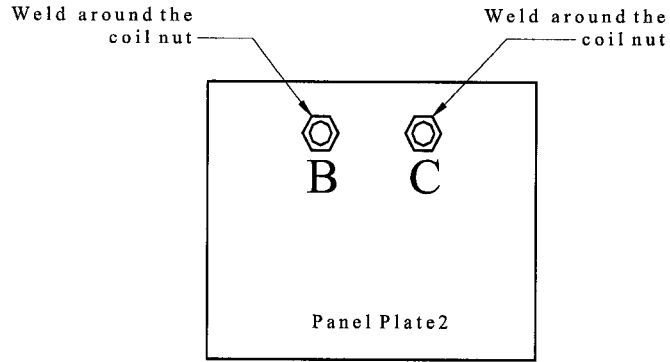
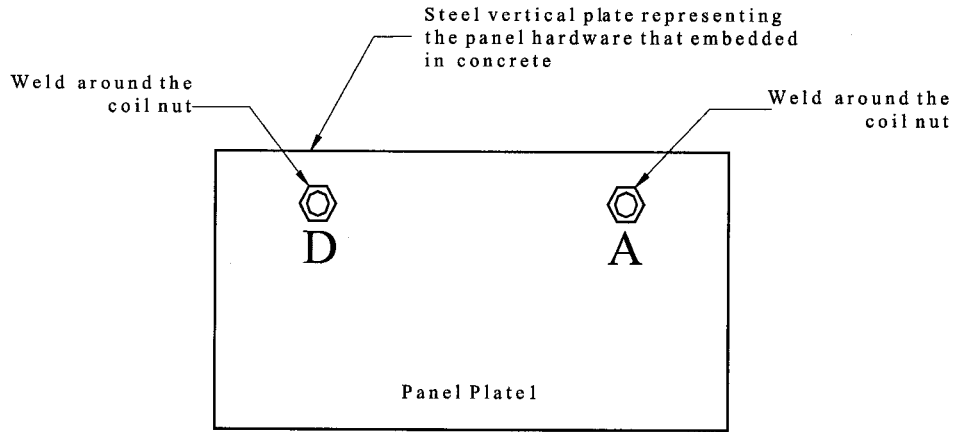
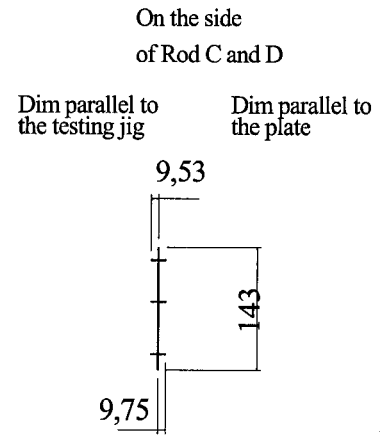
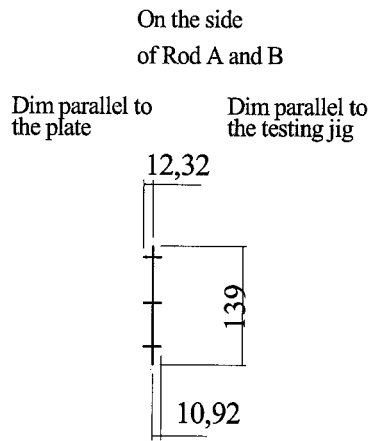
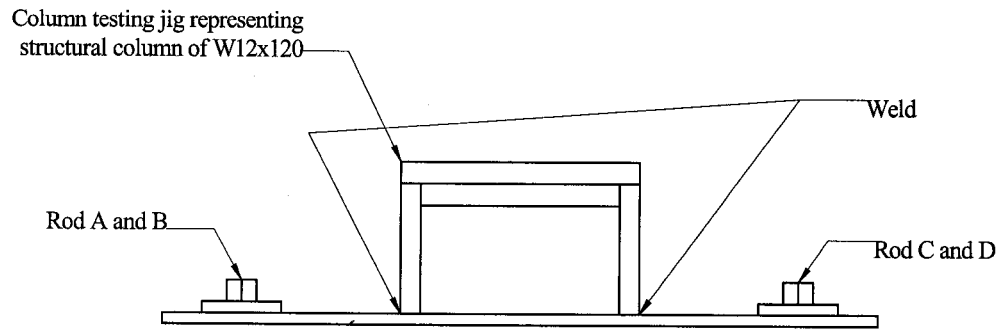


**Figure 10** – Sack’s Fixed and Pinned End Elastic Stiffness Coefficients vs. Ratio of Rod Length and Diameter for Flexible Panel Frame Connection (from Sack et al. 1989)

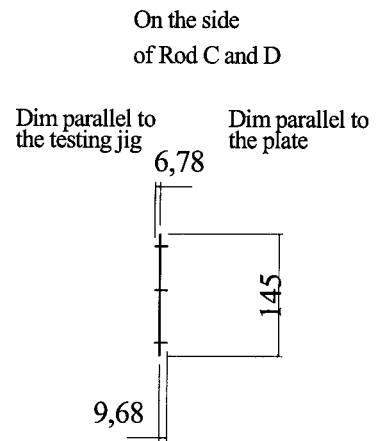
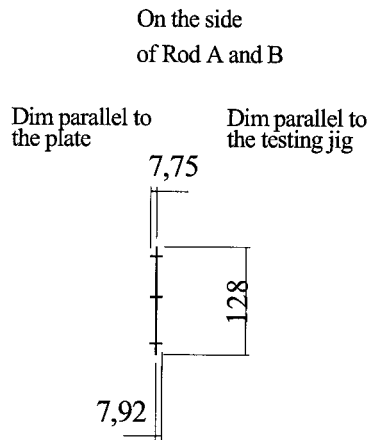


	Rod A	Rod B	Rod C	Rod D
Height (mm)	6.6	5.6	6.0	5.7
Width (mm)	8.7	9.7	8.6	6.9

**Figure 11 – Fillet Weld Size on the Nuts of Cantilever Tests**

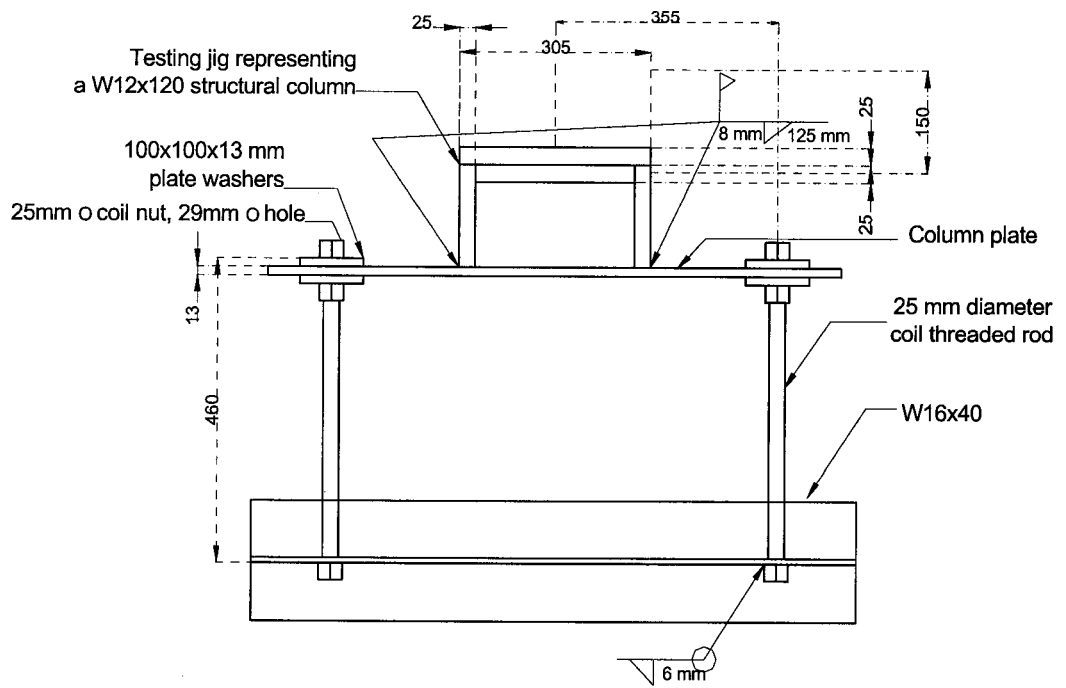


PP3

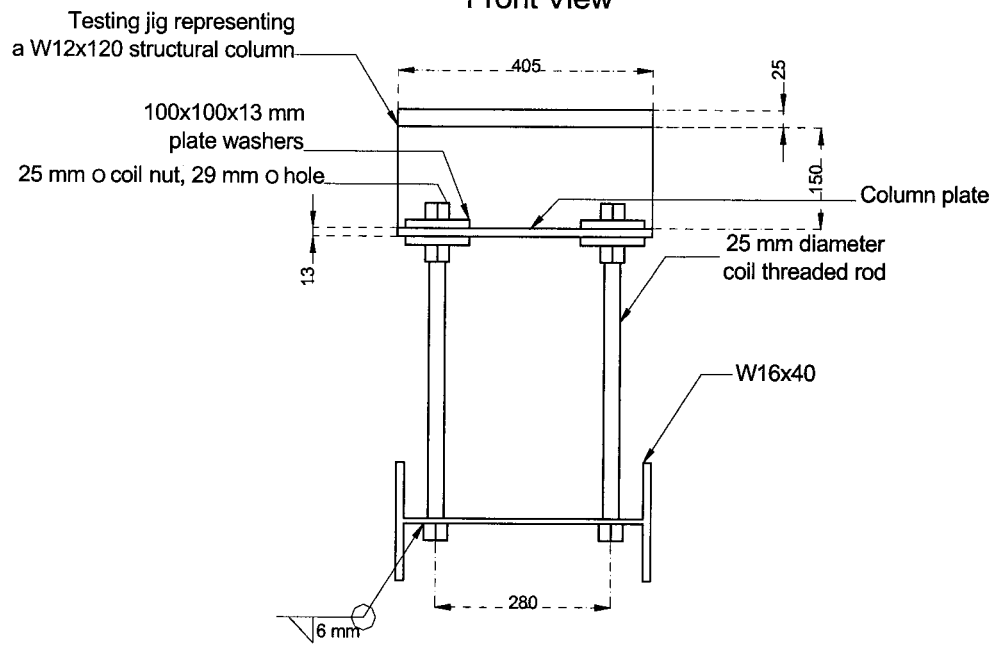


PP4

**Figure 12 – Fillet Weld Size on the Axial Tests (All units shown are in mm)**

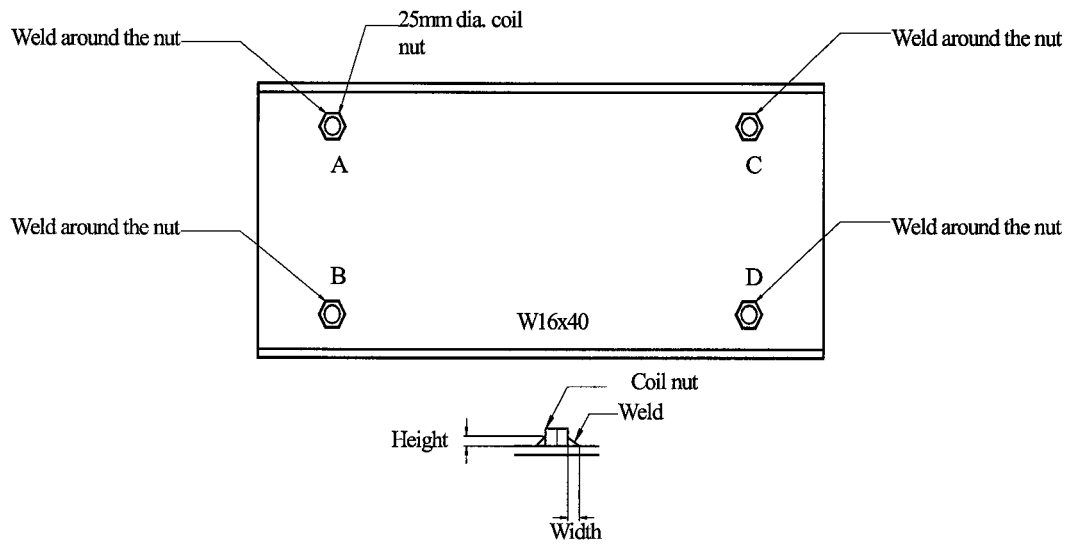


Front View



Side View

**Figure 13** – Tension and compression Tests Arrangement (All units shown are in mm)



	Rod A	Rod B	Rod C	Rod D
Height (mm)	6.2	7.6	4.4	5.6
Width (mm)	8.4	7.8	8.0	6.9

**Figure 14** – Fillet Weld Size on the Nuts of the Axial Tests

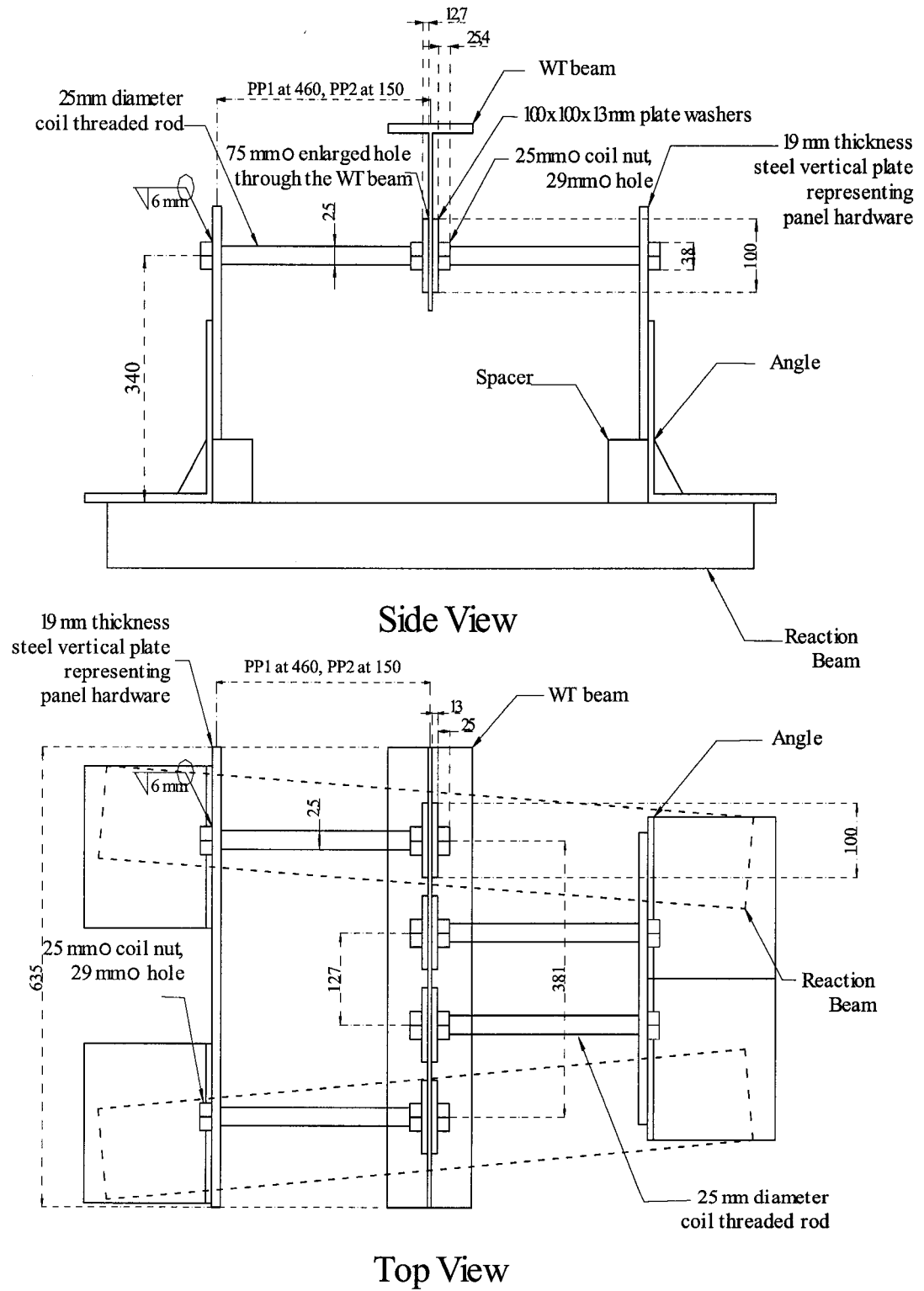


**Figure 15** – Cantilever Test Arrangement (All units shown are in mm)

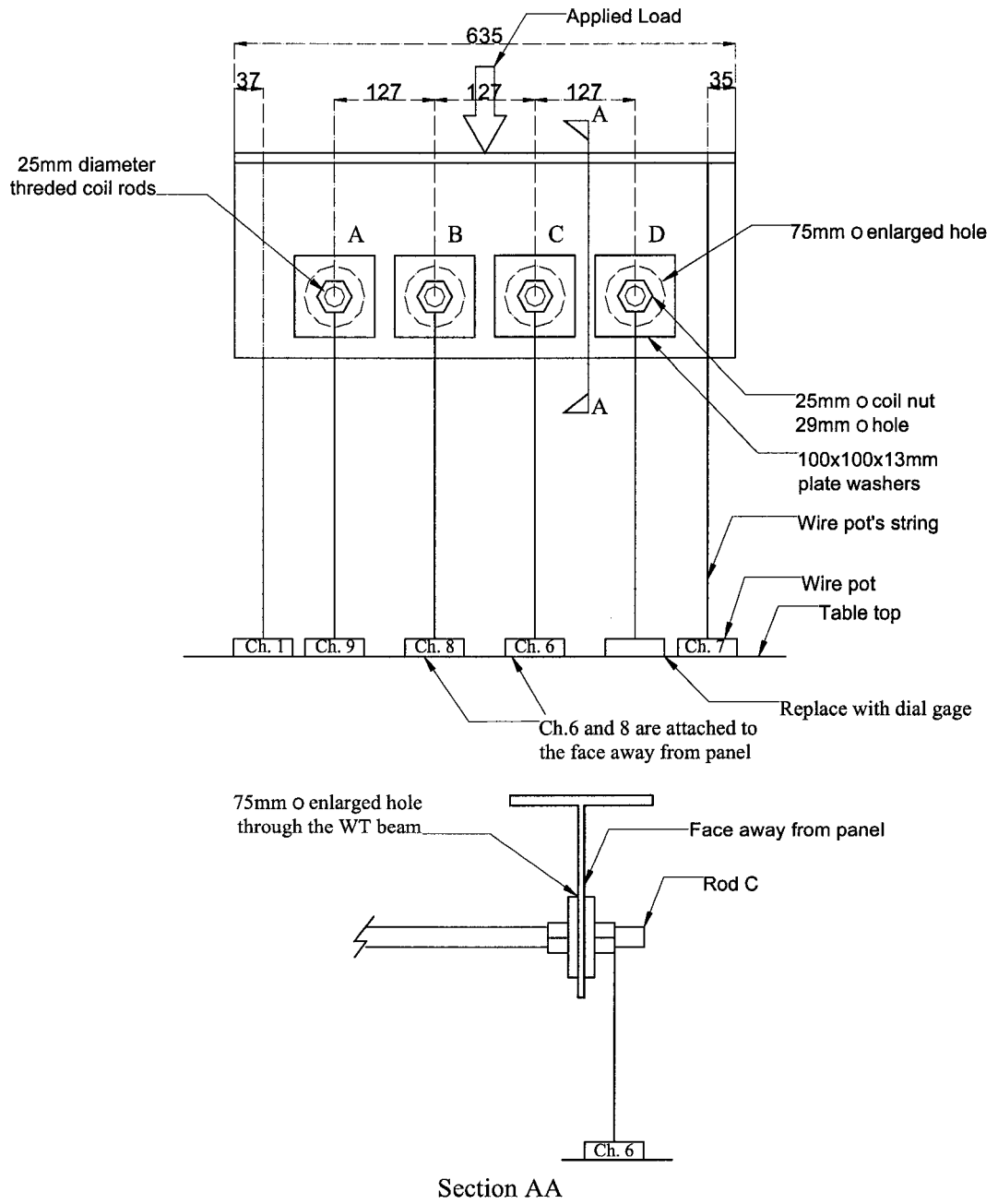
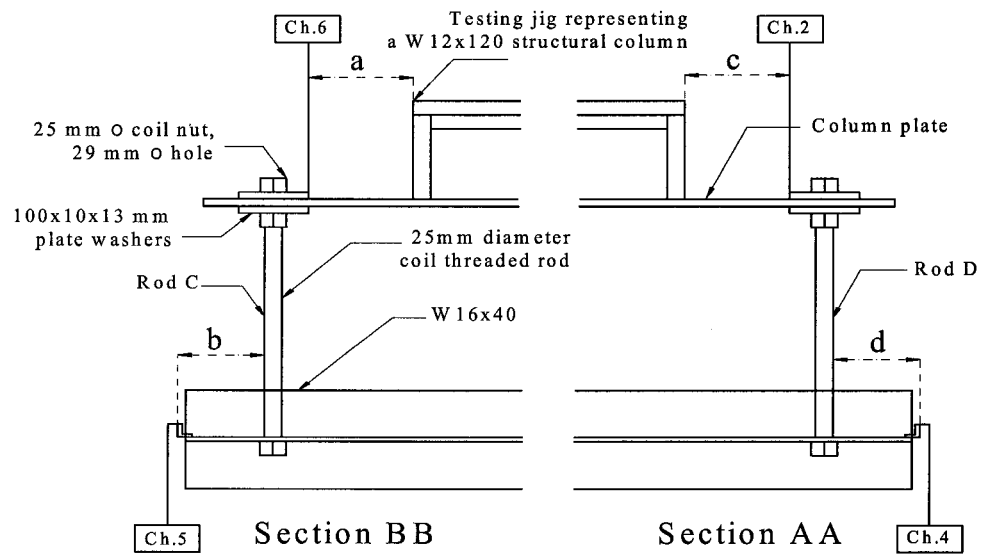
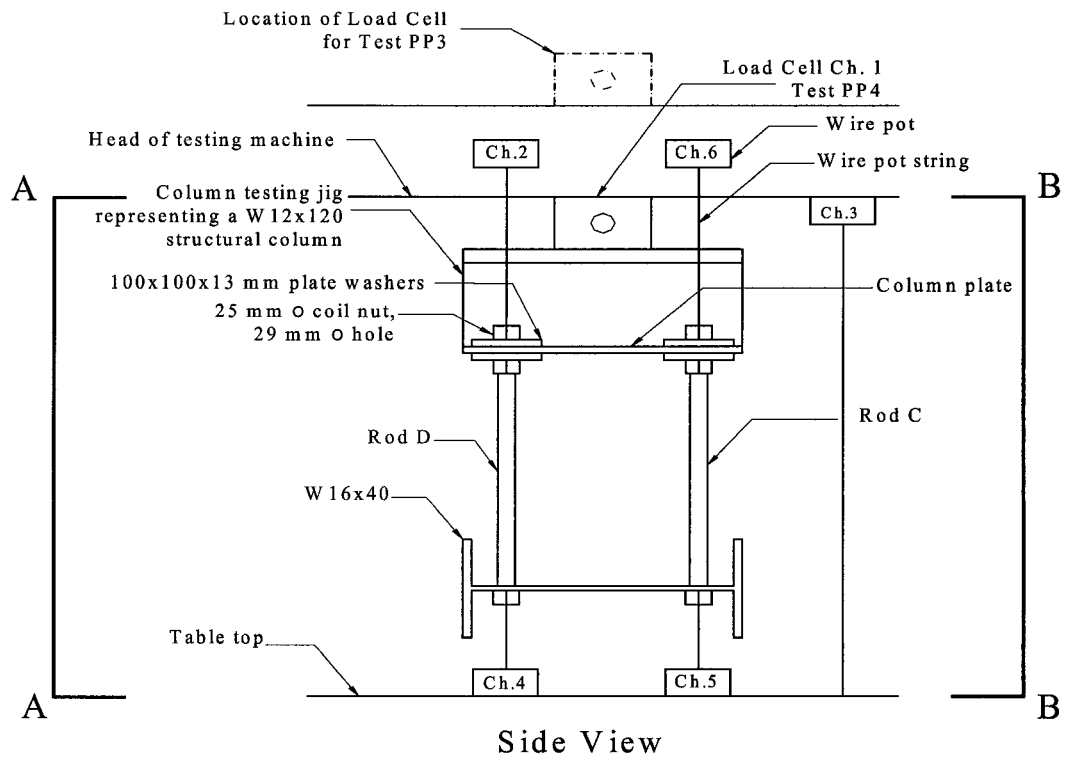


**Figure 16 – Cantilever Tests Instrumentation Lay Out**



	a (mm)	b (mm)	c (mm)	d (mm)
PP3 (Tension)	203	0	203	0
PP4 (Compression)	155.6	133.4	149.2	146.1

**Figure 17 – Tension and compression Tests Instrumentation Lay Out**



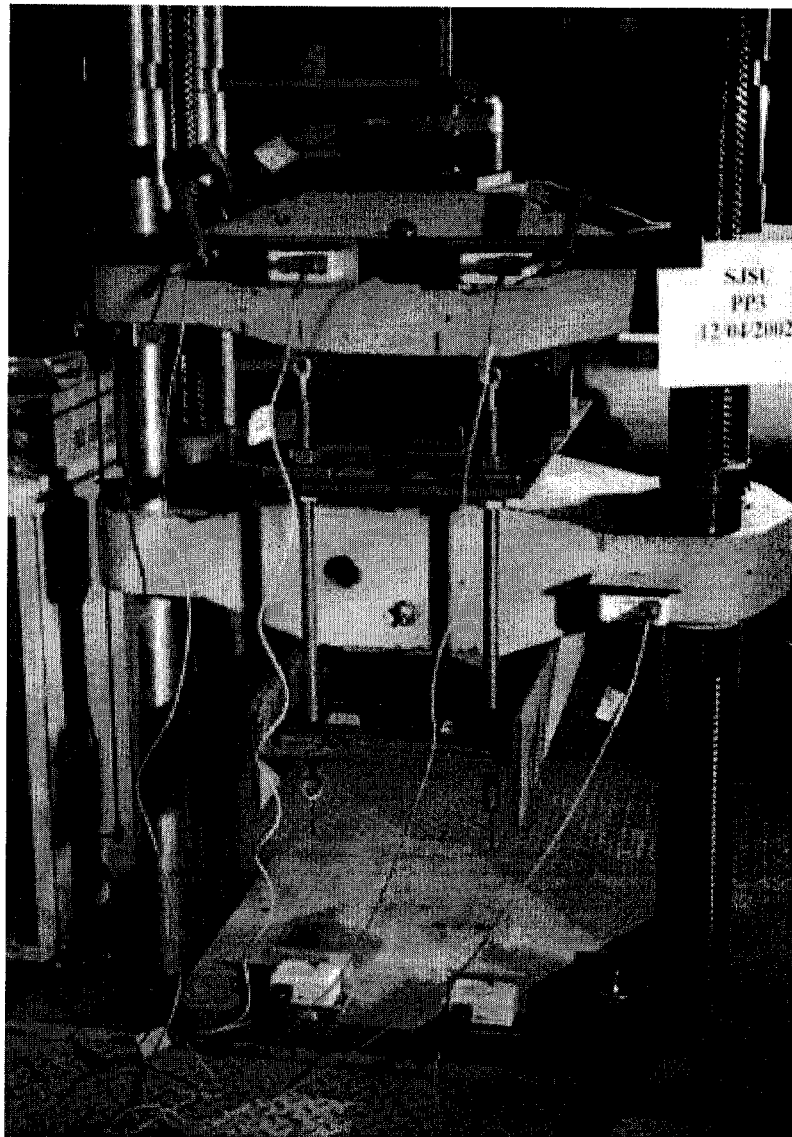


**Figure 18** – Testing Arrangement of Tension Test (PP3)

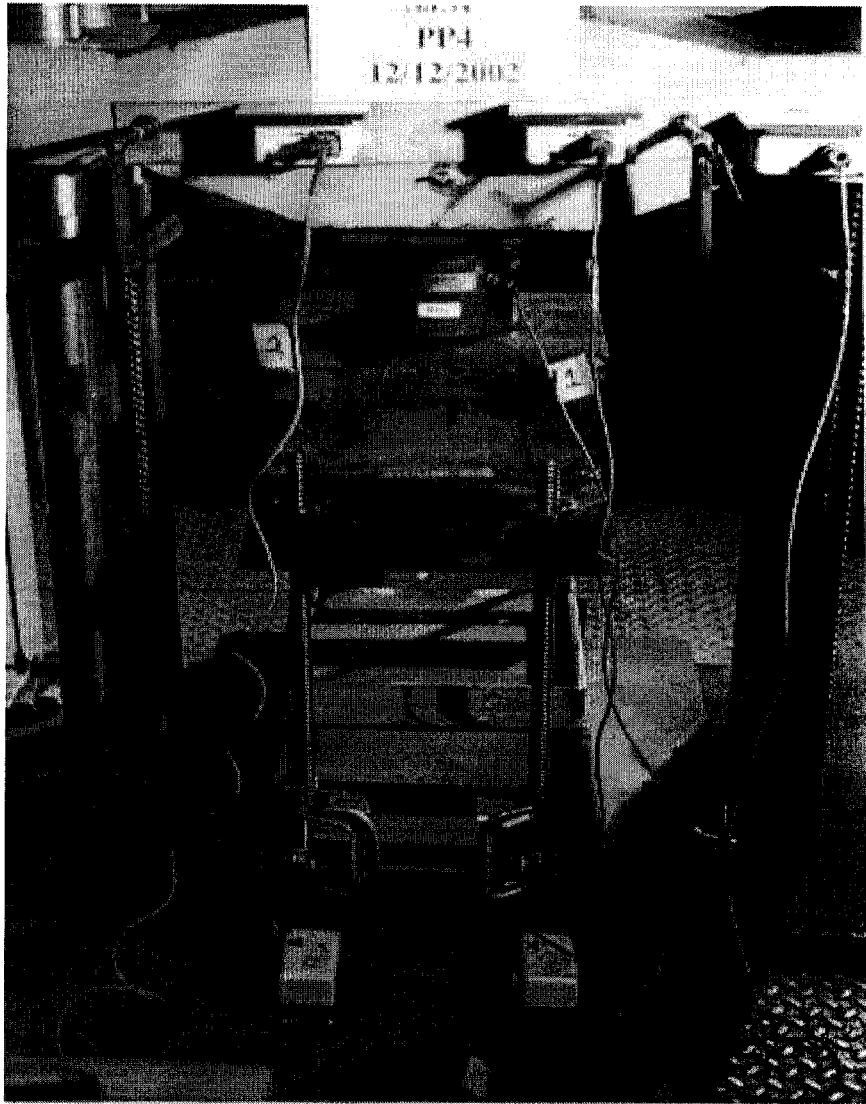


**Figure 19** – Testing Arrangement of Compression Test (PP4)

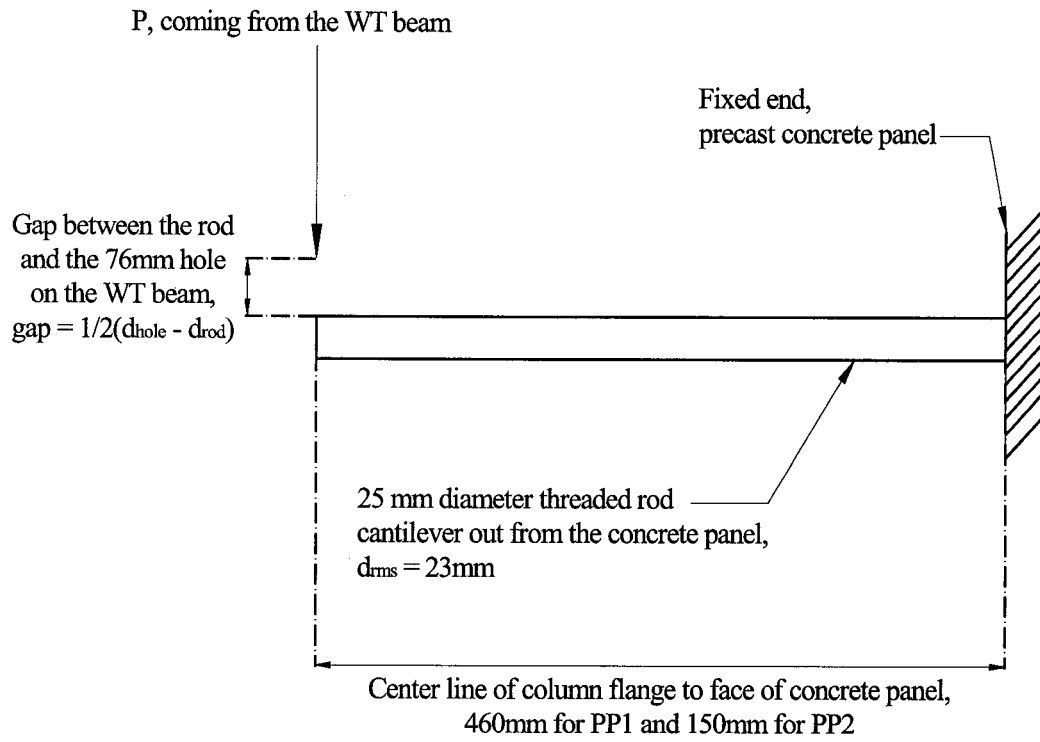


**Figure 20** – Prediction Model of the Cantilever Test

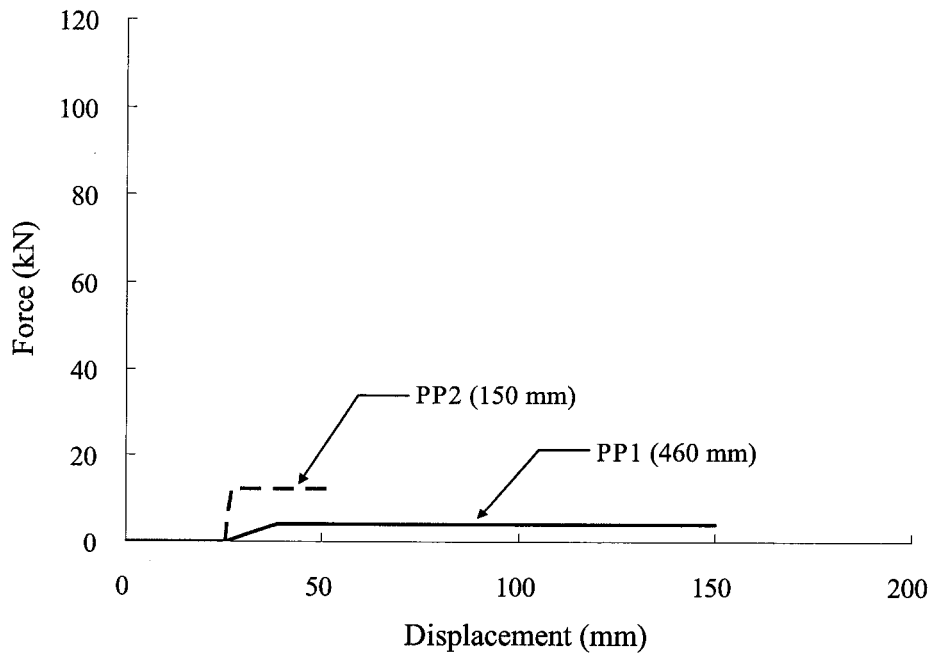


**Figure 21** – Predicted Results of the Cantilever Tests

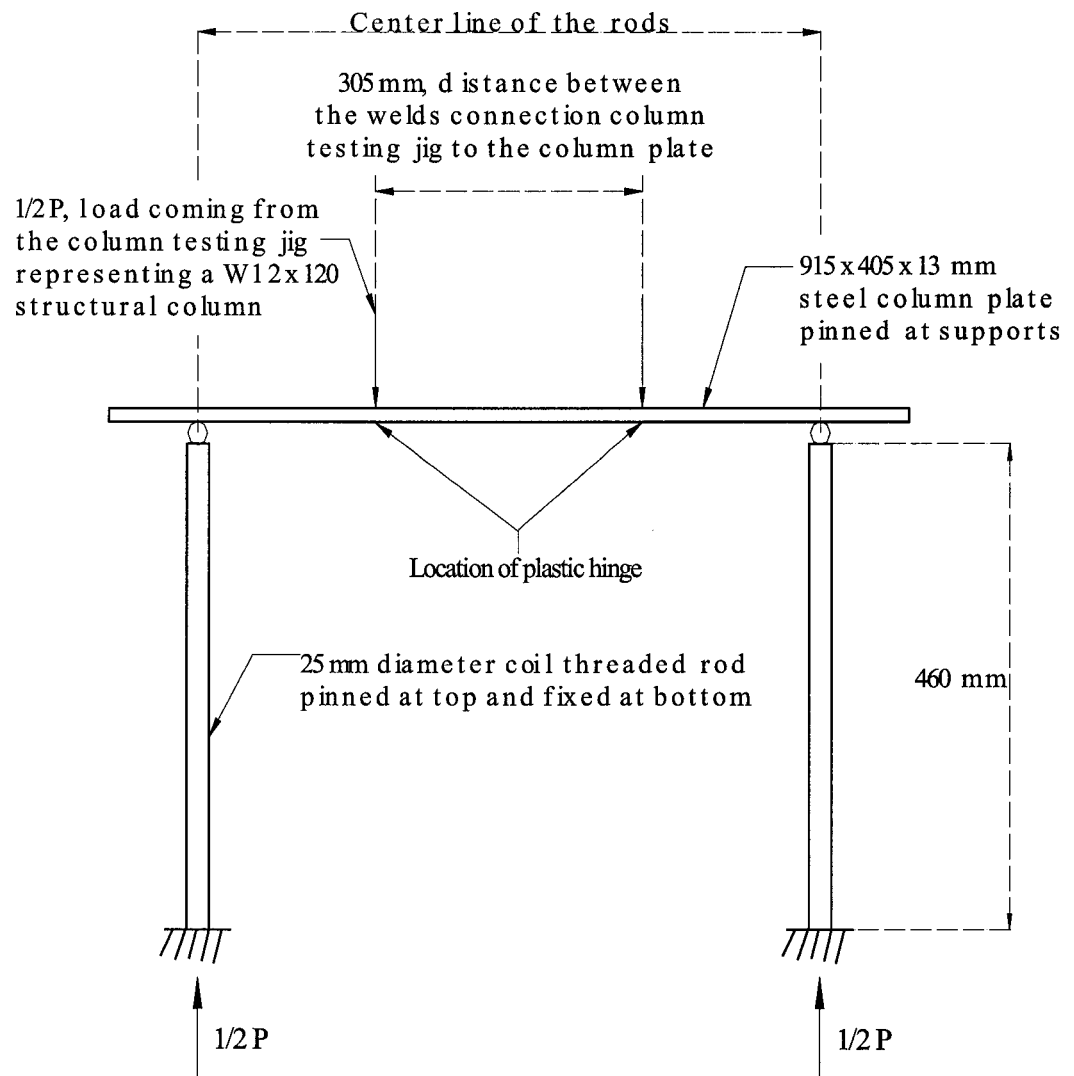


**Figure 22** – Prediction Model of the Axial Tests

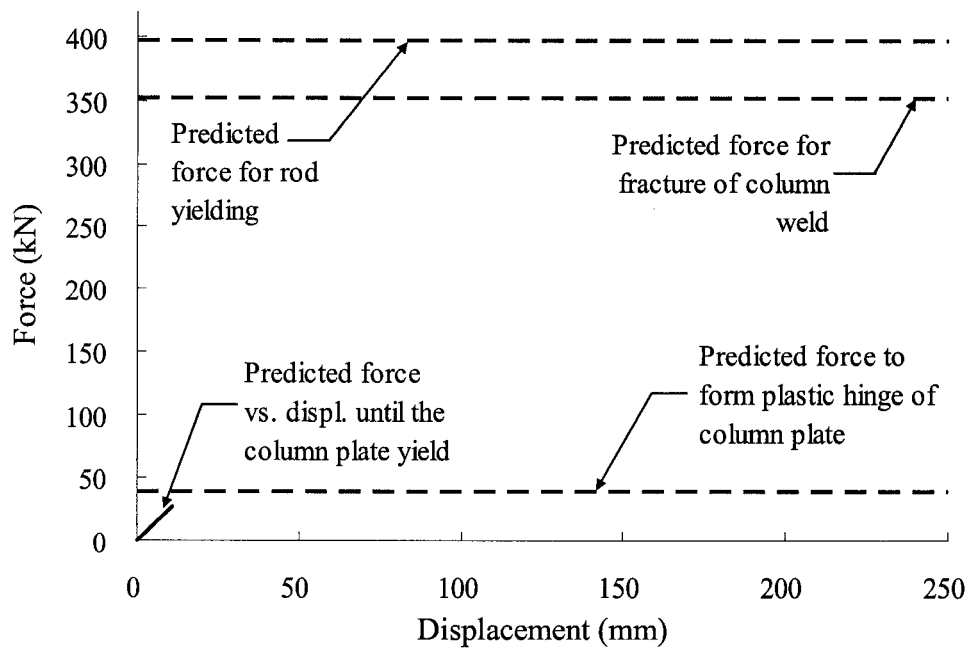


**Figure 23** – Predicted Results of the Axial Tests

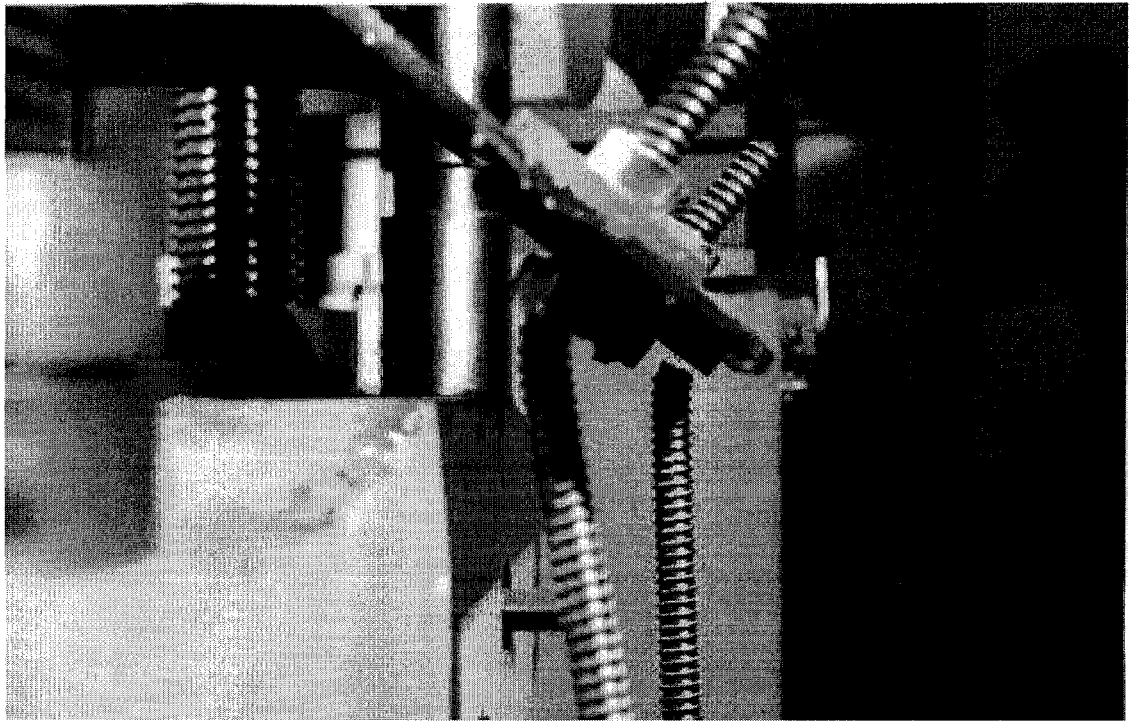


**Figure 24** – The Fractured Rod of PP3

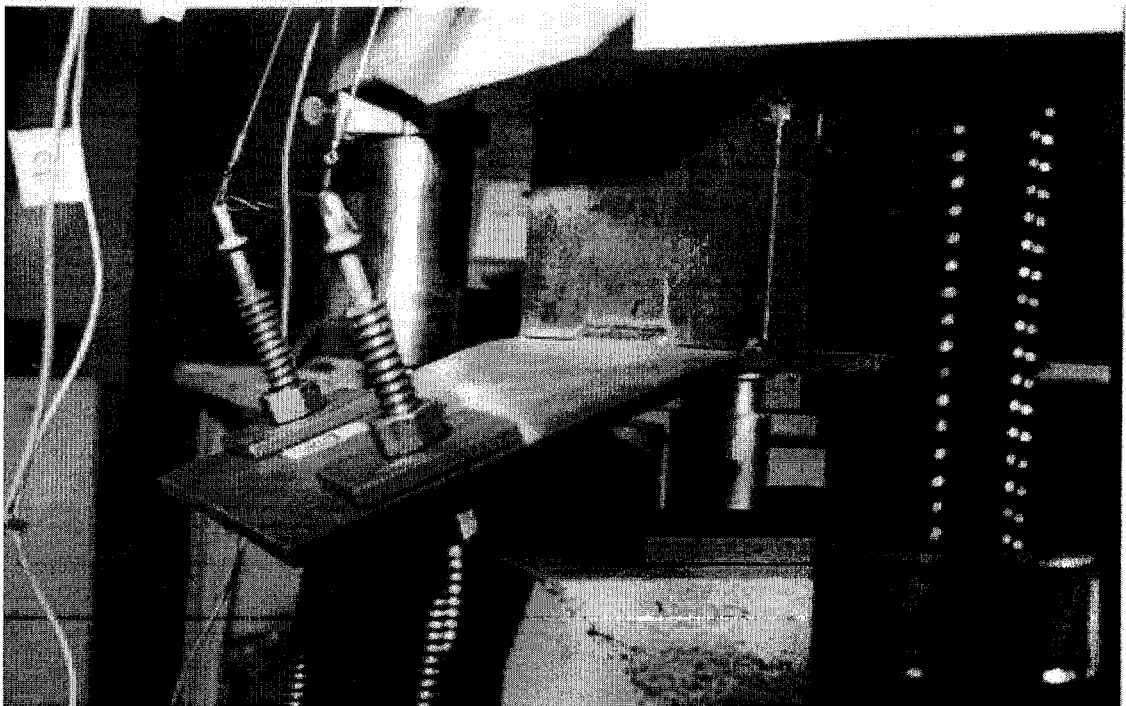


**Figure 25** – Bending of the Plate and Threaded Rods of PP3

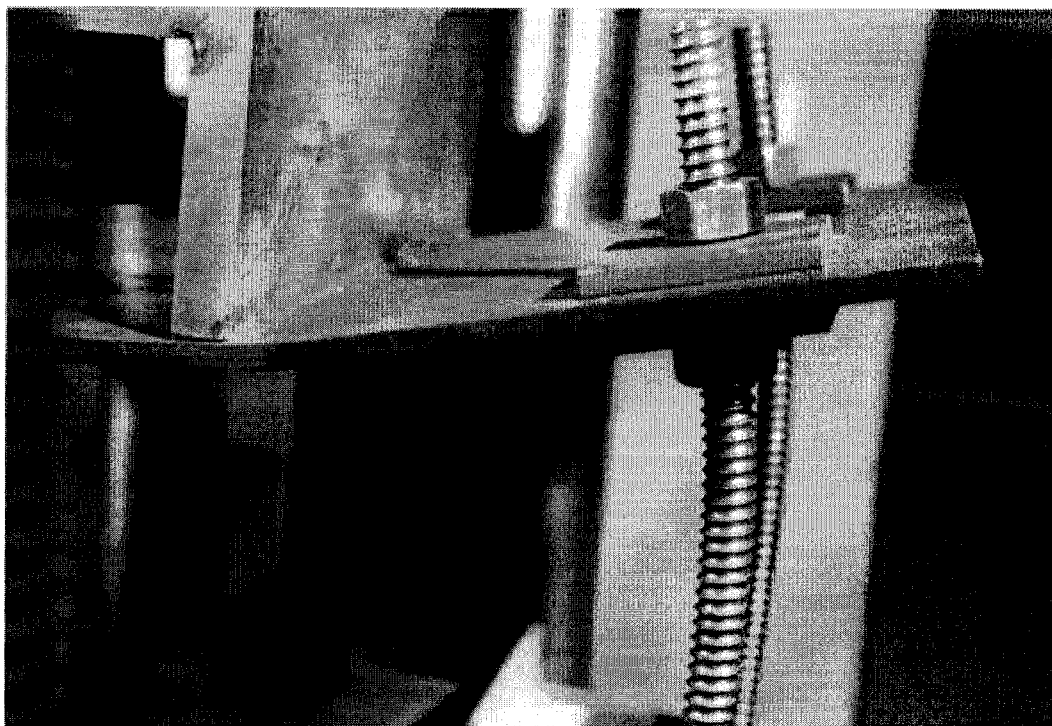


**Figure 26** – Gap at Backside of the Flange of the Column Testing Jig of PP4

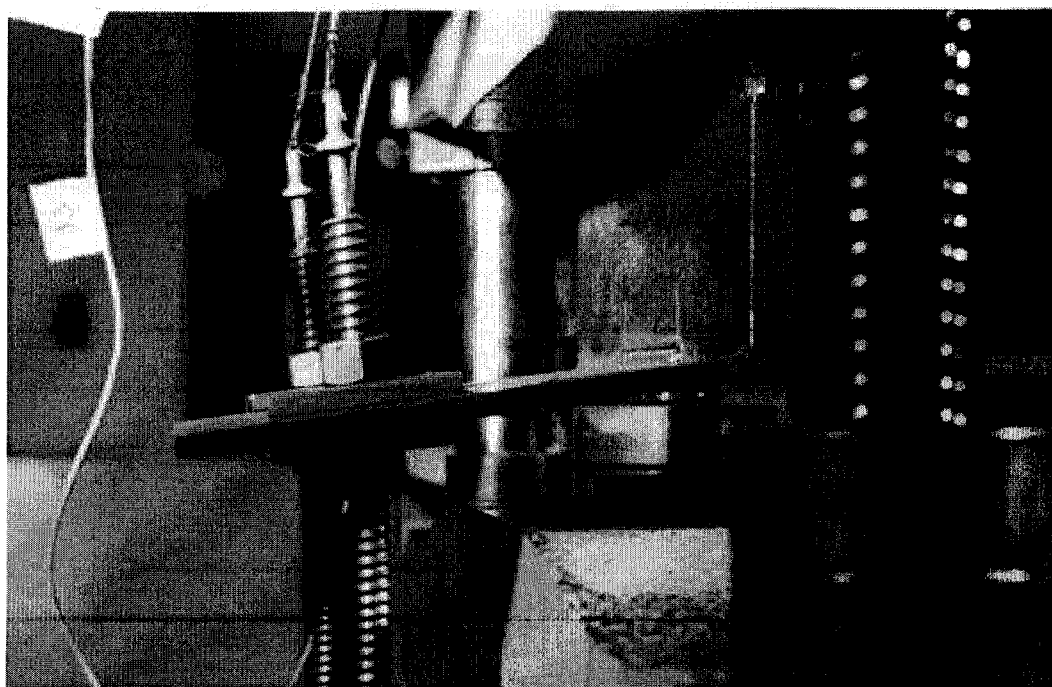


**Figure 27** – Bending of the Plate of PP3



**Figure 28** – Yield Lines Caused by Bending on the Plate of PP3

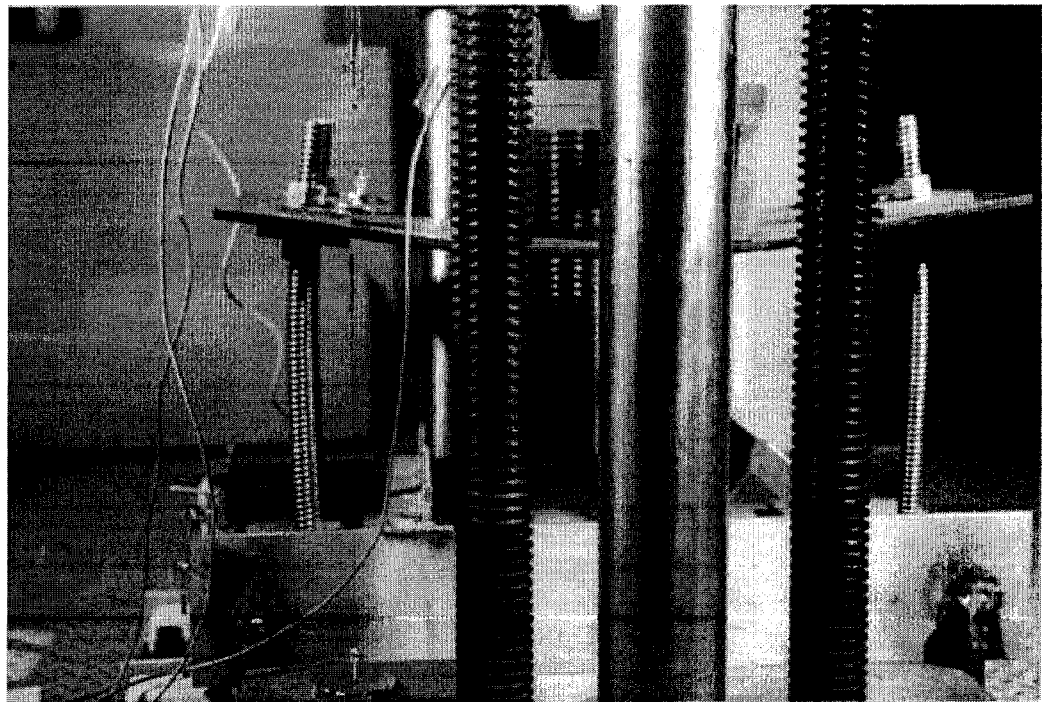


**Figure 29** – Initial Deformation of PP4



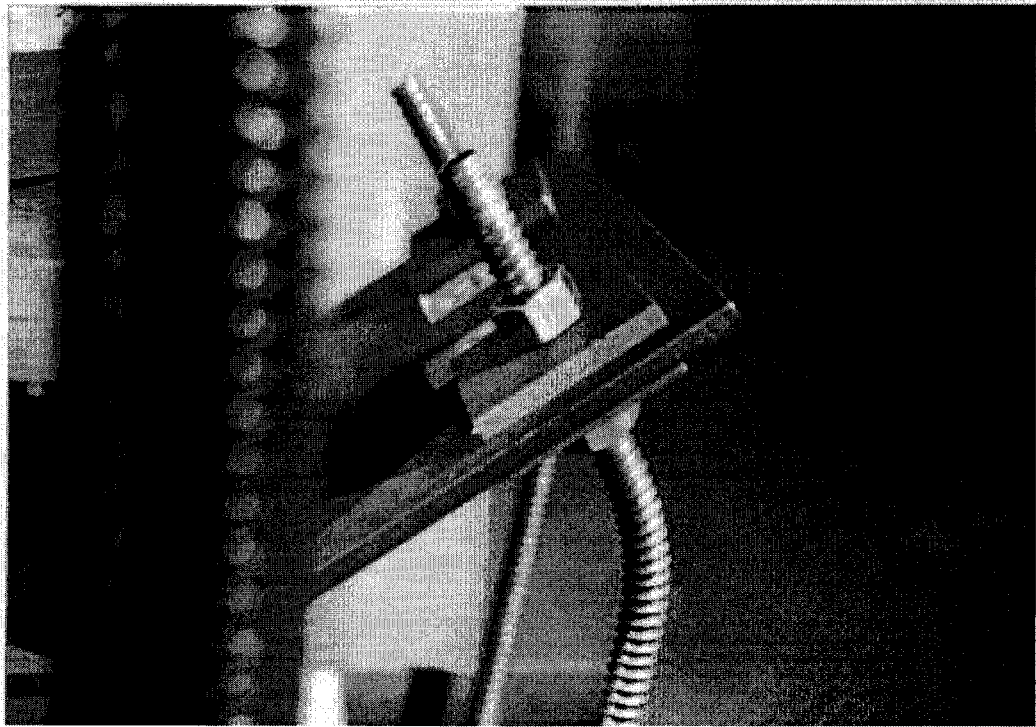


**Figure 30** – Bending of the Rods of PP4

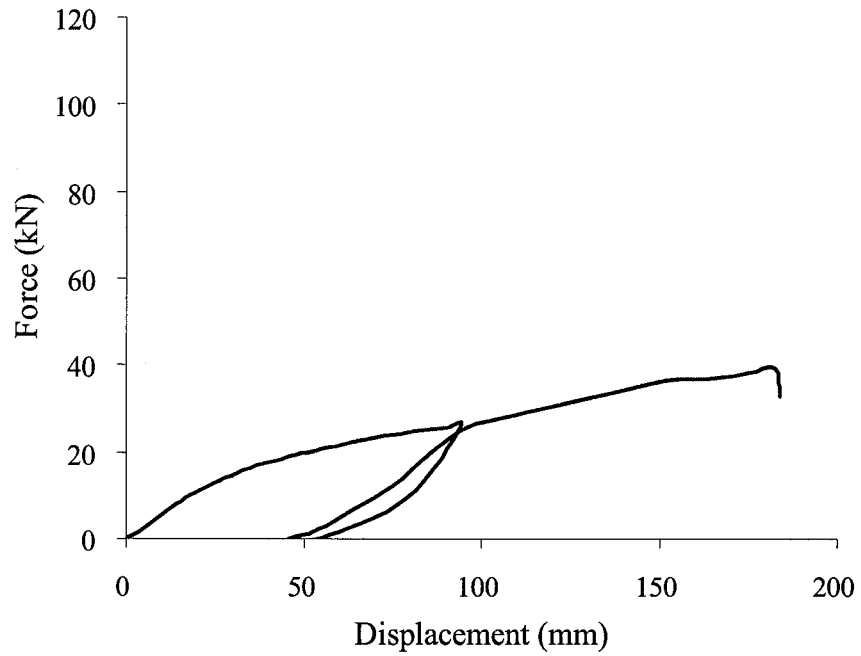


**Figure 31** – Force vs. Overall Displacement Curve of PP1

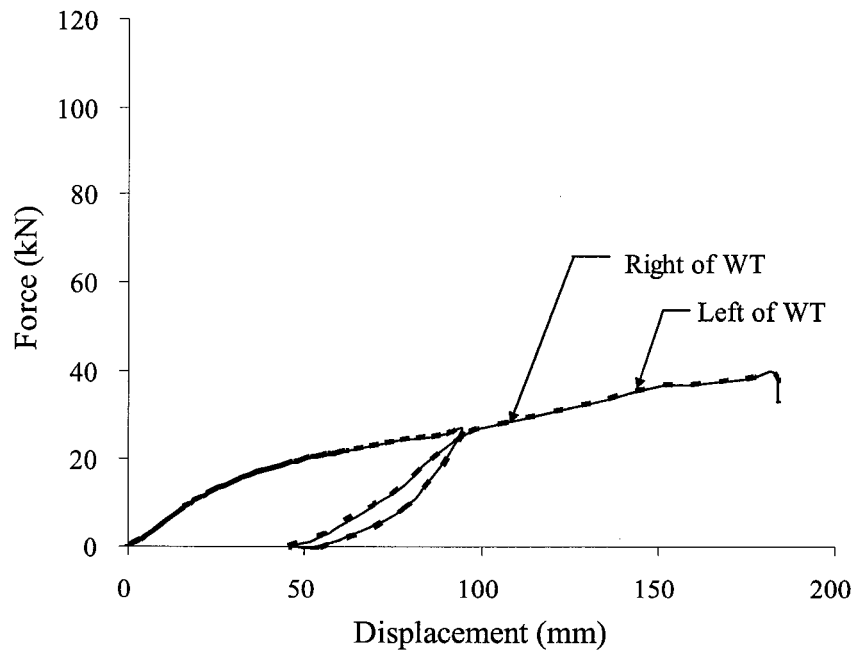


**Figure 32** – Force vs. Displacement of Two Ends of WT Beam of PP1

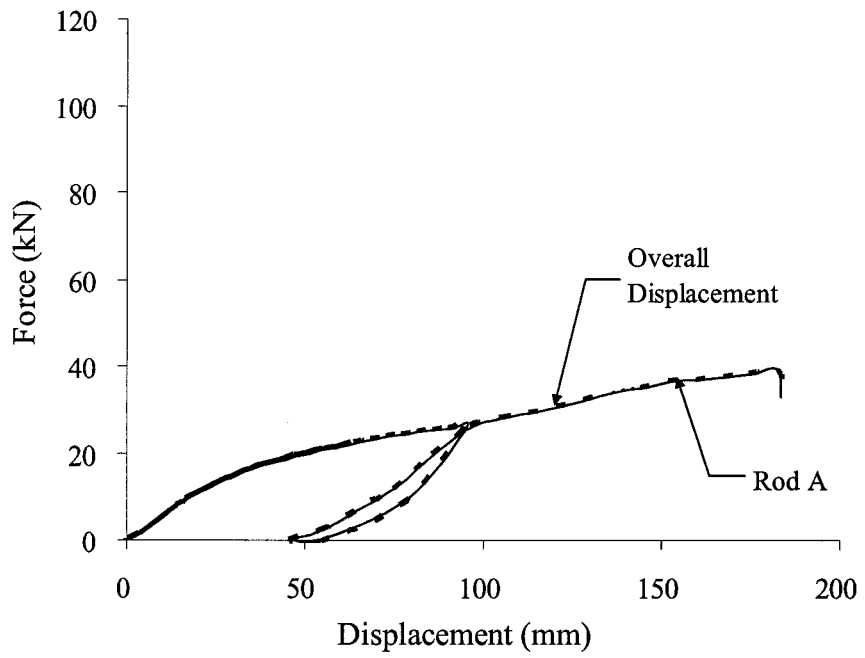


**Figure 33** – Force vs. Displacement of Rod A of PP1

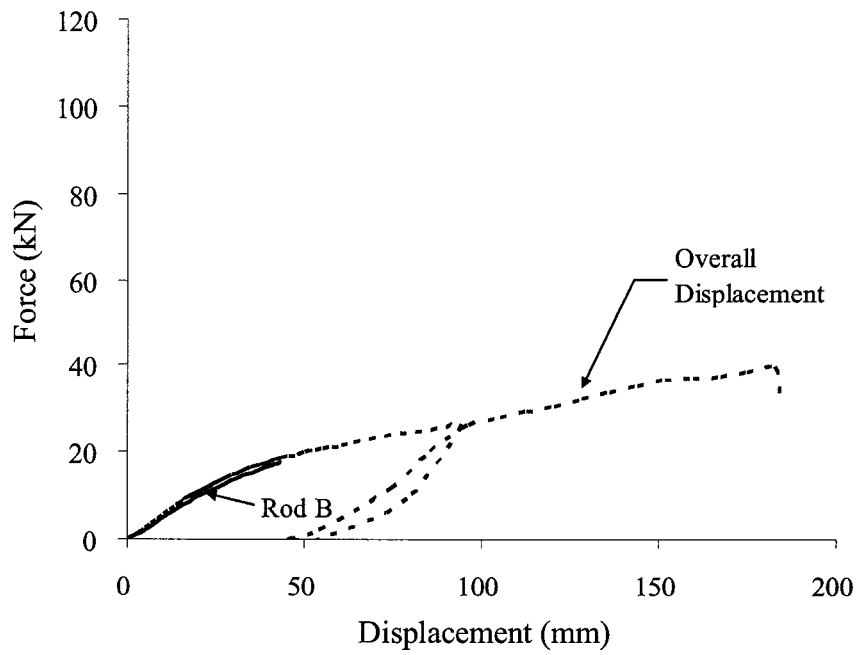


**Figure 34** – Force vs. Displacement of Rod B of PP1

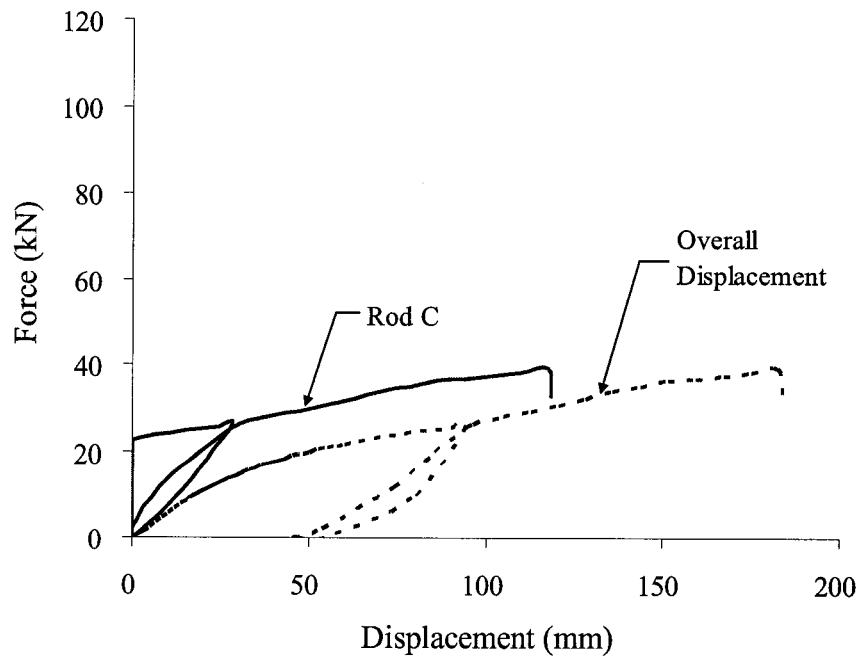


**Figure 35** – Force vs. Displacement of Rod C of PP1

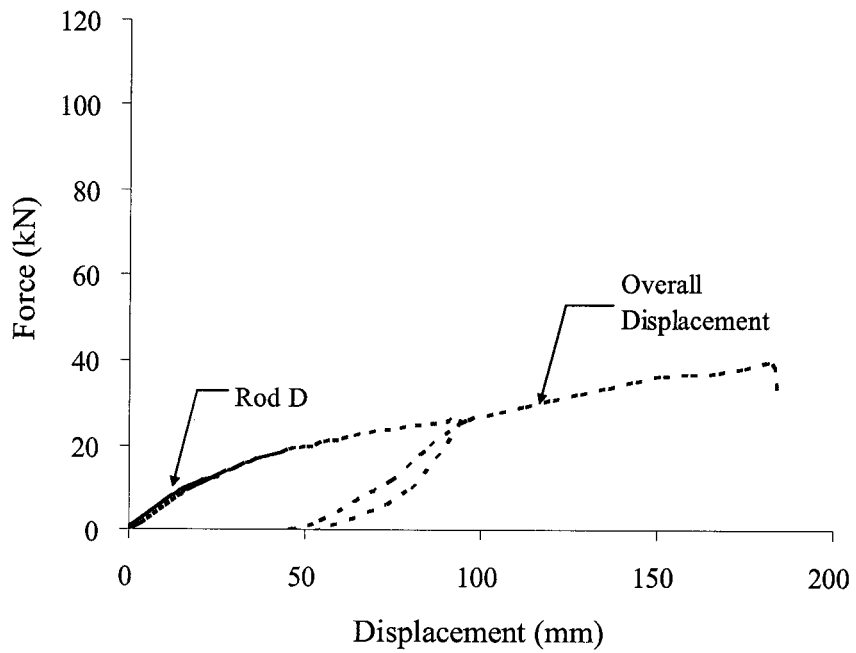


**Figure 36** – Force vs. Displacement of Rod D of PP1

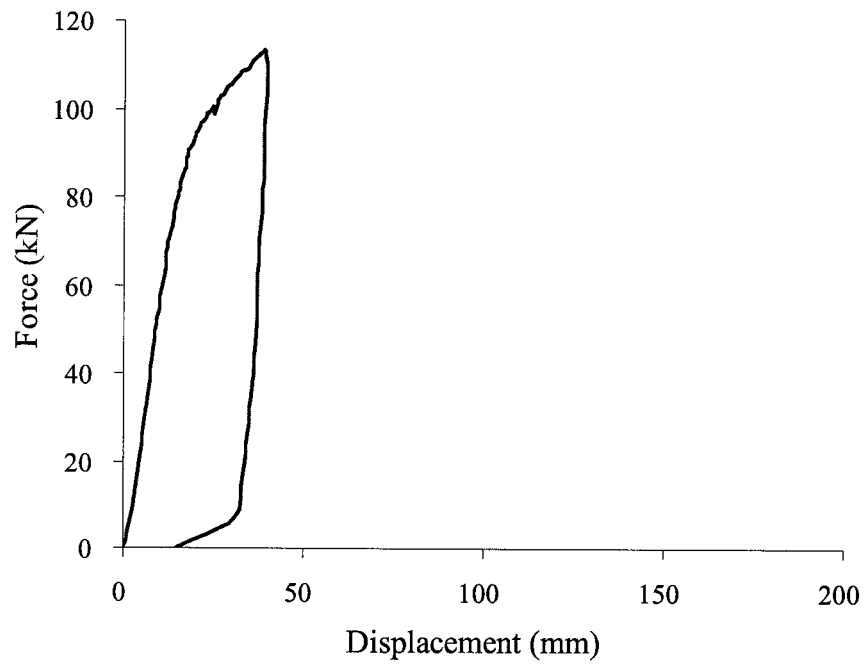


**Figure 37** – Force vs. Overall Displacement of PP2

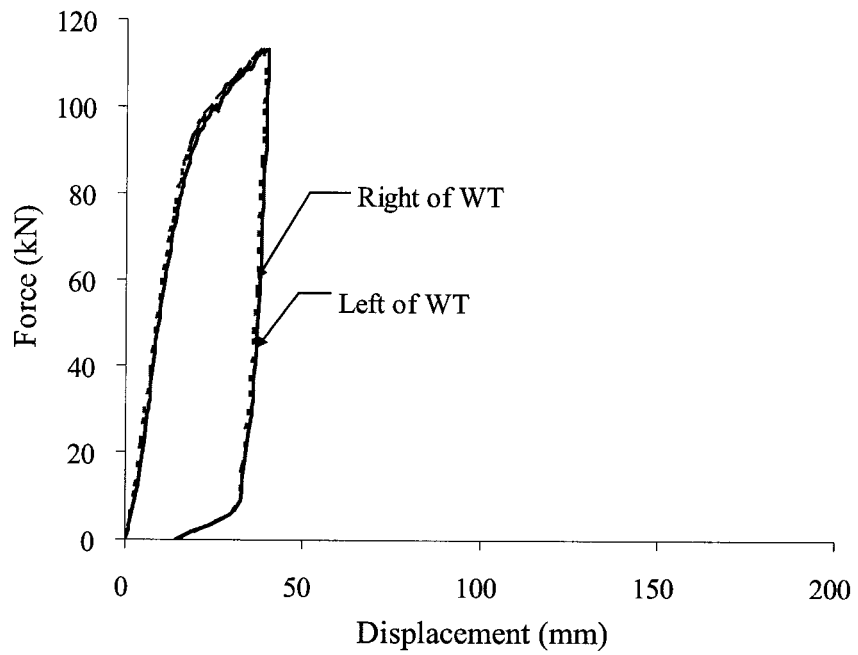


**Figure 38** – Force vs. Displacement of Two Ends of WT Beam of PP2

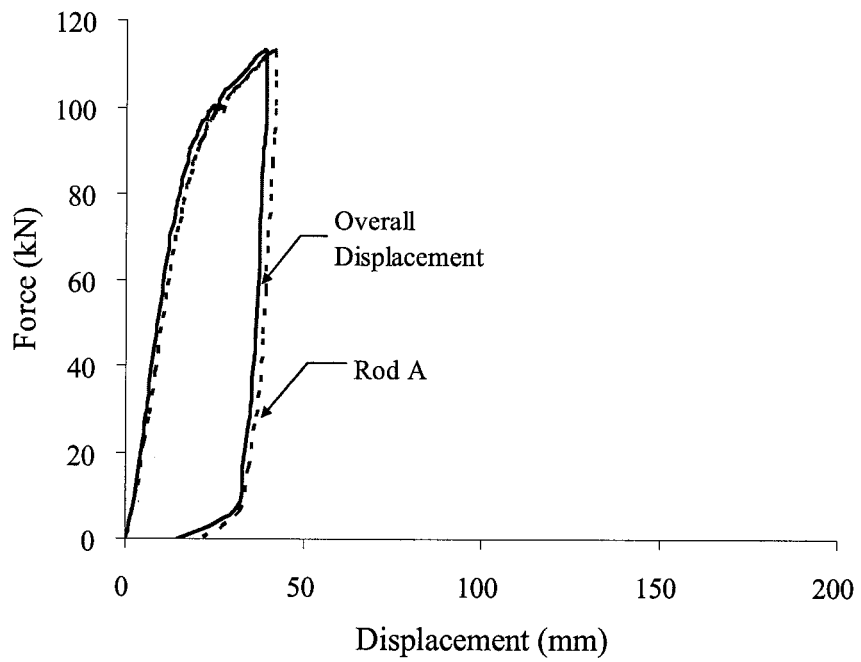


**Figure 39** – Force vs. Displacement of Rod A of PP2

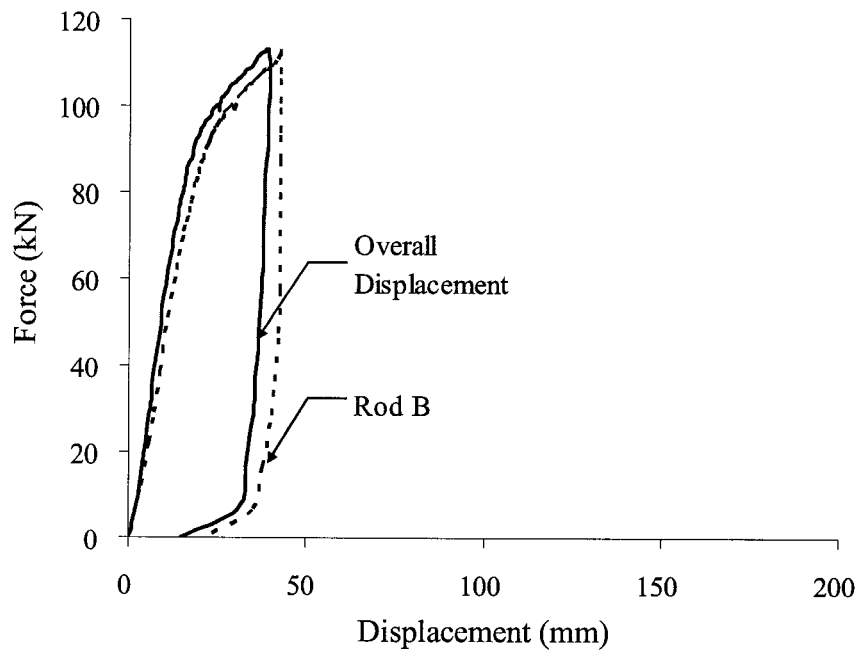


**Figure 40** – Force vs. Displacement of Rod B of PP2

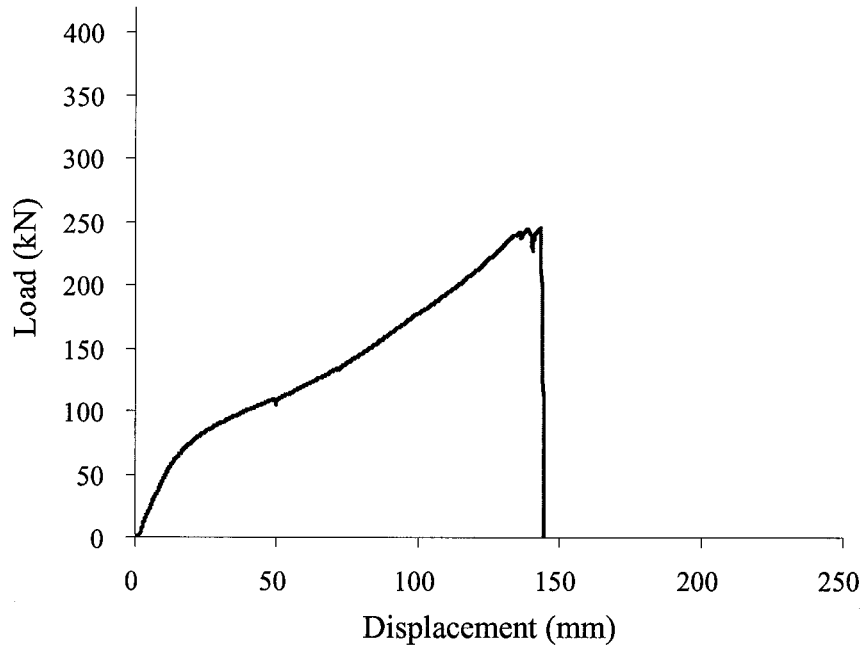


**Figure 41** – Force vs. Overall Displacement of PP3

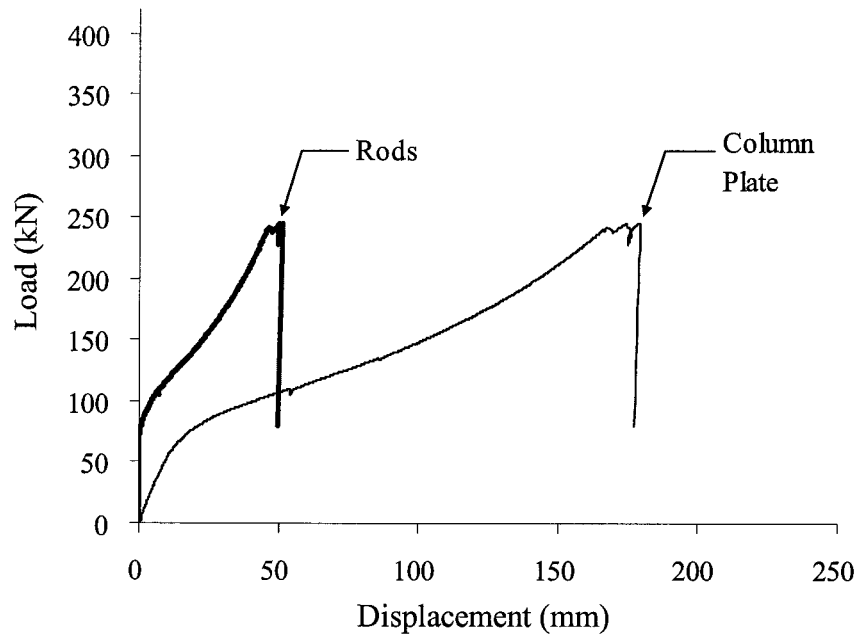


**Figure 42** – Force vs. Column Plate and Rods Displacement of PP3

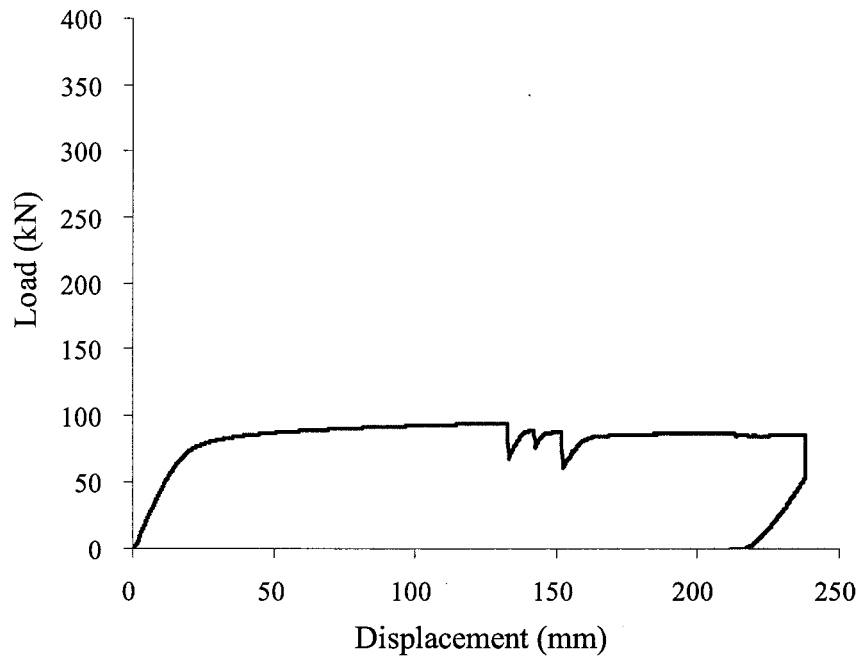


**Figure 43** - Force vs. Overall Displacement of PP4

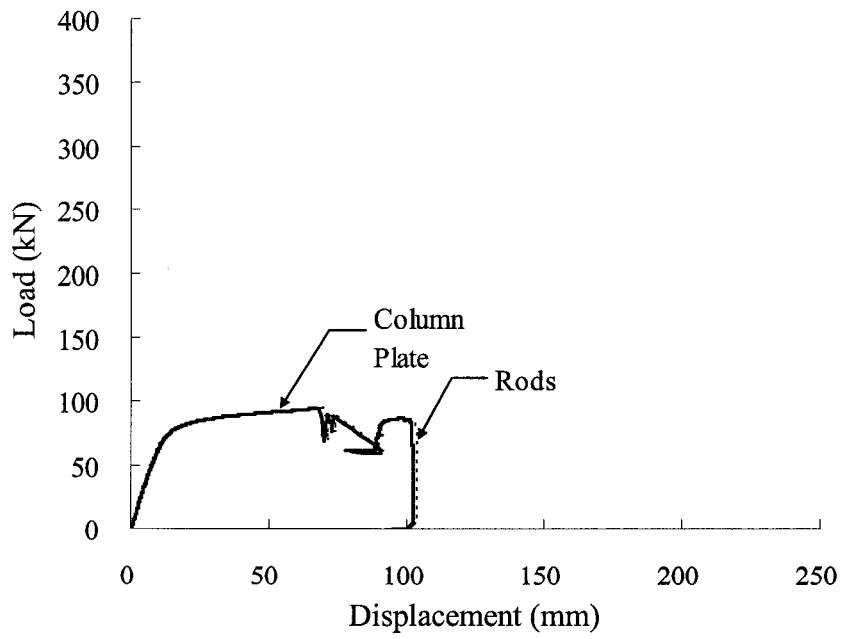


**Figure 44** - Force vs. Column Plate and Rods Displacement of PP4



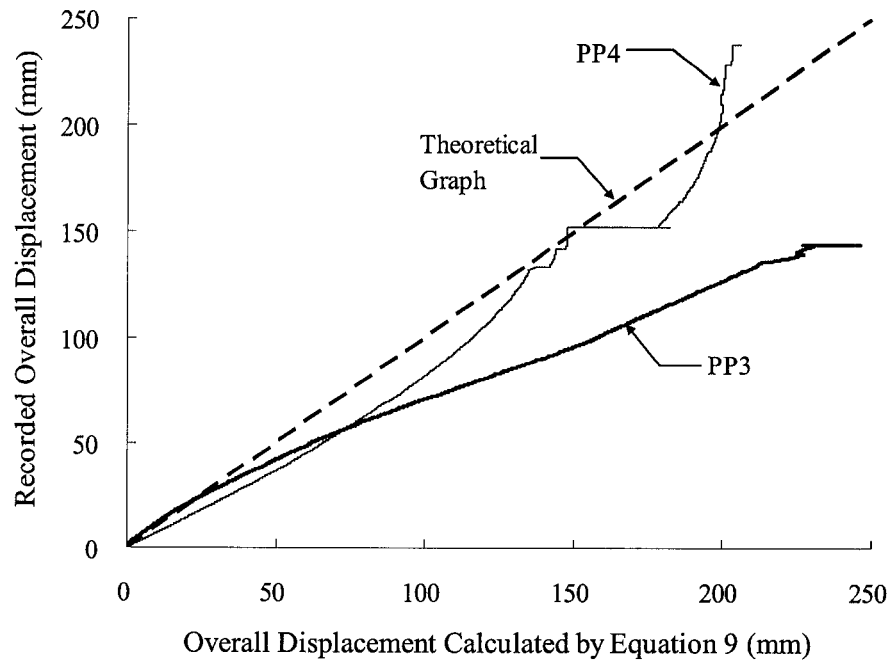


**Figure 45** – Comparison of Recorded Overall Displacement and Equation 9

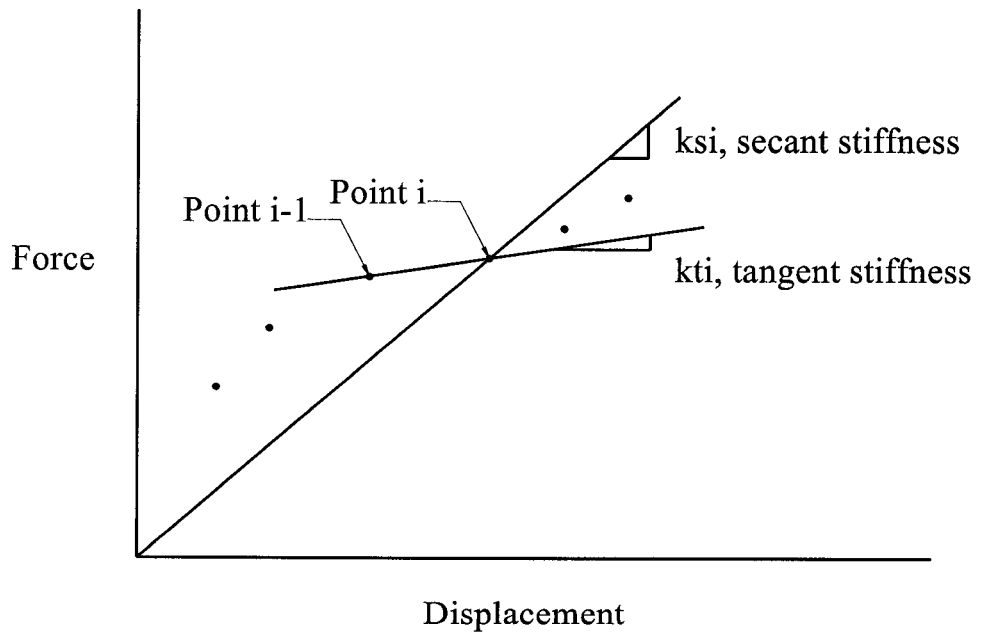


**Figure 46** – Definition of Secant and Tangent Stiffness

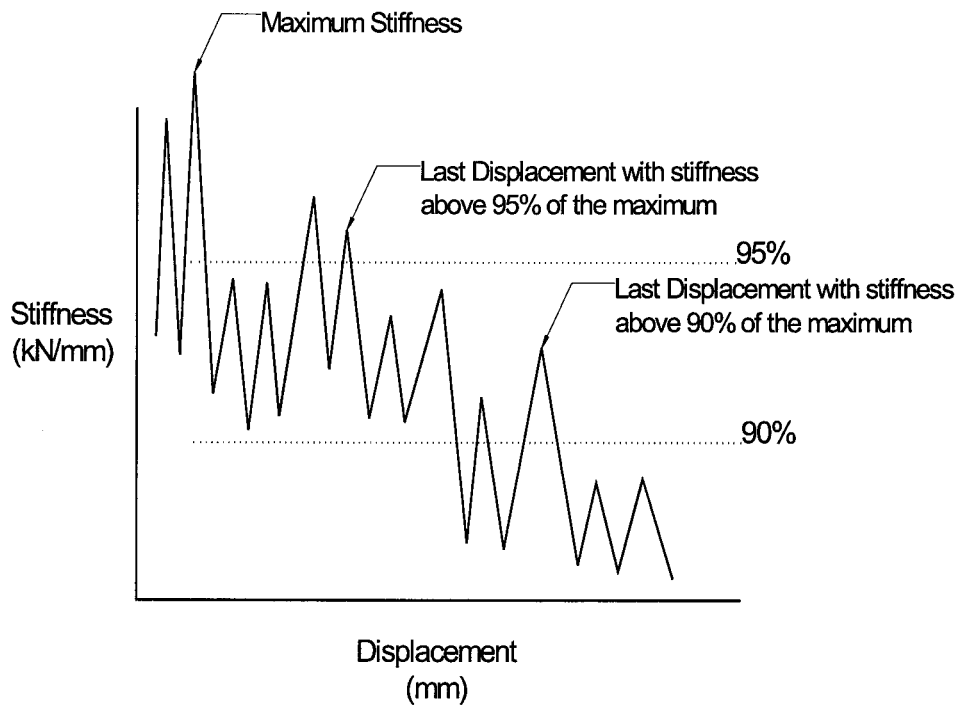


**Figure 47** – Method of Finding Yield Displacement

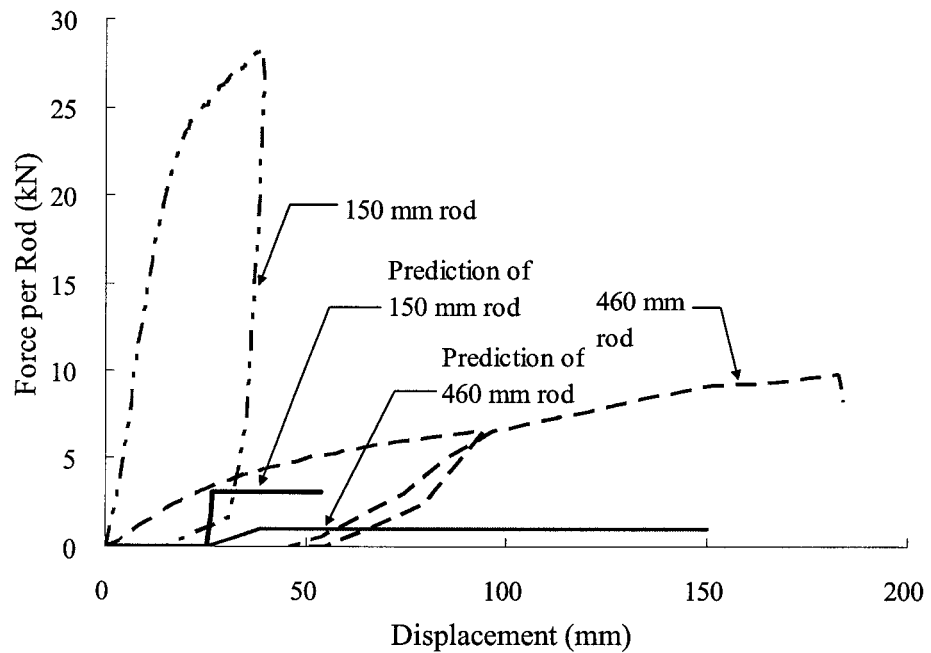


**Figure 48** – Comparison of Actual and Predicted Results for Cantilever Loading

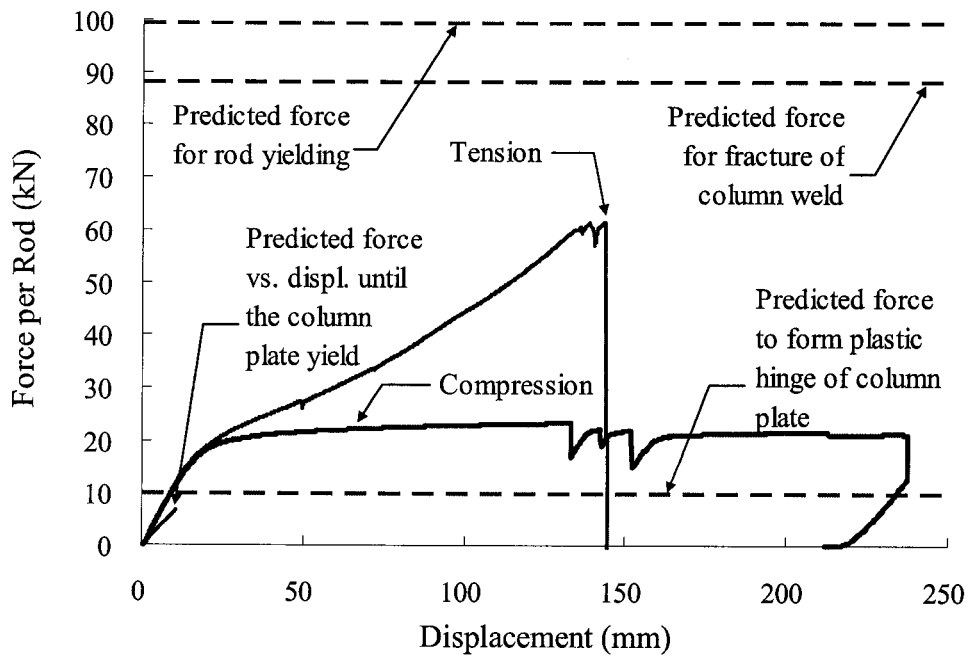


**Figure 49** – Comparison of Actual and Predicted Results for Axial Loading

**Appendix E**  
**Summary of Material Tests**

<b>Steel Coupon Test Results</b> <b>San Jose State University Structures Laboratory</b>
--

Coupon Specimen Number: Rod 1-1  
 Date of Testing: March 26, 2003  
 Testing conducted by: KMM, PJ, Kevin Chan, Carter Choi

Coupon Type: Rod-type  
 Specimen taken from: 1-inch diameter rod (2002) (1<sup>st</sup> piece)  
 Specimen Size: 2.25-inch length

**Measurement of specimen dimensions**

*Diameter:* Reading 1 = 0.499  
 Reading 2 = 0.499  
 Reading 3 = 0.501  
 Average = 0.500  
 Average Cross-Sectional Area = 0.196

Test Data

<u>Loading Point</u>	<u>Force</u>
Upper Yield	n/a
Ultimate	16.67 kips

Failure Type: Cup and Cone

Percent Elongation Data

Final Length Readings: 2.458

<b><u>Final Results</u></b>
-----------------------------

Yield Stress:	68.1 ksi	See Note 4
Ultimate Stress:	85.1 ksi	
2% Elongation:	22.9%	
8% Elongation:	n/a	

Notes

1. Testing conducted according to the ASTM E8-96 protocol.
2. All units are kips and inches.
3. Stress-strain data was not recorded during testing.
4. Ratio of 80% of ultimate stress was used to estimate yield stress.

<b>Steel Coupon Test Results</b> <b>San Jose State University Structures Laboratory</b>
--

Coupon Specimen Number: Rod 1-2  
 Date of Testing: March 26, 2003  
 Testing conducted by: KMM, PJ, Kevin Chan, Carter Choi

Coupon Type: Rod-type  
 Specimen taken from: 1-inch diameter rod (2002) (1<sup>st</sup> piece)  
 Specimen Size: 2.25-inch length

**Measurement of specimen dimensions**

*Diameter:* Reading 1 = 0.494  
 Reading 2 = 0.497  
 Reading 3 = 0.497  
 Average = 0.496  
 Average Cross-Sectional Area = 0.193

Test Data

<u>Loading Point</u>	<u>Force</u>
Upper Yield	n/a
Ultimate	14.68 kips

Failure Type: Cup and Cone

Percent Elongation Data

Final Length Readings: 2.481

<b><u>Final Results</u></b>
-----------------------------

Yield Stress:	60.9 ksi	See Note 4
Ultimate Stress:	76.1 ksi	
2% Elongation:	24.1%	
8% Elongation:	n/a	

Notes

1. Testing conducted according to the ASTM E8-96 protocol.
2. All units are kips and inches.
3. Stress-strain data was not recorded during testing.
4. Ratio of 80% of ultimate stress was used to estimate yield stress.

<b>Steel Coupon Test Results</b> <b>San Jose State University Structures Laboratory</b>
--

Coupon Specimen Number: Rod 1-3  
 Date of Testing: March 26, 2003  
 Testing conducted by: KMM, PJ, Kevin Chan, Carter Choi

Coupon Type: Rod-type  
 Specimen taken from: 1-inch diameter rod (2002) (1<sup>st</sup> piece)  
 Specimen Size: 2.25-inch length

**Measurement of specimen dimensions**

*Diameter:* Reading 1 = 0.494  
 Reading 2 = 0.492  
 Reading 3 = 0.494  
 Average = 0.493  
 Average Cross-Sectional Area = 0.191

Test Data

<u>Loading Point</u>	<u>Force</u>
Upper Yield	n/a
Ultimate	16.45 kips

Failure Type: Cup and Cone

Percent Elongation Data

Final Length Readings: 2.464

<b><u>Final Results</u></b>
-----------------------------

Yield Stress:	68.9 ksi	See Note 4
Ultimate Stress:	86.1 ksi	
2% Elongation:	23.2%	
8% Elongation:	n/a	

Notes

1. Testing conducted according to the ASTM E8-96 protocol.
2. All units are kips and inches.
3. Stress-strain data was not recorded during testing.
4. Ratio of 80% of ultimate stress was used to estimate yield stress.

**Steel Coupon Test Results**  
**San Jose State University Structures Laboratory**

Coupon Specimen Number: Rod 2-1  
Date of Testing: March 26, 2003  
Testing conducted by: KMM, PJ, Kevin Chan, Carter Choi

Coupon Type: Rod-type  
Specimen taken from: 1-inch diameter rod (2002) (2<sup>nd</sup> piece)  
Specimen Size: 2.25-inch length

**Measurement of specimen dimensions**

*Diameter:* Reading 1 = 0.503  
Reading 2 = 0.501  
Reading 3 = 0.501  
Average = 0.502  
Average Cross-Sectional Area = 0.198

**Test Data**

<u>Loading Point</u>	<u>Force</u>
Upper Yield	n/a
Ultimate	18.90 kips

Failure Type: Cup and Cone

**Percent Elongation Data**

Final Length Readings: 2.341

**Final Results**

Yield Stress:	76.4 ksi	See Note 4
Ultimate Stress:	95.5 ksi	
2% Elongation:	17.1%	
8% Elongation:	n/a	

**Notes**

1. Testing conducted according to the ASTM E8-96 protocol.
2. All units are kips and inches.
3. Stress-strain data was not recorded during testing.
4. Ratio of 80% of ultimate stress was used to estimate yield stress.



<b>Steel Coupon Test Results</b> <b>San Jose State University Structures Laboratory</b>
--

Coupon Specimen Number: Rod 2-2  
 Date of Testing: March 26, 2003  
 Testing conducted by: KMM, PJ, Kevin Chan, Carter Choi

Coupon Type: Rod-type  
 Specimen taken from: 1-inch diameter rod (2002) (2<sup>nd</sup> piece)  
 Specimen Size: 2.25-inch length

**Measurement of specimen dimensions**

*Diameter:* Reading 1 = 0.500  
 Reading 2 = 0.500  
 Reading 3 = 0.501  
 Average = 0.500  
 Average Cross-Sectional Area = 0.196

Test Data

<u>Loading Point</u>	<u>Force</u>
Upper Yield	n/a
Ultimate	18.66 kips

Failure Type: Cup and Cone

Percent Elongation Data

Final Length Readings: 2.364

<b><u>Final Results</u></b>
-----------------------------

Yield Stress:	76.2 ksi	See Note 4
Ultimate Stress:	95.2 ksi	
2% Elongation:	18.2%	
8% Elongation:	n/a	

Notes

1. Testing conducted according to the ASTM E8-96 protocol.
2. All units are kips and inches.
3. Stress-strain data was not recorded during testing.
4. Ratio of 80% of ultimate stress was used to estimate yield stress.

<b>Steel Coupon Test Results</b> <b>San Jose State University Structures Laboratory</b>
--

Coupon Specimen Number: Rod 2-3  
 Date of Testing: March 26, 2003  
 Testing conducted by: KMM, PJ, Kevin Chan, Carter Choi

Coupon Type: Rod-type  
 Specimen taken from: 1-inch diameter rod (2002) (2<sup>nd</sup> piece)  
 Specimen Size: 2.25-inch length

**Measurement of specimen dimensions**

*Diameter:* Reading 1 = 0.498  
 Reading 2 = 0.499  
 Reading 3 = 0.501  
 Average = 0.499  
 Average Cross-Sectional Area = 0.196

Test Data

<u>Loading Point</u>	<u>Force</u>
Upper Yield	n/a
Ultimate	18.67 kips

Failure Type: Cup and Cone

Percent Elongation Data

Final Length Readings: 2.354

<b><u>Final Results</u></b>
-----------------------------

Yield Stress:	76.2 ksi	See Note 4
Ultimate Stress:	95.3 ksi	
2% Elongation:	17.7%	
8% Elongation:	n/a	

Notes

1. Testing conducted according to the ASTM E8-96 protocol.
2. All units are kips and inches.
3. Stress-strain data was not recorded during testing.
4. Ratio of 80% of ultimate stress was used to estimate yield stress.

<b>Steel Coupon Test Results</b> <b>San Jose State University Structures Laboratory</b>
--

Coupon Specimen Number: Rod 3-1  
 Date of Testing: March 26, 2003  
 Testing conducted by: KMM, PJ, Kevin Chan, Carter Choi

Coupon Type: Rod-type  
 Specimen taken from: 1-inch diameter rod (2002) (3<sup>rd</sup> piece)  
 Specimen Size: 2.25-inch length

**Measurement of specimen dimensions**

*Diameter:* Reading 1 = 0.500  
 Reading 2 = 0.501  
 Reading 3 = 0.502  
 Average = 0.501  
 Average Cross-Sectional Area = 0.197

Test Data

<u>Loading Point</u>	<u>Force</u>
Upper Yield	n/a
Ultimate	17.13 kips

Failure Type: Cup and Cone

Percent Elongation Data

Final Length Readings: 2.395

<b><u>Final Results</u></b>
-----------------------------

Yield Stress:	69.6 ksi	See Note 4
Ultimate Stress:	87.0 ksi	
2% Elongation:	19.8%	
8% Elongation:	n/a	

Notes

1. Testing conducted according to the ASTM E8-96 protocol.
2. All units are kips and inches.
3. Stress-strain data was not recorded during testing.
4. Ratio of 80% of ultimate stress was used to estimate yield stress.

**Steel Coupon Test Results**  
**San Jose State University Structures Laboratory**

Coupon Specimen Number: Rod 3-2  
Date of Testing: March 26, 2003  
Testing conducted by: KMM, PJ, Kevin Chan, Carter Choi

Coupon Type: Rod-type  
Specimen taken from: 1-inch diameter rod (2002) (3<sup>rd</sup> piece)  
Specimen Size: 2.25-inch length

**Measurement of specimen dimensions**

*Diameter:* Reading 1 = 0.506  
Reading 2 = 0.505  
Reading 3 = 0.505  
Average = 0.505  
Average Cross-Sectional Area = 0.200

Test Data

<u>Loading Point</u>	<u>Force</u>
Upper Yield	n/a
Ultimate	17.36 kips

Failure Type: Cup and Cone

Percent Elongation Data

Final Length Readings: 2.474

**Final Results**

Yield Stress:	69.4 ksi	See Note 4
Ultimate Stress:	86.8 ksi	
2% Elongation:	23.7%	
8% Elongation:	n/a	

Notes

1. Testing conducted according to the ASTM E8-96 protocol.
2. All units are kips and inches.
3. Stress-strain data was not recorded during testing.
4. Ratio of 80% of ultimate stress was used to estimate yield stress.

<b>Steel Coupon Test Results</b> <b>San Jose State University Structures Laboratory</b>
--

Coupon Specimen Number: Rod 3-3  
 Date of Testing: March 26, 2003  
 Testing conducted by: KMM, PJ, Kevin Chan, Carter Choi

Coupon Type: Rod-type  
 Specimen taken from: 1-inch diameter rod (2002) (3<sup>rd</sup> piece)  
 Specimen Size: 2.25-inch length

**Measurement of specimen dimensions**

*Diameter:* Reading 1 = 0.470  
 Reading 2 = 0.471  
 Reading 3 = 0.471  
 Average = 0.471  
 Average Cross-Sectional Area = 0.174

Test Data

<u>Loading Point</u>	<u>Force</u>
Upper Yield	n/a
Ultimate	15.08 kips

Failure Type: Cup and Cone

Percent Elongation Data

Final Length Readings: 2.386

<b><u>Final Results</u></b>
-----------------------------

Yield Stress:	69.4 ksi	See Note 4
Ultimate Stress:	86.7 ksi	
2% Elongation:	19.3%	
8% Elongation:	n/a	

Notes

1. Testing conducted according to the ASTM E8-96 protocol.
2. All units are kips and inches.
3. Stress-strain data was not recorded during testing.
4. Ratio of 80% of ultimate stress was used to estimate yield stress.

**Steel Coupon Test Results**  
**San Jose State University Structures Laboratory**

Coupon Specimen Number: PL-1  
Date of Testing: March 26, 2003  
Testing conducted by: KMM, PJ, Kevin Chan, Carter Choi

Coupon Type: Plate-type  
Specimen taken from: 1/2x16 inch (2002)  
Specimen Size: 8-inch length

**Measurement of specimen dimensions**

<i>Width:</i> Reading 1 = 1.502	<i>Thickness:</i> Reading 1 = 0.512
Reading 2 = 1.500	Reading 2 = 0.506
Reading 3 = 1.501	Reading 3 = 0.505
Average = 1.501	Average = 0.508

Average Cross-Sectional Area = 0.763

**Test Data**

<u>Loading Point</u>	<u>Force</u>
Upper Yield	39.79 kips
Ultimate	56.03 kips

Failure Type: Cup and Cone

**Percent Elongation Data**

Final Length Readings: 10.19 in

**Final Results**

Yield Stress:	52.1 ksi
Ultimate Stress:	73.4 ksi
2% Elongation:	47.9%
8% Elongation:	27.4%

**Notes**

1. Testing conducted according to the ASTM E8-96 protocol.
2. All units are kips and inches.
3. Stress-strain data were not recorded during testing.

**Steel Coupon Test Results**  
**San Jose State University Structures Laboratory**

Coupon Specimen Number: PL-2  
Date of Testing: March 26, 2003  
Testing conducted by: KMM, PJ, Kevin Chan, Carter Choi

Coupon Type: Plate-type  
Specimen taken from: 1/2x16 inch (2002)  
Specimen Size: 8-inch length

**Measurement of specimen dimensions**

<i>Width:</i> Reading 1 = 1.503	<i>Thickness:</i> Reading 1 = 0.505
Reading 2 = 1.500	Reading 2 = 0.503
Reading 3 = 1.501	Reading 3 = 0.504
Average = 1.501	Average = 0.504

Average Cross-Sectional Area = 0.757

**Test Data**

<u>Loading Point</u>	<u>Force</u>
Upper Yield	40.96 kips
Ultimate	56.71 kips

Failure Type: Cup and Cone

**Percent Elongation Data**

Final Length Readings: 10.04 in

**Final Results**

Yield Stress:	54.1 ksi
Ultimate Stress:	74.9 ksi
2% Elongation:	46.0%
8% Elongation:	25.5%

**Notes**

1. Testing conducted according to the ASTM E8-96 protocol.
2. All units are kips and inches.
3. Stress-strain data were not recorded during testing.

**Appendix F**  
**Calibration Charts of Instrumentation**



## B.1 CALIBRATION CHARTS OF INSTRUMENTATION FOR PP1 AND PP2

**Table B1** – Calibration Data of Wire Pots for PP1 and PP2

Voltages in ( ) are in the dead zone of the wire pot.

Channel	1	6	7	8	9
Wire-Pot Number	5	6	4	1	2
Calibration Factor (Inch/Volt)	3.2372	0.7746	3.2336	3.5487	8.1695
R <sup>2</sup>	1.0000	1.0000	1.0000	0.9920	1.0000
Serial Number	B1051980	C1054470	B1051980	C1054469	A24885
0	0.7928	3.9028	0.7930	(0.0002)	0.4267
5	2.3359	10.3375	2.3382	0.0003	1.0400
10	3.8819	16.8123	3.8855	1.0366	1.6508
15				2.5959	(2.6874)
20				4.1395	(2.8803)
					(3.4972)

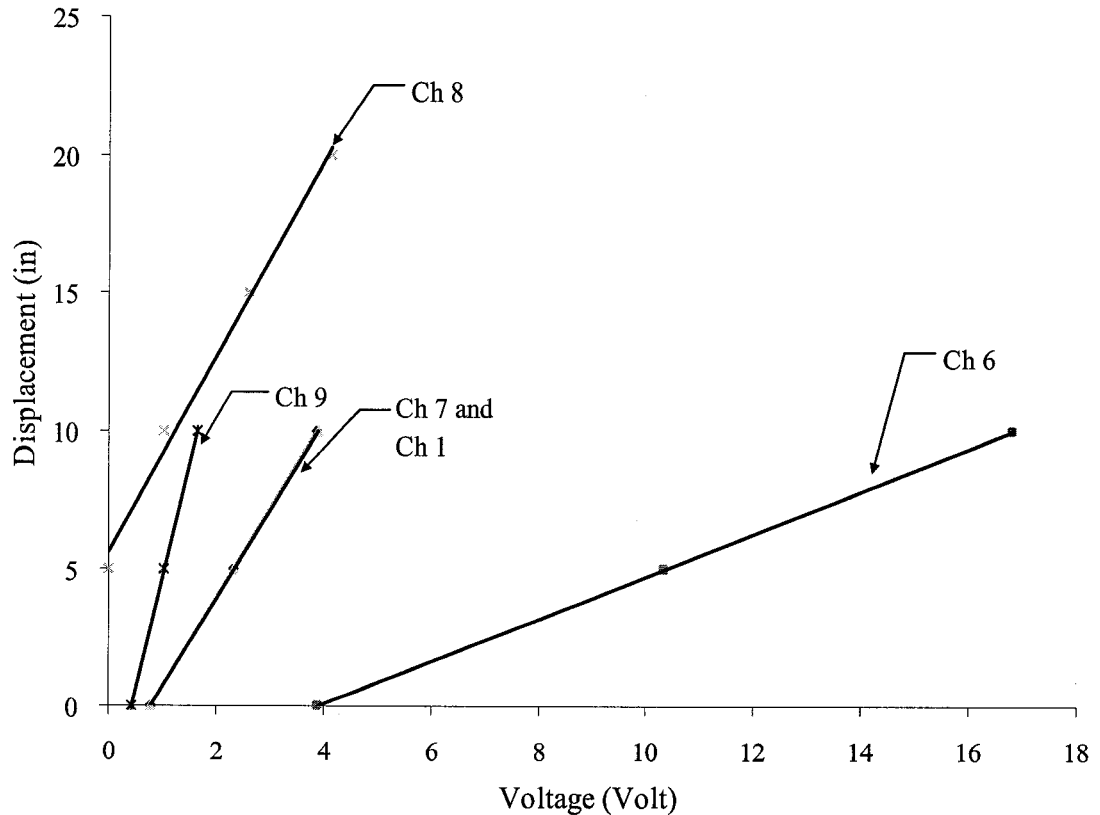


**Figure B2** – Plot of Calibration of Wire Pots Data for PP1 and PP2

## B.2 CALIBRATION CHARTS OF INSTRUMENTATION FOR PP3 AND PP4

**Table B3** – Calibration Data of Load Cell for PP3 and PP4

Testing Machine (lbs)	Signal Conditioner (lbs)	Fluke (volt)
30	0	-0.0041
10050	-2380	-0.1195
20100	-4800	-0.2405
30320	-7240	-0.3622
39900	-9540	-0.4774
50400	-12100	-0.6048
60130	-14440	-0.7225
70020	-16800	-0.8409
80400	-19320	-0.9665
51290	-12340	-0.6172
24900	-5980	-0.2992
100	-20	-0.0010

**Table B4** – Calibration Data of Load Cell for PP3 and PP4

	Signal Conditioner/Testing Machine	Fluke/Testing Machine
Calibration Factor	-0.2404	-0.00001201
R <sup>2</sup>	1.0000	0.9999

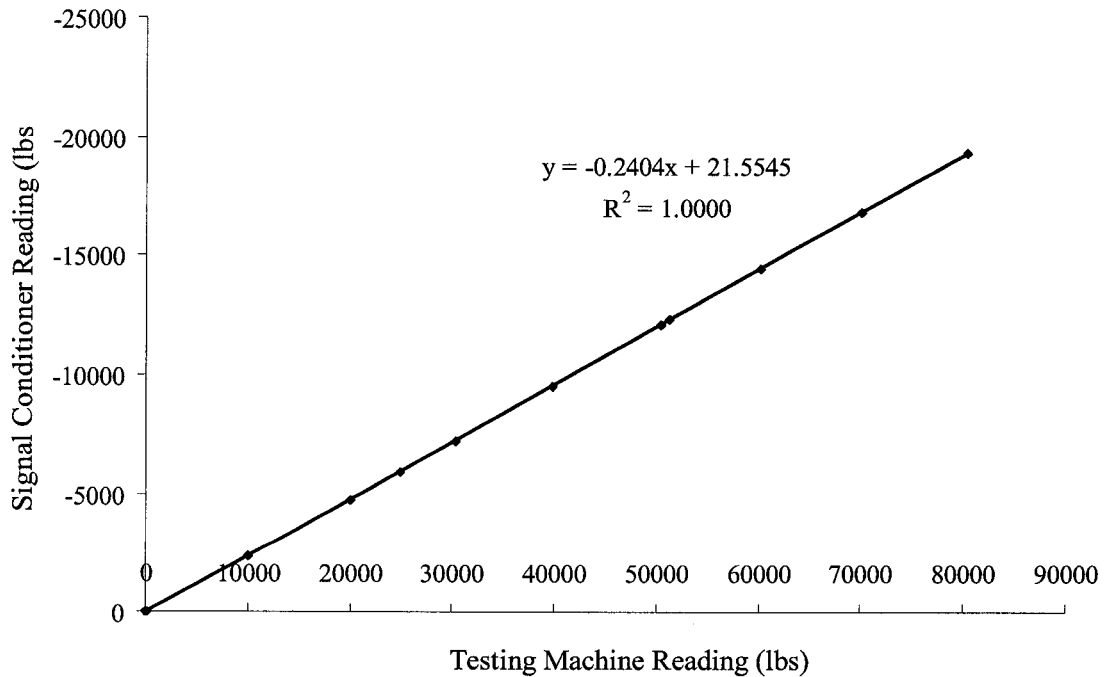


**Figure B5** – Plot of Calibration Data of Signal Conditioner and Testing Machine

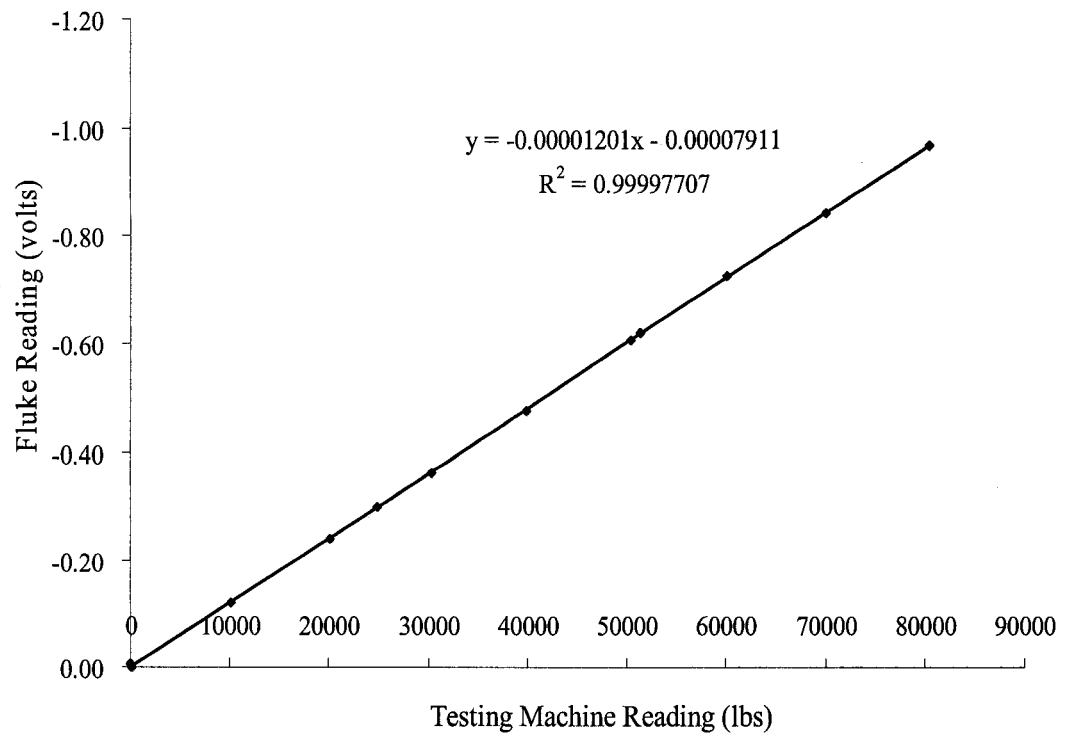


**Figure B6** – Plot of Calibration Data of Fluke and Testing Machine

**Table B7** – Calibration Data of Wire Pots for PP3 and PP4

Channel	2	3	4	5	6
Wire-Pot Number	4	1	5	3	6
Calibration Factor (Inch/Volt)	1.3406	1.3332	1.3414	2.6752	1.3259
R <sup>2</sup>	1	0.9974	1	1	1
Serial Number	B1052679	C1054469	B1051980	C1054518	C1054470
0	1.9765	2.5406	1.9541	1.6550	1.3088
5	5.6990	6.6110	5.6740	3.5270	5.0710
10	9.4360	10.0220	9.4090	5.3930	8.8510

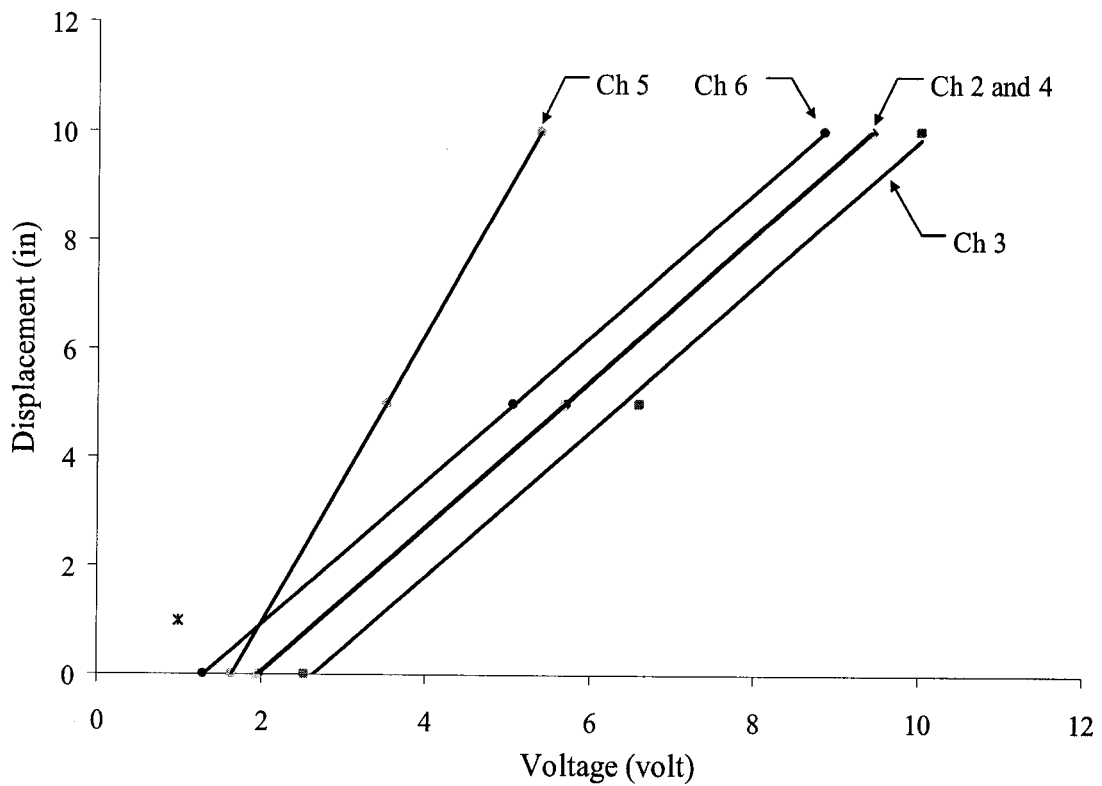


**Figure B8** – Plot of Calibration of Wire Pots Data for PP3 and PP4

**Appendix G**  
**Supporting Calculations**

## C.1 Calculating the Nominal Diameter and Cross Sectional Area of the Coil Threaded Rods

Nominal diameter:

$$A_{rms} = 0.785 \times (d_b - 0.9743/n)^2 \quad (\text{Salmon and Johnson, 1996})$$

$A_{rms}$  = nominal cross sectional area of the threaded rods.

$d_b$  = diameter of the threaded rods = 1 inch.

$n$  = number of threads per inch of threaded rods, 9 threads per inch was used for calculation.

For the 1-inch diameter threaded rod, its nominal area equals:

$$A_{rms} = 0.785 \times (1 - 0.9743/9)^2 = 0.624 \text{ in}^2 = 506.5 \text{ mm}^2$$

The nominal diameter of the threaded rod equals:

$$d_{rms} = 2 \times (A_{rms} / \Pi) = 0.891 \text{ inch} = 22.6 \text{ mm}$$

## C.2 Calculating the Failure Modes of Cantilever Tests

Yielding of the rod due to bending:

$M_y = F_y S_x$  = bending moment caused the rods to yield.

$F_y$  = yield strength of the steel = 36 ksi.

$S_x$  = section modulus =  $(\Pi \times d_{rms}^3)/32 = 0.0694 \text{ in}^3$  for 1-inch diameter threaded rod.

$$M_y = (36 \text{ ksi}) (0.0694 \text{ in}^3) = 2.50 \text{ kips-inch} = 282.5 \text{ kN-mm}$$

The force to cause the 6-inch length rod to reach  $M_y$ :

$$P = M_y / L = (2.50 \text{ kips-inch}) / (6 \text{ inch}) = 417 \text{ lbs.} = 1.85 \text{ kN}$$

The force to cause the 18-inch length rod to reach  $M_y$ :

$$P = M_y / L = (2.50 \text{ kips-inch}) / (18 \text{ inch}) = 139 \text{ lbs.} = 0.616 \text{ kN}$$

Plastic hinging of the rod due to bending:

$M_p = F_y Z_x$  = bending moment caused the rods to reach plastic hinge

$$Z_x = \text{plastic modulus} = d_{rms}^3/6 = 0.118 \text{ in}^3 \quad (\text{LRFD Volume I})$$

$$M_p = (36 \text{ ksi}) (0.118 \text{ in}^3) = 4.25 \text{ kip-inch.} = 480 \text{ kN-mm}$$

The force to cause the 6-inch length rod to reach  $M_p$ :

$$P = M_y / L = (4.25 \text{ kips-inch}) / (6 \text{ inch}) = 708 \text{ lbs.} = 3.14 \text{ kN}$$

The force to cause the 18-inch length rod to reach  $M_p$ :

$$P = M_y / L = (4.25 \text{ kips-inch}) / (18 \text{ inch}) = 236 \text{ lbs.} = 1.05 \text{ kN}$$

Rod failure due to shear:

$$V = 0.6 F_y A_{rms} = \text{shear force.}$$

$$V = (0.6) (36 \text{ ksi}) (0.624 \text{ in}^2) = 13.5 \text{ kips.} = 59.9 \text{ kN}$$

Bearing of the web of the WT beam:

$$R_n = 3.0F_u dt, \text{ nominal bearing strength of the web of the WT beam}$$

(Salmon and Johnson, 1996)

$$t = \text{thickness of the web} = 5/16 \text{ inch.}$$

$$d = \text{nominal diameter of the 1-inch rod} = 0.891 \text{ inch.}$$

$$F_u = \text{ultimate tensile strength of the material for the WT beam} = 36 \text{ ksi.}$$

$$R_n = 30.07 \text{ kips.} = 133.3 \text{ kN}$$

$$4R_n = 120.3 \text{ kips, 4 rods per test.} = 533.4 \text{ kN}$$

### **C.3 Calculating the Displacement of the Prediction Models of the Cantilever Tests**

Calculating displacement of the cantilever model with 1-inch diameter 6-inch length rods:

$$\Delta_{\text{total}} = \Delta_{\text{bending}} + \Delta_{\text{slip}}$$

$$\Delta_{\text{bending}} = FL^3/3EI$$

F = load that was applied to the rods.

L = length of the rods.

E = modulus of elasticity.

I = moment of inertia of the rods based on rms diameter.

For rod length of 6 inches:

At the yield force of 416.7 lb per rod, the rod would deflect

$$\Delta = (416.7 \text{ lb}) (6 \text{ in})^3 / 3(29000 \text{ ksi}) (0.0309 \text{ in}^4) = 0.03 \text{ inch} = 0.762 \text{ mm}$$

$$\Delta_{\text{slip}} = 1/2(d_{\text{hole}} - d_{\text{rod}}) = 1 \text{ inch} = 25.4 \text{ mm}$$

$\Delta_{\text{total}}$  at yield = 1 inch + 0.03 inch = 1.03 inch = 26.2 mm, when the rods reach their yield strength.

To estimate a lower bound for the deflection at the load causing plastic bending, the elastic bending formulas were used with the forces required for plastification.

When the plastic hinge force of 708.3 lb per rod was reached, the rod would deflect

$$\Delta = (708.3 \text{ lb}) (6 \text{ in})^3 / 3(29000 \text{ ksi}) (0.0309 \text{ in}^4) = 0.06 \text{ inch} = 1.52 \text{ mm}$$

$\Delta_{\text{total}}$  at plastic hinging = 1 inch + 0.06 inch = 1.06 inch = 26.9 mm, when the rods reached their plastic hinge strength.

Calculating displacement of the cantilever model with 1-inch diameter 18-inch length rods:

At the yield force of 138.9 lb per rod, the rod would deflect

$$\Delta = (138.9 \text{ lb}) (6 \text{ in})^3 / 3(29000 \text{ ksi}) (0.0309 \text{ in}^4) = 0.30 \text{ inch} = 7.62 \text{ mm}$$

$$\Delta_{\text{slip}} = 1/2 (d_{\text{hole}} - d_{\text{rod}}) = 1 \text{ inch} = 25.4 \text{ mm}$$

$\Delta_{\text{total}}$  at yield = 1 inch + 0.30 inch = 1.30 inch = 33.0 mm, when the rods reached their yield strength.

When the plastic hinge force of 236.1 lb per rod was reached, the rod would deflect

$$\Delta = (236.1 \text{ lb}) (6 \text{ in})^3 / 3(29000 \text{ ksi}) (0.0309 \text{ in}^4) = 0.51 \text{ inch} = 13.0 \text{ mm}$$

$\Delta_{\text{total}}$  at plastic hinging = 1 inch + 0.51 inch = 1.51 inch = 38.4 mm, when the rods reached their plastic hinge strength.



#### C.4 Calculating the Failure Modes of Axial Tests

Yielding of the column plate due to bending caused by axial load in the four rods:

$$M_y = F_y S_x$$

$$S_x = \text{section modulus} = (bt^2) / 6 = (16 \times 0.5^2) / 6 = 0.667 \text{ in}^3$$

$$M_y = (36 \text{ ksi}) (0.667 \text{ in}^3) = 24 \text{ kip-inch} = 2712 \text{ kN-mm}$$

The force to cause the plate to reach  $M_y$ :

$$P = M_y / 4 \text{ inches} = 6 \text{ kips.} = 26.6 \text{ kN}$$

Plastic hinging of the column plate due to bending caused by axial load:

$$M_p = F_y Z_x$$

$$Z_x = \text{plastic modulus} = (16 \times t^2) / 4 = (16 \times 0.5^2) / 4 = 1.0 \text{ in}^3$$

$$M_p = (36 \text{ ksi}) (1.0 \text{ in}^3) = 36 \text{ kip-inch} = 4068 \text{ kN-mm}$$

The force to cause the plate to reach  $M_p$ :

$$P = M_p / 4 \text{ inches} = 9 \text{ kips.} = 39.9 \text{ kN}$$

Yielding of a 1-inch diameter rod due to axial load:

$$P_y = A_{rms} F_y = (0.624 \text{ in}^2)(36 \text{ ksi}) = 22.45 \text{ kips} = 99.6 \text{ kN}$$

Buckling of a rod due to compression load:

$$P_{cr} = \Pi^2 EI / (KL)^2$$

$$E = \text{modulus of elasticity} = 29000 \text{ ksi.}$$

$$I = \text{moment of inertia of the rod} = (\Pi \times r^4) / 4$$

$$K = \text{effective-length factor} = 0.7, \text{ the rod was model as pinned on the top, fixed at the bottom.}$$

$$P_{cr} = 134.4 \text{ kips} = 596 \text{ kN}$$

Fracture of the weld between the column testing jig and the column plate due to tension load:

$$R_n = t_e \times F_y, \text{ strength of the weld under tension.}$$

$$F_y = \text{tensile strength of base metal} = 36 \text{ ksi}$$

$$t_e = \text{effective throat size} = 0.707a$$

$$a = \text{nominal size} = 5/16 \text{ inch}$$

$$t_e = 0.707 \times 5/16 = 0.221 \text{ inch}$$

$$R_n = 0.221 \text{ inch} \times 90 \text{ ksi} = 7.96 \text{ kips/inch.}$$

$$P = R_n \times 2L$$

$$L = \text{length of the weld} = 5 \text{ inches on each side of the column testing jig.}$$

$$P = (7.96 \text{ kips/inch}) (10 \text{ inches}) = 79.6 \text{ kips} = 353 \text{ kN}$$

Fracture of the weld between the nuts and the panel embed (represented by the web of the W16x40):

$$\text{Perimeter of the nut} = 3.9 \text{ inches} \quad (\text{LRFD Volume II})$$

$$a = 0.25 \text{ inch.}$$

$$t_e = 0.707 a = 0.177 \text{ inch.}$$

$$R_{nw} = 0.177 \text{ inch} \times 36 \text{ ksi} = 6.37 \text{ kips/inch.}$$

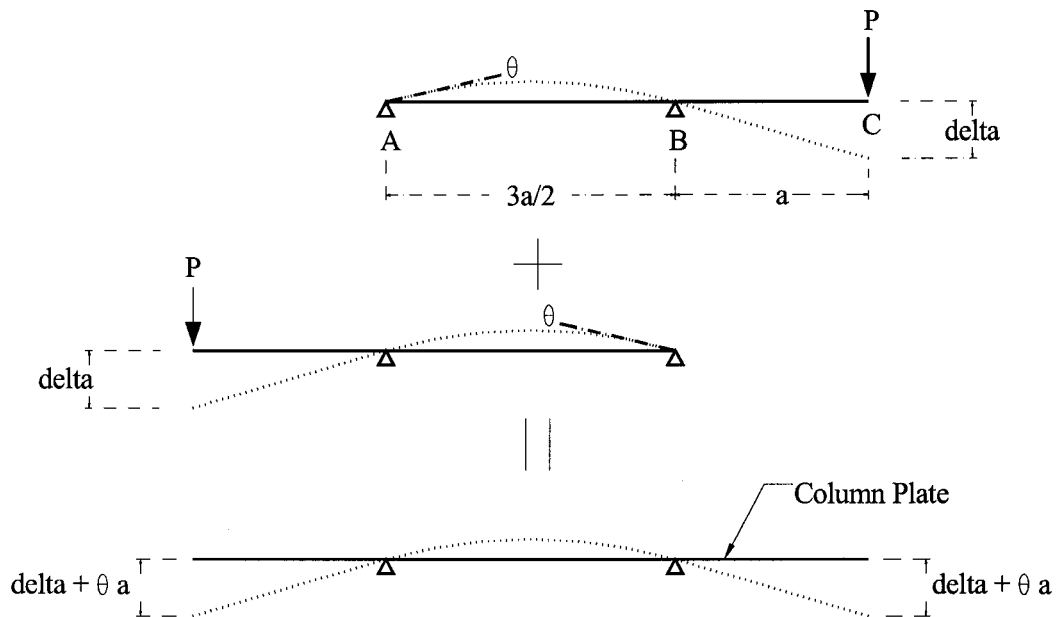
$$P = (6.37 \text{ kips/inch} \times 3.9 \text{ inch}) = 24.8 \text{ kips} = 110 \text{ kN, per nut.}$$

$$4P = 99.2 \text{ kips} = 440 \text{ kN, four nuts per test.}$$

### **C.5 Calculating the Displacement of the Prediction Models of the Axial Tests**

Calculating displacement of the tension and compression tests model with 1-inch diameter 18-inch length rods, post-buckling displacement of the rods was not calculated:

$$\Delta_{\text{overall}} = \Delta_{\text{column plate}} + \Delta_{\text{rods}}, \text{ until the plate reached its yield strength.}$$



$\Delta$  of column of column plate is calculated by using the double integration method and the above model:

Solving for reaction at A and B

$$\Sigma M_A = 0 = -P(a + 3a/2) + B(3a/2), \text{ sum of moment at A and solve for B}$$

$$B = 5P/3$$

$$\Sigma F_y = 0 = A + B - P, \text{ sum of forces in y direction and solve for A}$$

$$A = -2P/3$$

Solving for bending moment of the beam

$$M_1 = -2PX_1/3, 0 \leq X_1 \leq 3a/2$$

$$M_2 = -2PX_2/3 + 5P/3(X_2 - 3a/2) = PX_2 - 5Pa/2, 3a/2 < X_2 \leq 5a/2$$

Slope and elastic curve for  $X_1$

$$EI \frac{d^2v_1}{dx_1^2} = -2PX_1/3$$

$$EI \frac{dv_1}{dx_1} = -2PX_1^2/6 + C_1$$

$$EI v_1 = -2PX_1^3/18 + C_1X_1 + C_2$$

Slope and elastic curve for  $X_1$

$$EI \frac{d^2 v_2}{dx_2^2} = PX_2 - 5Pa/2$$

$$EI \frac{dv_2}{dx_2} = PX_2^2/2 - 5PaX_2/2 + C_3$$

$$EI v_2 = PX_2^3/6 - 5PaX_2^2/4 + C_3X_2 + C_4$$

Boundary condition at  $X_1 = 0, v_1 = 0$

$$v_1 = (-2PX_1^3/18 + C_1X_1 + C_2)/EI = 0, C_2 = 0$$

Boundary condition at  $X_1 = 3a/2, v_1 = 0$

$$v_1 = -3Pa^3/8 + C_1(3a/2) = 0, C_1 = Pa^2/4$$

Boundary condition at  $X_2 = 3a/2, v_2 = 0$

$$v_2 = 9Pa^3/16 - 45Pa^3/16 + 3aC_3/2 + C_4 = 0$$

Boundary condition of  $dv_1/dx_1 = dv_2/dx_2$  at  $X_1 = X_2 = 3a/2$

$$dv_1(3a/2)/dx_1 = dv_2(3a/2)/dx_2$$

$$-2P(3a/2)^2/6 + Pa^2/4 = P(3a/2)^2/2 - 5Pa(3a/2)/2 + C_3$$

$$C_3 = 17Pa^2/8$$

Substitute  $C_3 = 17Pa^2/8$  into  $v_2 = 9Pa^3/16 - 45Pa^3/16 + 3aC_3/2 + C_4 = 0$

$$C_4 = -15Pa^3/16$$

Solve  $\Delta$  at  $X_2 = 5a/2$  with  $v_2 = (PX_2^3/6 - 5PaX_2^2/4 + C_3X_2 + C_4)/EI$

$$v_2 = 50Pa^3/48EI$$

Solve  $\Theta$  at  $X_1 = 0$  with  $dv_1/dx_1 = (-2PX_1^2/6 + C_1)/EI$

$$\Theta = Pa^2/4EI$$

Solve for  $\Delta_{\text{column plate}}$

$$\Delta_{\text{column plate}} = v_2 + \Theta a$$

$$\Delta_{\text{column plate}} = 50Pa^3/48EI + (Pa^2/4EI)(a)$$

The load applied by the testing machine is notated as  $P$ . Therefore, use  $P = 0.5P$  in the  $\Delta_{\text{column plate}}$  equation.

$$\Delta_{\text{column plate}} = 50(0.5P)(a^3)/48EI + (0.5P)(a^3)/4EI$$

The rods are assumed to have same behavior under both tension and compression:

$\Delta_{\text{rods}} = (0.25PL) / A_{\text{rms}}E$ , assumed to be the same under both tension and compression forces.

P = load applied by the testing machine.

a = distance from the flange of the column testing jig to the center of the rod = 8 inches.

E = modulus of elasticity = 29000 ksi.

I = moment of inertia = 0.167 in<sup>4</sup>

$A_{\text{rms}}$  = nominal cross sectional area of the rods = 0.624 in<sup>2</sup>

L = length of the rods = 18 inches.

The column plate yield at the load of P = 6 kips, according to the failure mode calculation in C.4:

$$\Delta_{\text{column plate}} = 0.330 + 0.079 = 0.409 \text{ inch} = 10.4 \text{ mm}$$

$$\Delta_{\text{rods}} = (0.25PL) / A_{\text{rms}}E = (0.25) (6 \text{ kips}) (18 \text{ inch}) / (0.624 \text{ in}^2) (29000 \text{ ksi}) = 0.0115 \text{ inch} = 0.292 \text{ mm}$$

$$\Delta_{\text{overall}} = \Delta_{\text{column plate}} + \Delta_{\text{rods}} = 0.409 \text{ inch} + 0.0115 \text{ inch} = 0.420 \text{ inch} = 10.7 \text{ mm},$$

when the plate reached its yield stress.